2013 台灣工程計算力學暨邊界元素法研討會

Engineering Numerical Analysis and BEM in Taiwan 2013

論文集

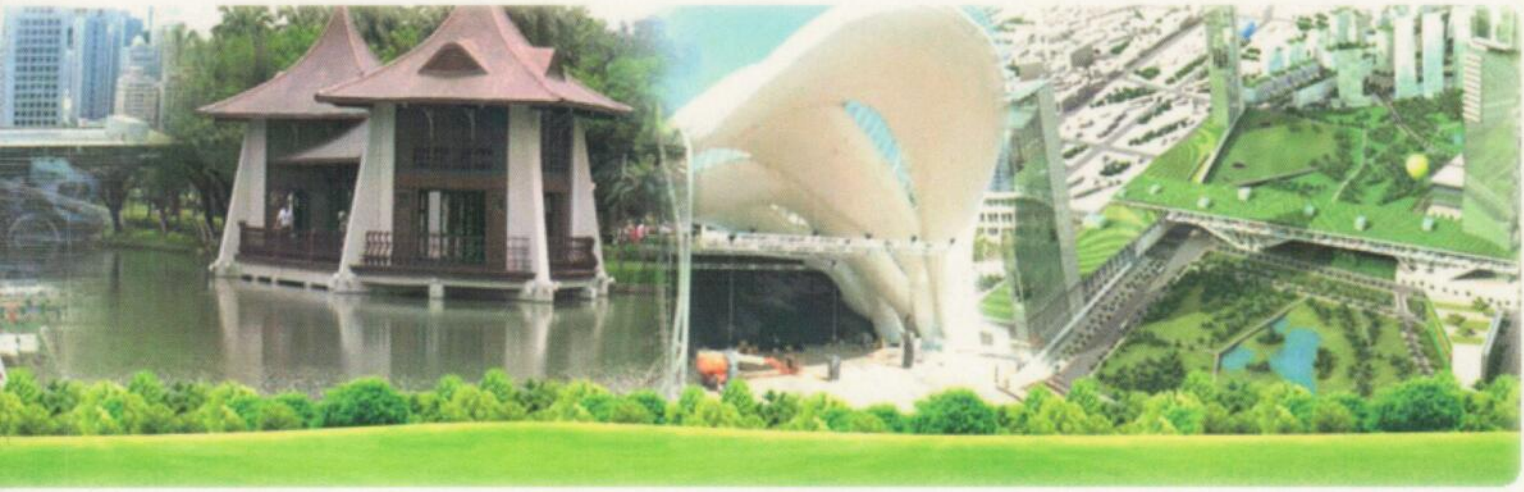

國立中興大學

National Chung Hsing University

2013 年 3 月 20 日

2013 台灣工程計算力學暨邊界元素法研討會
Engineering Numerical Analysis and BEM in Taiwan 2013

主　　旨： 2010 年於海洋大學舉辦了第一屆邊界元素法相關研討會，提供數學與工程學者同好能有再一次相互觀摩切磋的機會。之後，2011 年由成大數學系承辦了第二屆研討會，2012 年第三屆研討會由逢甲大學航太系舉辦。本次第四屆研討會配合美國國家工程院士也是邊界元素法大師的美國University of Minnesota理工學院院長Steven L. Crouch之來訪舉辦；乃為傳承此一薪火，提供一個平臺，使國內學者在工程計算力學及邊界元素法與相關數學或數值方法上得以互相切磋、交流與學習。

主辦單位：國立中興大學土木工程學系

協辦單位：中華民國大地工程學會(TGS)

主講人、主持人 ：

Steven L. Crouch	美國國家工程院士 University of Minnesota 理工學院院長
陳正宗	國立台灣海洋大學河海工程系終身特聘教授
陳立憲	國立台北科技大學土木工程系副教授
陳昭旭	國立成功大學資源工程系教授
夏育群	國立成功大學航空太空工程系教授
方富民	國立中興大學土木工程系教授
馮正一	國立中興大學水土保持學系教授
壽克堅	國立中興大學土木工程系教授兼系主任

時　　間：2013 年 3 月 20(星期三)

地　　點：台中市國光路 250 號國立中興大學土木系
土木環工大樓地下室工學院第三會議室

議程

時　間 (2013/3/20)	演 講 主 題	主 講 人	主持人
09:00-09:20	報　到		
09:20-09:30	開幕與貴賓致詞	薛富盛	壽克堅
09:30-10:30	**On the Displacement Discontinuity Method** 位移不連續法之發展	**Steven L. Crouch**	
10:30-10:50	休　息		
10:50-11:50	**Review of the dual BEM and recent development of null-field integral equation approach by ntou/msv** 對偶邊界元素法回顧及其近期發展	陳正宗	壽克堅
11:50-13:00	午　餐　休　息		
13:00-13:30	**Boundary Element Analysis of the Stress Concentration in 3D Anisotropic Bodies** 邊界元素法分析三維異向體之應力集中	夏育群	陳正宗
13:30-14:00	**Analysis of Rock Fracture Mechanics Using the BEM** 邊界元素法應用於岩石之破壞力學性質分析	陳昭旭	
14:00-14:30	**Simulation of Seismic Signals Induced by Landslide by Numerical Coupling of PFC and FLAC** 研究顆粒流與連體數值耦合方法模擬山崩產生之震動訊號	馮正一	
14:30~14:40	休　息		
14:40~15:10	**Applications in Computational Wind Engineering** 計算風工程之應用	方富民	陳立憲
15:10~15:40	**Indentation Fracture with coupling of DEM and FDM** 耦合分離元素與有限差分法模擬貫切破壞	陳立憲	
15:40~16:10	**Applications of Displacement Discontinuity Method** 位移不連續法之應用	壽克堅	

On the Displacement Discontinuity Method

位移不連續法之發展

Steven L. Crouch

美國 **University of Minnesota** 理工學院院長

"On the Displacement Discontinuity Method"

Steven L. Crouch
College of Science and Engineering
University of Minnesota

Introduction

The displacement discontinuity method was devised nearly 40 years ago as a way to compute the displacements and stresses induced by excavations in tabular ore deposits in an assumed linearly elastic body of rock. A tabular ore deposit is one that is thin in one dimension and extensive in the other two, for example, a narrow coal seam. For such problems the seam can be treated as a crack containing a compressible filling, and the relative displacements between the two surfaces of the crack—the displacement discontinuities—then determine the displacements, strains, and stresses elsewhere in the rock. This approach can also be used to represent the effects of intersecting joints or faults in the rock in the vicinity of the seam.

Since its introduction, the displacement discontinuity method has been enhanced and refined by a number of researchers and used to tackle a variety of problems in applied mechanics, including viscoelasticity, transient thermoelasticity, and elastodynamics. Several variants of the basic approach have been devised to deal with applications related to simulation of crack propagation in brittle materials, including hydraulic fracturing technology.

This talk gives an updated summary of the basic method, shows the connection between its "indirect" and "direct" formulations, and presents a simplified treatment of the relatively new Galerkin formulation of the method. Finally, some thoughts are ventured on possible future developments and applications of the displacement discontinuity method.

On the Displacement Discontinuity Method

by

Steven L. Crouch

(with major input from John A. L. Napier,
Department of Mining Engineering,
University of Pretoria, South Africa)

Department of Civil Engineering
University of Minnesota

Overview of Presentation

- Historical background
- Original development of method; influence function approach
- Applications
- Alternate development of method using Volterra's formula
- Galerkin formulation
- Conclusions

COLLEGE OF Science & Engineering
UNIVERSITY OF MINNESOTA Driven to Discover

Historical background

Method originally developed to address problems in mining; modeling of thin vein or seam-like ore deposits. Early contributions by:

- **P. Hackett** (1959) — longwall mine working modeled as a crack (Hackett attributes idea to R. Hill)
- **D. S. Berry** (1960; 1963) — 2D and 3D mine subsidence modeling
- **M. D. G. Salamon** (1963) — 3D "face element principle"; development of analog computer technique
- **A. M. Starfield** (1968) — First 2D and 3D digital computer models
- **F. H. Deist** (1969) — "MINSIM" replaced analog computer for designing 3D mine layouts in South Africa
- **S. L. Crouch** (1973; 1976) — Coined term "displacement discontinuity method" for general 2D model

These developments were done in parallel with work by **Rizzo et al.** on boundary integral equation techniques for elasticity problems.

COLLEGE OF Science & Engineering
UNIVERSITY OF MINNESOTA Driven to Discover

The basic idea: divide a line crack into N elements

An "influence function" approach

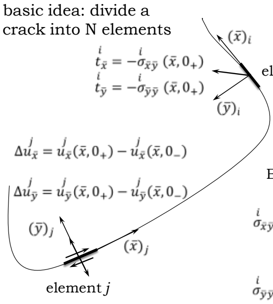

$$\overset{i}{t}_{\bar{x}} = -\overset{i}{\sigma}_{\bar{x}\bar{y}}\,(\bar{x},0_+)$$
$$\overset{i}{t}_{\bar{y}} = -\overset{i}{\sigma}_{\bar{y}\bar{y}}\,(\bar{x},0_+)$$

Use collocation to avoid strong singularities at element endpoints!

$$\Delta\overset{j}{u}_{\bar{x}} = \overset{j}{u}_{\bar{x}}(\bar{x},0_+) - \overset{j}{u}_{\bar{x}}(\bar{x},0_-)$$
$$\Delta\overset{j}{u}_{\bar{y}} = \overset{j}{u}_{\bar{y}}(\bar{x},0_+) - \overset{j}{u}_{\bar{y}}(\bar{x},0_-)$$

By superposition…

$$\overset{i}{\sigma}_{\bar{x}\bar{y}} = \sum_{j=1}^{N} \overset{ij}{A}_{\bar{x}\bar{x}}\Delta\overset{j}{u}_{\bar{x}} + \sum_{j=1}^{N} \overset{ij}{A}_{\bar{x}\bar{y}}\Delta\overset{j}{u}_{\bar{y}}$$
$$\overset{i}{\sigma}_{\bar{y}\bar{y}} = \sum_{j=1}^{N} \overset{ij}{A}_{\bar{y}\bar{x}}\Delta\overset{j}{u}_{\bar{x}} + \sum_{j=1}^{N} \overset{ij}{A}_{\bar{y}\bar{y}}\Delta\overset{j}{u}_{\bar{y}}$$

Note: Each element has its own local $\bar{x}$, $\bar{y}$ coordinate system.

COLLEGE OF Science & Engineering
UNIVERSITY OF MINNESOTA Driven to Discover

The system of equations

If there are N displacement discontinuity elements along the crack(s), and if the shear and normal tractions $(\sigma_{\bar{x}\bar{y}})_0$ and $(\sigma_{\bar{y}\bar{y}})_0$ are specified at each one, then, for $i = 1$ to N,

$$\sum_{j=1}^{N} \overset{ij}{A}_{\bar{x}\bar{x}}\Delta\overset{j}{u}_{\bar{x}} + \sum_{j=1}^{N} \overset{ij}{A}_{\bar{x}\bar{y}}\Delta\overset{j}{u}_{\bar{y}} = (\overset{i}{\sigma}_{\bar{x}\bar{y}})_0$$
$$\sum_{j=1}^{N} \overset{ij}{A}_{\bar{y}\bar{x}}\Delta\overset{j}{u}_{\bar{x}} + \sum_{j=1}^{N} \overset{ij}{A}_{\bar{y}\bar{y}}\Delta\overset{j}{u}_{\bar{y}} = (\overset{i}{\sigma}_{\bar{y}\bar{y}})_0$$

$2N$ equations in $2N$ unknowns.

Note: If the displacement discontinuities vary linearly along the element then there are two collocation points per element and the system of algebraic equations is $4N$ by $4N$

COLLEGE OF Science & Engineering
UNIVERSITY OF MINNESOTA Driven to Discover

Derivation of formulas using displacement potentials (Papkovitch-Neuber functions)

The following expressions satisfy the displacement equations of equilibrium for an isotropic, linearly elastic solid in two dimensions:

$$u_x = -(1-2\nu)\frac{\partial}{\partial x}\Phi + 2(1-\nu)\frac{\partial}{\partial y}\Psi - y\frac{\partial}{\partial x}\Lambda$$
$$u_y = 2(1-\nu)\frac{\partial}{\partial y}\Phi + (1-2\nu)\frac{\partial}{\partial x}\Psi - y\frac{\partial}{\partial y}\Lambda$$

Where ν is Poisson's ratio, $\Lambda = \partial\Psi/\partial x + \partial\Phi/\partial y$, and displacement potentials Φ and Ψ satisfy Laplace's equation:

$$\nabla^2\Phi = \frac{\partial^2}{\partial x^2}\Phi + \frac{\partial^2}{\partial y^2}\Phi = 0\,;\; \nabla^2\Psi = 0$$

Note: A similar representation is available for 3D problems in terms of *three* potentials, $\Phi(x,y,z), \Psi_x(x,y,z)$, and $\Psi_y(x,y,z)$.

COLLEGE OF Science & Engineering
UNIVERSITY OF MINNESOTA Driven to Discover

Derivation (cont'd)

The associated stress components are

$$\sigma_{xx} = 2G\,[\frac{\partial^2}{\partial y^2}\Phi + 2\frac{\partial^2}{\partial x \partial y}\Psi + y\,\frac{\partial^2}{\partial y^2}\Lambda\,]$$

$$\sigma_{yy} = 2G\,[\frac{\partial^2}{\partial y^2}\Phi - y\,\frac{\partial^2}{\partial y^2}\Lambda\,]$$

$$\sigma_{xy} = 2G\,[\frac{\partial^2}{\partial y^2}\Psi - y\,\frac{\partial^2}{\partial x \partial y}\Lambda\,]$$

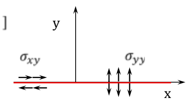

Where G is the shear modulus (and again $\Lambda = \partial\Psi/\partial x + \partial\Phi/\partial y$).

(1) $\Psi = 0, \Phi \neq 0$: The line (or plane) $y = 0$ is free from shear stress σ_{xy} for $-\infty \leq x \leq \infty$;

(2) $\Psi \neq 0, \Phi = 0$: The line $y = 0$ is free from normal stress σ_{yy} for $-\infty \leq x \leq \infty$;

(3) $\Psi \neq 0, \Phi \neq 0$: Superposition of (1) and (2).

Derivation (cont'd)

A displacement discontinuity over the line segment $-a \leq x \leq a, y = 0$:

To express in terms of local coordinates:

Replace x and y with $\bar{x}$ and $\bar{y}$ — there is no preferred orientation in the problem. (Infinite body; isotropic elasticity.)

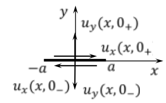

$$\Delta u_x(x) = u_x(x, 0_+) - u_x(x, 0_-)$$

$$\Delta u_y(x) = u_y(x, 0_+) - u_y(x, 0_-)$$

$$\Psi(x, y) = -\int_{-a}^{a} \Delta u_x(x') g(x - x', y) dx'$$

$$\Phi(x, y) = -\int_{-a}^{a} \Delta u_y(x') g(x - x', y) dx'$$

Where $g(x, y) = -\frac{1}{4\pi(1-\nu)} \ln\sqrt{x^2 + y^2}$

Example element types ($i = x \; or \; y$)

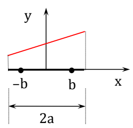

<u>Linearly varying displacement discontinuity</u>:

$$\Delta u_i(x) = \tfrac{1}{2}\left(1 - \frac{x}{b}\right)\Delta u_i(-b) + \tfrac{1}{2}\left(1 + \frac{x}{b}\right)\Delta u_i(b)$$
$$= \alpha_1(x)(\Delta u_i)_1 + \alpha_2(x)(\Delta u_i)_2$$

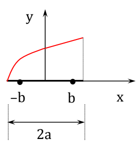

<u>A crack tip element</u>:

$$\Delta u_i(x) = \Delta u_i(-b)\frac{1}{\sqrt{a-b}}\sqrt{x+a}\,; \; -a \leq x \leq 0$$

$$\Delta u_i(x) = \Delta u_i(b)\frac{1}{b+2a}(x + 2a)\,; \; 0 \leq x \leq a$$

Compute Ψ and Φ, then find displacements u_x and u_y and stresses σ_{xx}, σ_{yy}, and σ_{xy}.

Applications (with emphasis on problems in geomechanics)

"Easy" problems:

- Crack closure & frictional sliding along pre-defined crack/fracture geometries (relatively easy for both 2D and 3D)
- Crack propagation in tension (easy for 2D, less so for 3D)

Areas of need:

- 3D modeling of mixed mode fractures and shear bands
- Elastodynamics (e.g. simulation of seismic events)
- Hydraulic fracturing with fluid flow
- Fracture of composite materials

$\Delta u_x(x) = u_x(x, 0_+) - u_x(x, 0_-)$

To express in terms of local coordinates:

Replace x and y with $\bar{x}$ and $\bar{y}$ — there is no preferred orientation in the problem. (Infinite body; isotropic elasticity.)

Simulation of crack growth in tension — procedure

Maximum tensile stress criterion:

- Crack propagates in radial direction, perpendicular to direction of greatest tension (i.e. $\sigma_{r\theta} = 0$)
- $\sigma_{\theta\theta}$ must reach a critical value, $\sqrt{2\pi r}\sigma_{\theta\theta} = K_{Ic}$, where K_{Ic} is the fracture toughness

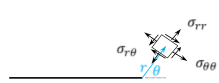

r is "small"

$$\sigma_{r\theta} = \frac{1}{2\sqrt{2\pi r}} cos\frac{\theta}{2}[K_I sin\theta + K_{II}(3cos\theta - 1)]$$

$$\sigma_{\theta\theta} = \frac{1}{2\sqrt{2\pi r}} cos\frac{\theta}{2}[K_I cos^2\frac{\theta}{2} - \frac{3}{2}K_{II} sin\theta]$$

Simulation of crack growth — procedure (cont'd)

Compute K_I and K_{II} numerically:

$$K_I \approx \frac{G}{4(1-\nu)}\sqrt{\frac{2\pi}{a}}\,\Delta u_{\hat{y}}(0) \qquad K_{II} \approx \frac{G}{4(1-\nu)}\sqrt{\frac{2\pi}{a}}\,\Delta u_{\hat{x}}(0)$$

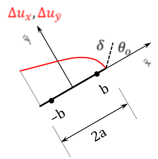

Then, use formulas

(1) $\cos\frac{\theta_o}{2}[K_I \sin\theta_o + K_{II}(3\cos\theta_o - 1)] = 0;\ \sigma_{r\theta} = 0$

(2) $\cos\frac{\theta_o}{2}\left[K_I \cos^2\frac{\theta_o}{2} - \frac{3}{2}K_{II}\sin\theta_o\right] = K_{Ic}$

Solve (1) for θ_o; extend crack by amount δ if (2) is satisfied ($\delta \ll 2a$).

A simple example — 2D simulation of crack growth (maximum tensile stress criterion)

Two pressurized "starter cracks," each 0.4 mm long

Pressure p applied *to starter cracks only* in 0.5 MPa increments, from 0 to 500 Mpa

Shear modulus: $G = 30 \times 10^3$ Mpa

Poisson's ratio: $\nu = 0.2$

Fracture toughness: $K_{Ic} = 1$ MPa m$^{1/2}$

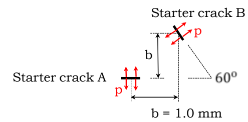

Use linearly varying displacement discontinuities and crack tip elements.

COLLEGE OF Science & Engineering
UNIVERSITY OF MINNESOTA Driven to Discover

Load step 100 (pressure = 50 MPa)

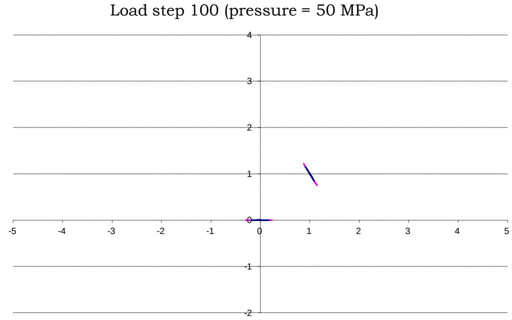

COLLEGE OF Science & Engineering
UNIVERSITY OF MINNESOTA Driven to Discover

Load step 200 (pressure = 100 MPa)

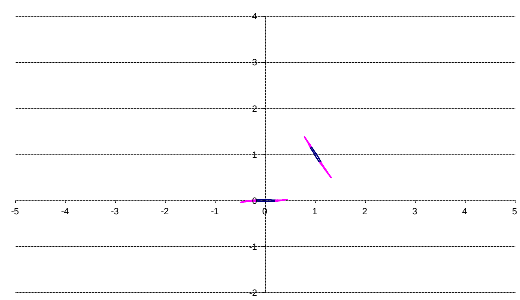

COLLEGE OF Science & Engineering
UNIVERSITY OF MINNESOTA Driven to Discover

Load step 300 (pressure = 150 MPa)

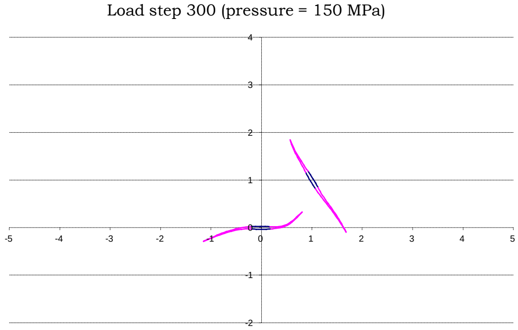

COLLEGE OF Science & Engineering
UNIVERSITY OF MINNESOTA Driven to Discover

Load step 400 (pressure = 200 MPa)

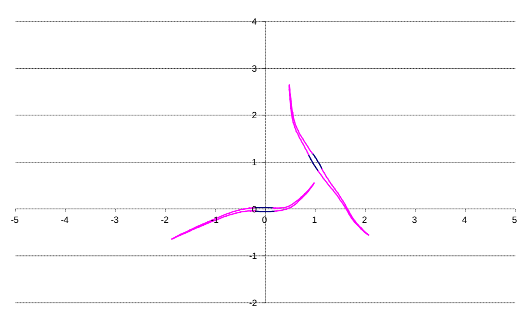

COLLEGE OF Science & Engineering
UNIVERSITY OF MINNESOTA Driven to Discover

Load step 500 (pressure = 250 MPa)

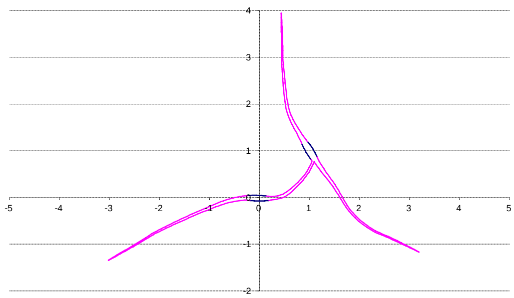

Alternate development of the method using Volterra's formula

A line crack Γ with surfaces Γ^+ and Γ^-;

Displacements $u_i(\boldsymbol{\xi})$ at point $\boldsymbol{\xi} = (\xi_x, \xi_y)$ due to displacement discontinuities $\Delta u_j(\boldsymbol{x}) = u_j^+(\boldsymbol{x}) - u_j^-(\boldsymbol{x})$;

Volterra's formula is:

$$u_i(\boldsymbol{\xi}) = \int_\Gamma T_{ij}(\boldsymbol{\xi}, \boldsymbol{x}) \Delta u_j(\boldsymbol{x}) dS(\boldsymbol{x})$$

$T_{ij}(\boldsymbol{\xi}, \boldsymbol{x})$ gives the traction in the j-direction at point $\boldsymbol{x}$ (the sample point) due to a unit concentrated force in the i-direction at point $\boldsymbol{\xi}$ (the load point).

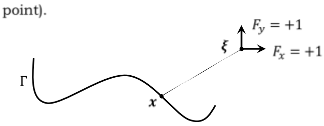

COLLEGE OF Science & Engineering — UNIVERSITY OF MINNESOTA Driven to Discover

The stresses associated with displacements $u_i(\boldsymbol{\xi})$ are

$$\sigma_{ij}(\boldsymbol{\xi}) = \int_\Gamma S_{ijk}(\boldsymbol{\xi}, \boldsymbol{x}) \Delta u_k(\boldsymbol{x}) dS(\boldsymbol{x})$$

<u>Numerical approximation</u>

Divide crack Γ into N line segments of length $S_J = 2a_J$ and write

$$u_i(\boldsymbol{\xi}) = \sum_{J=1}^{N} \int_{S_J} T_{ij}(\boldsymbol{\xi}, \boldsymbol{x}) \Delta u_j(\boldsymbol{x}) dS(\boldsymbol{x})$$

$$\sigma_{ij}(\boldsymbol{\xi}) = \sum_{J=1}^{N} \int_{S_J} S_{ijk}(\boldsymbol{\xi}, \boldsymbol{x}) \Delta u_k(\boldsymbol{x}) dS(\boldsymbol{x})$$

These equations can be used to develop a "direct" version of the displacement discontinuity method. (The kernel S_{ijk} is hypersingular.)

COLLEGE OF Science & Engineering — UNIVERSITY OF MINNESOTA Driven to Discover

Comparison with influence function approach

A simple demonstration problem: Compute u_x at point (ξ_x, ξ_y) due to a <u>known</u> displacement discontinuity $\Delta u_x(x)$, $\Delta u_y(x)$ over a single element $-a \le x \le a$, $y = 0$.

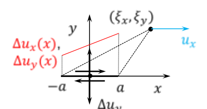

<u>Influence function approach</u>. Integrate concentrated displacement discontinuity Δu_x, Δu_y over element to specify Ψ and Φ; differentiate to compute u_x at point (ξ_x, ξ_y).

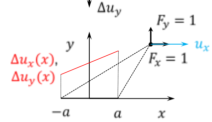

<u>"Direct" approach</u>. Apply unit concentrated load $F_x = 1$, $F_y = 1$ at point (ξ_x, ξ_y), integrate effects of load, multiplied by $\Delta u_x(x)$ and $\Delta u_y(x)$, over element to compute u_x at point (ξ_x, ξ_y).

(Note: In practice $\Delta u_y(x)$, $\Delta u_y(x)$ are defined at collocation points.)

COLLEGE OF Science & Engineering — UNIVERSITY OF MINNESOTA Driven to Discover

Consider effects from the element $-a \le x \le a$, $y = 0$

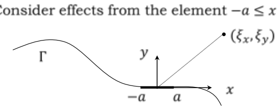

$$u_i(\xi_x, \xi_y) = \int_{-a}^{a} T_{ij}(x - \xi_x, y - \xi_y) \Delta u_j(x) dx$$

where, for example,

$$T_{xx}(x - \xi_x, y - \xi_y) = (1 - 2\nu)\frac{\partial g}{\partial y} - (x - \xi_x)\frac{\partial^2 g}{\partial x \partial y}$$

with $\quad g(x - \xi_x, y - \xi_y) = -\dfrac{1}{4\pi(1-\nu)} ln\sqrt{(x - \xi_x)^2 + (y - \xi_y)^2}$

Easy to show that

$$(x - \xi_x)\frac{\partial^2 g}{\partial x \partial y} = -\frac{\partial g}{\partial y} - (y - \xi_y)\frac{\partial^2 g}{\partial y^2}$$

COLLEGE OF Science & Engineering — UNIVERSITY OF MINNESOTA Driven to Discover

Expression for $u_x(\xi_x, \xi_y)$:

$$T_{xx} = 2(1-\nu)\frac{\partial g}{\partial y} + (y - \xi_y)\frac{\partial^2 g}{\partial y^2}$$

$$T_{xy} = -(1-2\nu)\frac{\partial g}{\partial x} - (y - \xi_y)\frac{\partial^2 g}{\partial x \partial y}$$

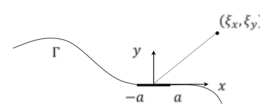

$$u_x(\xi_x, \xi_y) = \int_{-a}^{a} \Delta u_x(x)\left\{2(1-\nu)\frac{\partial g(x - \xi_x, y - \xi_y)}{\partial y} + (y - \xi_y)\frac{\partial^2 g(x - \xi_x, y - \xi_y)}{\partial y^2}\right\}dx$$

$$+ \int_{-a}^{a} \Delta u_y(x)\left\{-(1-2\nu)\frac{\partial g(x - \xi_x, y - \xi_y)}{\partial x} - (y - \xi_y)\frac{\partial^2 g(x - \xi_x, y - \xi_y)}{\partial x \partial y}\right\}dx$$

Set $\dfrac{\partial}{\partial x} = -\dfrac{\partial}{\xi_x}$; $\dfrac{\partial}{\partial y} = -\dfrac{\partial}{\xi_y}$ $\quad$ Then let $y = 0$; $x = x'$

COLLEGE OF Science & Engineering — UNIVERSITY OF MINNESOTA Driven to Discover

$$u_x(\xi_x,\xi_y) = \int_{-a}^{a} \Delta u_x(x')\left\{-2(1-\nu)\frac{\partial g(x'-\xi_x,\xi_y)}{\partial \xi_y} - \xi_y \frac{\partial^2 g(x'-\xi_x,\xi_y)}{\partial {\xi_y}^2}\right\}dx'$$

$$+ \int_{-a}^{a}\Delta u_y(x')\left\{(1-2\nu)\frac{\partial g(x'-\xi_x,\xi_y)}{\partial\xi_x} + \xi_y\frac{\partial^2 g(x'-\xi_x,\xi_y)}{\partial\xi_x\partial\xi_y}\right\}dx'$$

Papkovitch-Neuber approach (with $x = \xi_x, y = \xi_y$) gives the <u>same</u> result.

$$u_x(x,y) = \int_{-a}^{a} \Delta u_x(x')\left\{-2(1-\nu)\frac{\partial g(x-x',y)}{\partial y} - y\frac{\partial^2 g(x-x',y)}{\partial y^2}\right\}dx'$$

$$+ \int_{-a}^{a}\Delta u_y(x')\left\{(1-2\nu)\frac{\partial g(x-x',y)}{\partial x} + y\frac{\partial^2 g(x-x',y)}{\partial x\partial y}\right\}dx'$$

Galerkin formulation

An averaging process that allows the system of equations to be written in terms of the displacement discontinuities at the element endpoints (i.e. the nodes), thereby avoiding internal collocation.

A simple illustration: How does Galerkin compare with collocation?

- N equal length elements along a straight line ($N+1$ nodes)
- Displacement discontinuity Δu_y on element J varies linearly between nodes $j-1$ and j; $(\Delta u_y)_{j-1}$ and $(\Delta u_y)_j$ are the nodal point values.

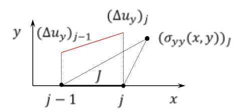

- Stress at (x,y) due to element J is $(\sigma_{yy}(x,y))_J$

By superposition, the stress at point (x,y) due to the contributions of all N elements is

$$\sigma_{yy}(x,y) = \sum_{J=1}^{N}(\sigma_{yy}(x,y))_J$$

Can also sum over $N+1$ nodal points: $\sigma_{yy}(x,y) = \sum_{j=0}^{N}(\sigma_{yy}(x,y))_j$

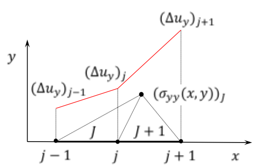

Galerkin:

Formation of i-th equation in system:

$$\int_{x_{i-1}}^{x_{i+1}} \psi(x)\,\sigma_{yy}(x,0)dx = \sum_{j=0}^{N+1}\lim_{\varepsilon\to 0}\int_{x_{i-1}}^{x_{i+1}}\psi(x)\,(\sigma_{yy}(x,\varepsilon))_j \mathrm{d}x$$

where $\psi(x)$ is a weight function

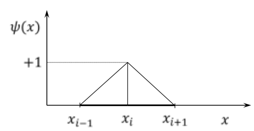

$$\psi(x) = 1 + \frac{1}{2a}(x-x_i);\ \ x_{i-1} \le x \le x_i$$

$$\psi(x) = 1 - \frac{1}{2a}(x-x_i);\ \ x_i \le x \le x_{i+1}$$

$$\psi(x) = 0;\ \ x \le x_{i-1} \text{ and } x \ge x_{i+1}$$

- Compare with collocation approach for simple crack problem
- All integrations can be done analytically (no special crack tip logic used for this simple example!)
- $\sigma_{yy} = (\sigma_{yy})_0$ for all N elements; get system of equations:

$$\sum_{j=0}^{N-1} A^{ij}_{yy}\Delta u^{j}_{y} = (\sigma_{yy})^{i}_0;\ \ i = 0 \text{ to } N-1$$

Two co-planar cracks

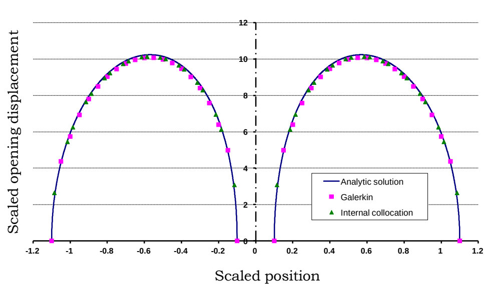

Conclusions

1. The influence function formulation of the displacement discontinuity method gives the same results as the direct boundary integral approach using Volterra's formula.
2. For the simple 2D crack problem considered in this presentation, the Galerkin formulation of the method is no more accurate than the internal element collocation formulation for equivalent numbers of degrees of freedom.
3. The displacement discontinuity method can be used to model crack growth (and crack interactions) in complex fracture networks. Many questions about the physics of crack growth remain to be answered, however, especially for 3D problems.

"Computational Modeling of Composite and Functionally Graded Materials"

Steven L. Crouch
Department of Civil Engineering
College of Science and Engineering
University of Minnesota

Abstract

A numerical method is described for solving two- and three-dimensional elasticity problems for materials with multiple circular and spherical voids and inclusions. The method uses series expansions of orthogonal functions (Fourier series in two dimensions; spherical harmonics in three dimensions) to represent the displacements and tractions on all the circular or spherical boundaries. The solutions are expressed in terms of truncated infinite series and are semi-analytical in the sense that the numerical errors can be made arbitrarily small by increasing the number of terms in the series. The coefficients in the series can be determined by using a boundary integral approach (i.e. Somigliana's formula) or by superposition of the general solution for arbitrary loading of a single circular or spherical void, together with addition formulas that re-expand the solution for one void in terms of the coordinates for another. In either case, a system of linear algebraic equations can be formed to find the unknown coefficients, and these equations can be conveniently solved by iteration.

The numerical method is well-suited to modeling elastic materials involving numerous voids or inclusions, and these features can be arbitrarily close together, provided they do not actually touch. Different types of interface conditions can easily be adopted, including spring-type interfaces, explicit "interphases," partial de-bonding, and a "membrane –type" interface known as the Gurtin-Murdoch model, which includes a surface tension term and can account for size effects in nano-composites.

An important application of the numerical method is the computation of effective material properties for materials with numerous voids and inclusions. The ability to include the interaction effects of all the voids and inclusions allows one to accurately determine these properties for any arrangement of these features.

Computational Modeling of Composite and Functionally Graded Materials

by

Steven L. Crouch

(with major input from Sonia Mogilevskaya, Department of Civil Engineering, University of Minnesota)

Department of Civil Engineering
University of Minnesota

Composite Materials

Polymer matrix, rubber particles (after Sjögren & Berglund, 1999)

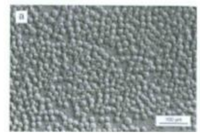

Functionally graded material

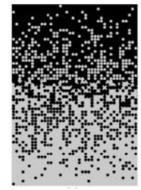

Fiber-reinforced ceramic material

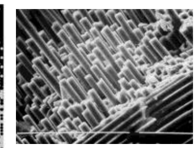

Applications: Aerospace, electronics, marine, construction, etc.

COLLEGE OF Science & Engineering UNIVERSITY OF MINNESOTA Driven to Discover

Interphases

Micrographs (Crasto et al.,1988)

Perfect bond

Uniform interphase layer

Micrograph (Mascia et al., 1993)

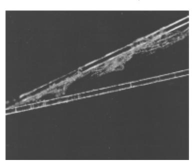

Coated fibers

COLLEGE OF Science & Engineering UNIVERSITY OF MINNESOTA Driven to Discover

Nano Materials

Nanochannel-array Materials

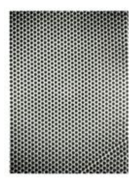

Filters for particle sizing, unidirectional conductors, etc.

Quantum Dots

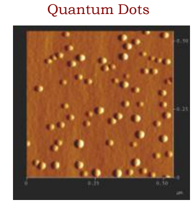

Particles made of semiconductor or metallic material capable of confining electrons and/or holes in three dimensions.

COLLEGE OF Science & Engineering UNIVERSITY OF MINNESOTA Driven to Discover

Conventional Numerical Methods

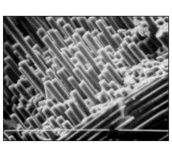

2D model

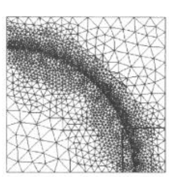

3D model

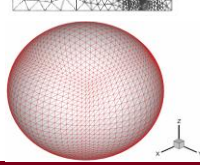

Large numbers of degrees of freedom

COLLEGE OF Science & Engineering UNIVERSITY OF MINNESOTA Driven to Discover

Our Approach

William Thomson (Lord Kelvin)

1824–1907

Peter Guthrie Tait

1831–1901

- Direct boundary integral method or superposition of the solutions for each single feature
- Approximation of the unknowns by Fourier Series or series of scalar or vector spherical harmonics
- Complex (2D problems) or real variables (3D problems)

Jean Baptiste Joseph Fourier

1768–1830

COLLEGE OF Science & Engineering UNIVERSITY OF MINNESOTA Driven to Discover

Series of Orthogonal Functions

Fourier series (2D)

$$f(\varphi)=\sum_{m=-N}^{N} e^{im\varphi} C_m$$

$$e^{im\varphi}=\cos(m\varphi)+i\sin(m\varphi)$$

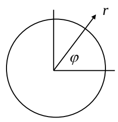

Series of surface spherical harmonics (3D)

$$f(\theta,\varphi)=\sum_{n=0}^{N}\sum_{m=-n}^{n} Y_n^m(\theta,\varphi)C_{nm}$$

$$Y_n^m(\theta,\varphi)=\sqrt{\frac{(2n+1)(n-m)!}{4\pi(n+m)!}}\,e^{im\varphi}\underbrace{P_n^m(\cos\theta)}_{\text{Associated Legendre polynomial}}$$

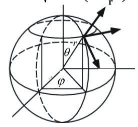

- Complete orthogonal system on the surface of a circle/sphere
- Any smooth function can be represented by a truncated series of these functions with any desired accuracy

Semi-analytical Solution of the Problem of N Particles (Fibers); Elastostatics

Series of surface spherical harmonics (3D)

Decompose unknowns into a series of spherical harmonics
↓
Use addition theorems
↓
Set up system of algebraic equations using orthogonal properties of spherical harmonics
↓
Solve the system to find coefficients
↓
Evaluate fields

Fourier series (2D)

Decompose unknowns into complex Fourier series
↓
Use addition theorems
↓
Set up system of algebraic equations using orthogonal properties of Fourier series
↓
Solve the system to find coefficients
↓
Evaluate fields

College of Science & Engineering
University of Minnesota
Driven to Discover

Solutions of Transient Problems (Example: Heat Conduction)

$$\nabla^2 T=\frac{\partial T}{\partial t}$$

⇩ Laplace transform

- Modified Helmholtz equation
- Analytical solution for a single cavity
- Superposition for multiple cavities

} Laplace domain

⇩ Inverse Laplace transform

$$T(x,t)$$

College of Science & Engineering
University of Minnesota
Driven to Discover

Addition Theorems

Re-expansion formulae (2D example): express Fourier series for j-th circle in terms of quantities for k-th circle

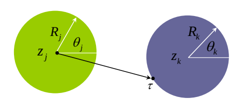

$$g_j^m(\tau)=R_j^m/(\tau-z_j)^m=R_j^m(\tau-z_k+z_k-z_j)^{-m}$$

$$=\frac{R_j^m}{(z_k-z_j)^m}\left(1+\frac{\tau-z_k}{z_k-z_j}\right)^{-m}=g_j^m(z_k)\sum_{\ell=0}^{\infty}\binom{m+\ell-1}{\ell}\left(\frac{\tau-z_k}{z_k-z_j}\right)^{\ell}$$

$$=g_j^m(z_k)\sum_{\ell=0}^{\infty}\binom{m+\ell-1}{\ell}g_k^{\ell}(z_j)g_k^{-\ell}(\tau)$$

College of Science & Engineering
University of Minnesota
Driven to Discover

Fast Solvers

Rokhlin 1985, Greengard and Rokhlin 1987

V.Rokhlin

L. Greengard

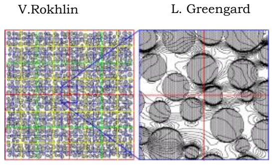

College of Science & Engineering
University of Minnesota
Driven to Discover

Comparison of the Algorithm Efficiency

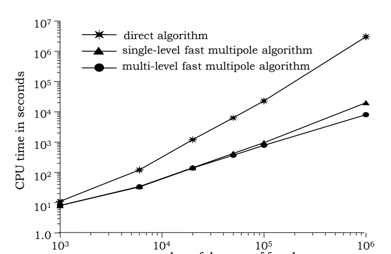

College of Science & Engineering
University of Minnesota
Driven to Discover

Applications

- Elastic Composites (perfect bonding, imperfect interfaces, interface layers, graded interfaces, material surfaces, debonding)
- Boundary Effects (free boundaries, dissimilar materials)
- Elastic-Viscoelastic Composites
- Transient Heat Conduction
- Chemistry (diffusive reactions)

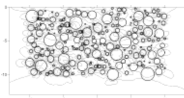

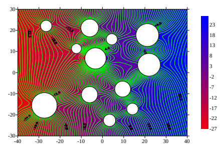

Contour of u_x at t = 10 sec

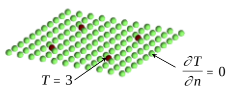

Interface Models

- Spring-type interface

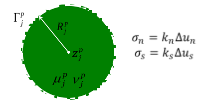

- Partial de-bonding

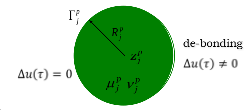

- Explicit presence of interphase layers

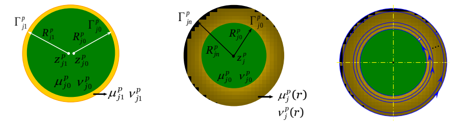

Example — Two Inclusions with Interphase Layers

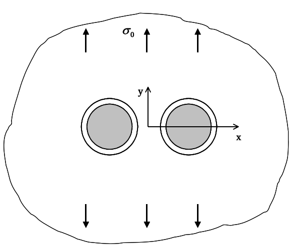

material	n	E/E_{matrix}
inhomog	0.2537	38.9
matrix	0.2647	1.0
soft coating	0.2647	0.067
stiff coating	0.2647	20.0

$\delta_1 = 10^{-6}$; $\delta_2 = 10^{-3}$

6 – 9 terms in Fourier series

Results

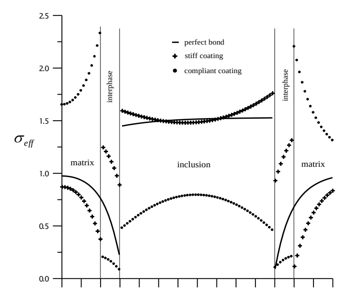

Example — Inclusion with Interface Crack (Toya, 1974)

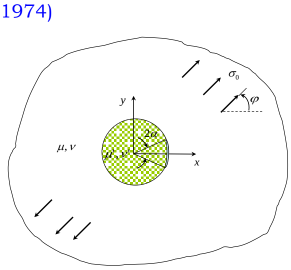

Radial and Shear Sresses; Open Circles — computed (N=180); Solid Lines — analytical solution

$\mu' = 44.2 GN/m^2, \nu' = 0.22, \mu = 2.39 GN/m^2, \nu' = 0.35$

$\alpha = \varphi = 30^\circ$

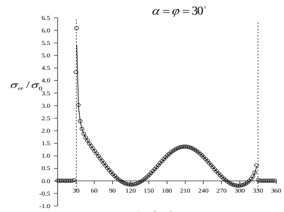

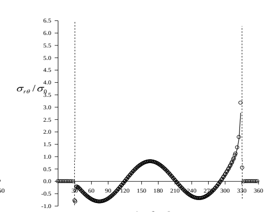

(a) (b)

Radial and Shear Displacement Discontinuities; Open Circles — computed (N=180); Solid Lines — analytical solution

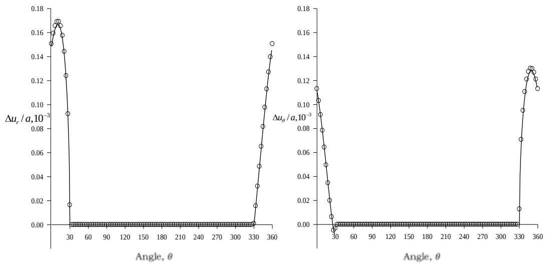

Size-dependent Mechanics of Materials

Experimental results and direct atomistic simulations of nano-materials indicate that:

- Mechanical behavior is inherently size dependent
- Traditional analysis is not able to account for size effects
- Size dependence is due to surface effects

COLLEGE OF Science & Engineering
UNIVERSITY OF MINNESOTA Driven to Discover

Gurtin & Murdoch's (1975) Model for a Material Surface

The interface Σ between the inhomogeneity and the matrix is modeled as a material surface of vanishing thickness that is characterized by elastic constants (Lamé parameters) μ_0, λ_0 and surface tension σ_0.

Surface constitutive equations

Surface stress tensor

$$\mathbf{S} = \sigma_0 \mathbf{I}_\ell + (\lambda_0 + \sigma_0)(tr\,\boldsymbol{\varepsilon}^{sur})\mathbf{I}_\ell + 2(\mu_0 - \sigma_0)\boldsymbol{\varepsilon}^{sur} + \sigma_0 \nabla_\Sigma \mathbf{u}$$

Continuity of displacements

$$\mathbf{u}^{inh} = \mathbf{u}^{matrix}$$

Surface equilibrium conditions

$$\Delta\boldsymbol{\sigma}\mathbf{n} = div_\Sigma \mathbf{S},\ \Delta\boldsymbol{\sigma} = \boldsymbol{\sigma}^{inh} - \boldsymbol{\sigma}^{matrix}$$

COLLEGE OF Science & Engineering
UNIVERSITY OF MINNESOTA Driven to Discover

Mechanical Properties of the Material Surface

Elastic properties

Fleshly cleaved iron (Gurtin & Murdoch, 1978)

$\mu_0 = 2.5\ N/m,\ \lambda_0 = -8\ N/m$

Anodic alumina (Miller & Shenoy, 2000)

a) $\mu_0 = -6.2178\ N/m,\ \lambda_0 = 3.48912\ N/m$ [100]

b) $\mu_0 = -0.3755\ N/m,\ \lambda_0 = 6.842\ N/m$ [111]

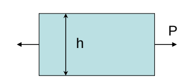

$P = E^b h\varepsilon$

Surface tension

$0.7\ N/m \le \sigma_0 \le 2\ N/m$ (Sharma & Ganti, 2004)

$P \ne E^b h\varepsilon$

$P = (E^b h + 2E^s)\,\varepsilon$

COLLEGE OF Science & Engineering
UNIVERSITY OF MINNESOTA Driven to Discover

2D Example

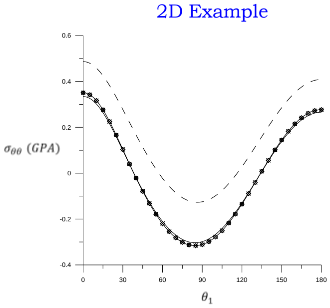

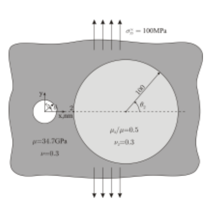

$\mu_{10} = -6.2178\ N/m,\ \lambda_{10} = 3.48912\ N/m$

$\sigma_{10} = 0.72\ N/m$

× (i) $\mu_{20} = \lambda_{20} = \sigma_{20} = 0$

◇ (ii) $\mu_{20} = \mu_{10},\ \lambda_{20} = \lambda_{10},\ \sigma_{20} = 0$

— (iii) $\mu_{20} = \mu_{10},\ \lambda_{20} = \lambda_{10},\ \sigma_{20} = \sigma_{10}$

--- Classical solution

COLLEGE OF Science & Engineering
UNIVERSITY OF MINNESOTA Driven to Discover

Modeling of Graded Composite Materials

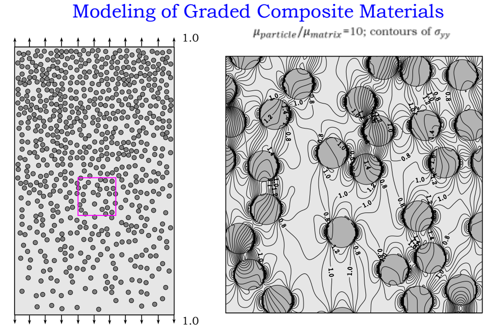

COLLEGE OF Science & Engineering
UNIVERSITY OF MINNESOTA Driven to Discover

Modeling of Graded Composite Materials (Cont'd)

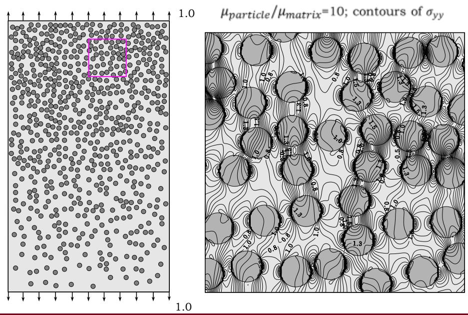

Homogenization; Computation of Effective Material Properties

Homogenization: RVE

Three length scales

$$\ell_1 \le \ell_2 \le \ell_3$$

Microscale (greater than the size of the inhomogeneities)

Mesoscale (statistically homogeneous)

Macroscale (less than the size of the composite body)

Volumetric averaging, elasticity

$$\langle \sigma_{kj} \rangle = \frac{1}{V}\left[\int_{V_m} \sigma_{kj}\,dv + \sum_{n=1}^{N}\int_{V_n} \sigma_{kj}\,dv\right]$$

$$\langle \varepsilon_{kj} \rangle = \frac{1}{V}\left[\int_{V_m} \varepsilon_{kj}\,dv + \sum_{n=1}^{N}\int_{V_n} \varepsilon_{kj}\,dv\right]$$

$$V_m = V - \sum_{n=1}^{N} V_n$$

Effective properties

$$\langle \sigma_{ij} \rangle = C_{ijk\ell} \langle \varepsilon_{k\ell} \rangle$$

Stresses

Strains

Effective elastic properties tensor

Homogenization

Embedding Method

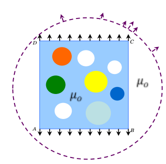

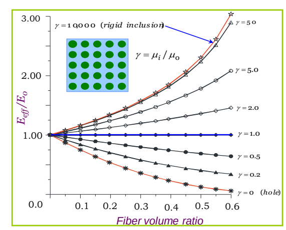

- Embed a domain of interest in a fictitious circular domain
- Apply load at boundary of circle to satisfy (in a least squares sense) boundary conditions on the (rectangular) physical domain

Maxwell's Approach

Maxwell JC, Treatise on electricity and magnetism, vol.1, 3rd edition, Oxford, UK, Clarendon Press, 1892 (1st edition 1873)

- A cluster of spherical particles enclosed by a sphere of matrix material is immersed in the matrix
- At large distances all the particles are considered to be located at the same point (at the center of the sphere)
- At large distances the cluster gives the same contribution to the field as the sphere with the effective conductivity

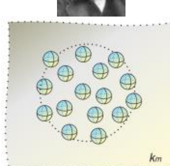

Maxwell's definition of the effective conductivity:

$$k_{eff} = k_m \frac{k_p(1+2c)+2k_m(1-c)}{k_p(1-c)+k_m(2+c)}$$ — the solution is of order c,

where $c = Na_p^3 / a_{sph}^3$ is the volume fraction

Extension of Maxwell's Approach

- Interactions among the inhomogeneities (reinforcements) are accounted for.
- The effect on the fields due to the cluster are accounted for via the asymptotic behavior at infinity.
- The original geometrical distribution of the inhomogeneities (reinforcements) is preserved.

How It Works

A cluster of isotropic inhomogeneities
in an isotropic matrix.

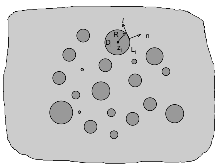

An equivalent inhomogeneity
in an isotropic matrix

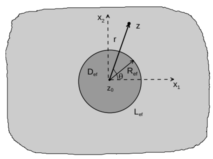

- Solve the problem for the cluster; determine R_{ef}, μ_{ef}, ν_{ef}
- Solve the problem for the equivalent inhomogeneity
- Compare the far-field solutions for the fields (e.g.) displacements

Are the Fields Really the Same?

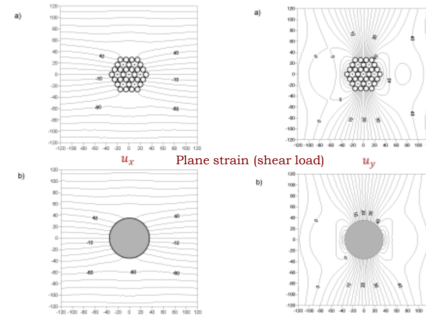

Example: Square Symmetry

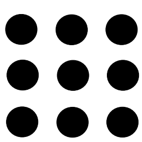

$$\begin{bmatrix}\sigma_{11}\\ \sigma_{22}\\ \sigma_{33}\\ \sigma_{12}\\ \sigma_{13}\\ \sigma_{23}\end{bmatrix}=\begin{bmatrix}c_{11}^{ef} & c_{12}^{ef} & c_{13}^{ef} & 0 & 0 & 0\\ c_{12}^{ef} & c_{11}^{ef} & c_{13}^{ef} & 0 & 0 & 0\\ c_{13}^{ef} & c_{13}^{ef} & c_{33}^{ef} & 0 & 0 & 0\\ 0 & 0 & 0 & c_{44}^{ef} & 0 & 0\\ 0 & 0 & 0 & 0 & c_{66}^{ef} & 0\\ 0 & 0 & 0 & 0 & 0 & c_{66}^{ef}\end{bmatrix}\begin{bmatrix}\varepsilon_{11}\\ \varepsilon_{22}\\ \varepsilon_{33}\\ 2\varepsilon_{12}\\ 2\varepsilon_{13}\\ 2\varepsilon_{23}\end{bmatrix}$$

6 material constants

Results

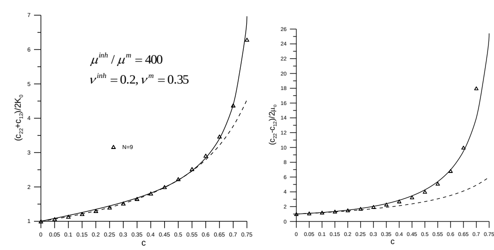

— Periodic solution (V. I. Kushch)

- - - Non-interacting

Results

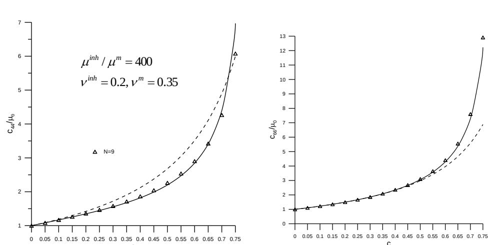

— Periodic solution (V. I. Kushch)

- - - Non-interacting

Experiment and Results

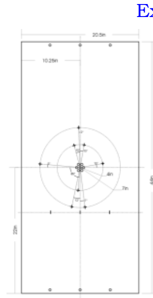

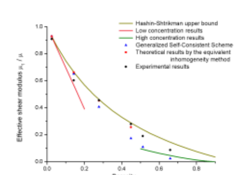

Shear modulus is determined through uniaxial tension test!

"In theory, there is no difference between theory and practice. But, in practice, there is." (Jan L. A. van de Snepscheut)

Conclusions

- A powerful method for simulation of the fields (including transient fields) in elastic, viscoelastic composite, and porous materials has been created.
- The method accurately takes into account interactions between reinforcements (particles, pores, fibers) in the material.
- Various effects at the fiber/matrix interfaces (e.g. perfect bond, homogeneously imperfect interfaces, uniform interphase layers, Gurtin and Murdoch model) can be included.
- The method is efficient, fast, and provides accurate results.
- A variety of mechanical (e.g. viscoelastic) models can be incorporated.

Conclusions (cont'd)

- Maxwell's concept can be generalized to allow for accurate estimates of the effective properties of composite materials.
- The concept is attractive: No need for averaging the fields - the method automatically provides the relationships between the average values of fields.
- The problems of the clusters in infinite domains permit accurate solutions that precisely account for interactions.
- The method provides reasonably accurate results in the wide range of volume fractions and/or porosities.
- The method could be useful for estimation of the overall properties of a material based on the small samples (scanning electron micrograph, X-ray, etc.).

Collaborators

Sonia Mogilevskaya

Henryk Stolarski

Volodymyr Kushch (in chair); with Andrew Drescher

Joe Labuz

Students

Jianlin Wang (2D elasticity, fast solutions, embedding method)

Andrey Pyatigorets (2D viscoelastic composites, experiment)

Yun Huang (2D viscoelastic porous media)

Lisa Gordeliy (3D trasient heat conduction, 2D thermoelasticity, surface effects)

Olesya Koroteeva (3D effective thermal properties)

Hamid Sadraie (3D elasticity)

Interns

Benoit Legros (boundary effects)

Alexandre Dejoie (boundary effects)

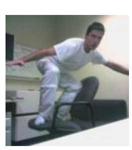

Nicolas Brusselaars (dissimilar materials)

Matthieu Jammes (surface effects)

Alessandro La Grotta (surface effects)

Adrien Benusiglio (equivalent inhomogeneity)

Thank you for your attention.

Questions?

Review of the dual BEM and recent development of null-field integral equation approach by ntou/msv

對偶邊界元素法回顧及其近期發展

陳正宗

國立台灣海洋大學河海工程系終身特聘教授

Review of the Dual BEM and Recent Development of Null-Field Integral Equation Approach by NTOU/MSV

Jeng-Tzong Chen

jtchen@mail.ntou.edu.tw, Department of Harbor and River Engineering & Department of Mechanical and Mechatronic Engineering, National Taiwan Ocean University, Keelung, 202-24, Taiwan

Key words: *Dual BEM/BIEM, Rank deficiency, Null-field BIEM, Degenerate boundary, Harbor resonance, SH wave, Focusing*

Abstract

In this lecture, the development of dual BEM is reviewed since its appearance in 1986 by Hong and Chen. The academic activity of BEM community in Taiwan is also reported. Methods to deal with hypersigularity are also examined. A novel method using the singular value decomposition (SVD) for problems with degenerate boundaries is proposed to distinguish the rank deficiency due to the rigid body mode and the degenerate boundary. Applications of the dual BEM to civil engineering and military problems are reviewed. To avoid singularities, a null-field integral equation approach in companion with an addition theorem (or so called degenerate kernel or separable kernel) is proposed. Several gains, exponential convergence, free of singularity and boundary layer effect, are achieved. Applications to circular, elliptical (2D), spherical and spheriroidal boundaries (3D) with emphasis on harbor resonance and SH wave scattering of hill and canyon are done. Focusing effect in harbor engineering and earthquake engineering are addressed.

References

[1] H.-K. Hong, J.T. Chen: Derivations of integral equations of elasticity, ASCE, J. Eng. Mech., 114(6), pp.1028-1044, 1988.

[2] J.T. Chen: Recent development of dual BEM in acoustic problems, In Fourth World Congress on Computational Mechanics, Keynote lecture, BuenosAires, Argentina, 1998.

[3] J.T. Chen, H.-K. Hong: Review of dual boundary element methods with emphasis on hypersingular integrals and divergent series, ASME, Appl. Mech. Rev., 52(1), pp.17-33, 1999.

[4] J.T. Chen: On the rank-deficiency problems in boundary integral formulation using the Fredholm alternative theorem and singular value decomposition technique, In Fifth World Congress on Computational Mechanics. Keynote lecture, Vienna, Austria, 2002.

[5] J.T. Chen: Dual BEM since 1986, In APCOM’07 & EPMESC XI, Keynote lecture, Kyoto, Japan, 2007.

[6] J.T. Chen: Development of dual BEM in Taiwan, In The 3rd Asia-Pacific Int. Conf. on Comp. Meth. in Engrg (ICOME 2009), Plenary lecture, Nanjing, China, 2009.

[7] J.T. Chen: Review of BEM development in Taiwan and recent advances by NTOU/MSV group, In GCWCOME2012, Plenary lecture, Changsha, China, 2012.

[8] J.T. Chen, I.L. Chen, K.H. Chen: Treatment of rank-deficiency in acoustics using SVD, J. Comput. Acoust., 14 (2), pp.157-183, 2006.

[9] J.T. Chen, S.R. Lin, K.H. Chen, Degenerate scale problem when solving Laplace equation by BEM and its treatment, Int. J. Numer. Meth. Eng., 62(2), pp.233-261, 2005.

[10] I.L. Chen, J.T. Chen, M.T. Liang: Analytical study and numerical experiments for radiation and scattering problems using the CHIEF method, J. Sound Vib., 248(5), pp.809-828, 2001.

[11] I.L. Chen, J.T. Chen, S.R. Kuo, M.T. Liang: A new method for true and spurious eigensolutions of arbitrary cavities using the CHEEF method, J. Acoust. Soc. Am., 109(3), pp.982-999, 2001.

[12] J.T. Chen, Y.J. Lin, Y.T. Lee, C.F. Wu: Water wave interaction with surface-piercing porous cylinders using null-field integral equations, Ocean Eng., 38, pp.409-418, 2011.

[13] J.T. Chen, J.W. Lee, W.S. Shyu: SH wave scattering by a semi-elliptical hill using null-field integral equation method and a hybrid method, Geophys. J. Int., 188, pp.177-194, 2012.

[14] J.T. Chen, J.W. Lee, C.F. Wu, I.L. Chen: SH-wave diffraction by a semi-circular hill revisited: a null-field boundary integral equation method using degenerate kernels. Soil Dyn. Earthqu. Eng., 31, pp.729-736, 2011.

[15] J.T. Chen, P.Y. Chen, C.T. Chen: Surface motion of multiple alluvial valleys for incident plane SH-waves by using a semi-analytical approach, Soil Dyn. Earthqu. Eng., 28, pp.58-72, 2008.

Review of the dual BEM and recent development of the null-field BIEM by NTOU/MSV

Jeng-Tzong Chen (海大河工 陳正宗)
Life-time Distinguished Professor
Dept. Harbor and River Engineering
Dept. Mechanical and Mechatronic Engineering
Taiwan Ocean University

10:50-11:50, March 20 (Wed.), 2013

BEM4-Taiwan2013.ppt

NEWS 2013

- Two BEM people win the academician of NAE

Crouch
Elasticity
fracture

For contributions to simulation methodology for the behavior of fractured rock masses.

Chew
Electro
magnetics

For contributions to large-scale computational electromagnetics of complex structur

---

EABE Editors

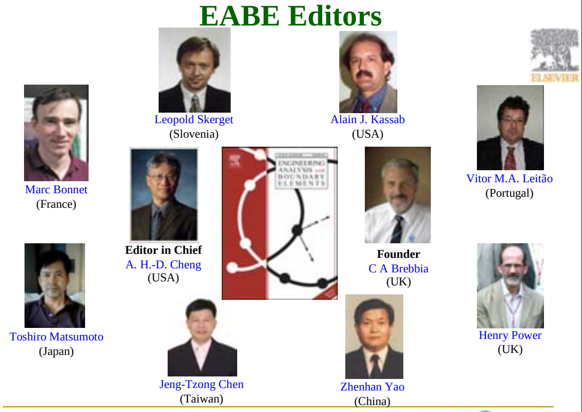

BEM History in Taiwan

BEM Workshop in Taiwan

- **1986** NTU IAM Rizzo, Shippy & Mukherjee
  12↓ (Civil Engineering and Applied Mech.)
- **1998** NSC Alex Cheng and Taiwan Professors
  12↓ (College of Engineering)
- **2010** NTOU-HRE-MSV First Taiwan BEM meeting
  1↓ (Mathematics and Engineering)
- **2011** NCTS(South) Second Taiwan BEM meeting
  1↓ (Mathematics and Engineering)
- **2012** Feng Chia University Third Taiwan BEM meeting
  (Mathematics and Engineering) Taiwan SIAM 2012

History (Workshop in 1986)

I was a TA at that time.

F. J. Rizzo

D. J. Shippy

S. Mukherjee
Winner of Rizzo Award 2013

History (Workshop in 1998) - I
(Five generations together)


C. S. Yeh, NTU
土木國家講座


C. H. Chen, NTU
電機國家講座


D. L. Young, NTU
教育部學術獎


C. R. Chou, NTOU


H.-K. Hong, NTU
國科會三傑出


C. Lai, NTU

台灣 台南 成功大學

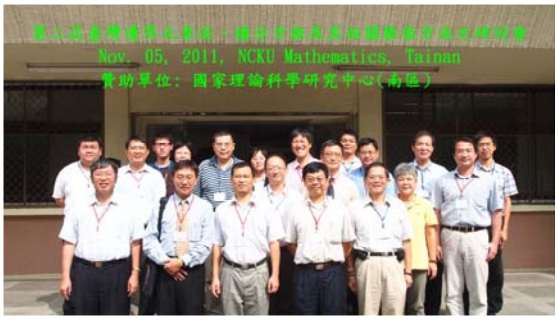

成功大學八十週年慶

History (Workshop in 1998) - II
(Five generations together)


A. H.-D. Cheng, Mississippi Univ.


C. C. Ma, NTU
國科會三傑出


國研院副院長
K. C. Wu, NTU
國科會三傑出


J. T. Chen, NTOU
教育部學術獎


S. S. Hsiao, NTOU


I. L. Chen, NKMU

BEM III-Taiwan, Oct.06, 2012

NTOU, Keelung, Taiwan

ICOME 2012, Kyoto, Japan Dec.12-14, 2012
(Hosted by 西村直志教授 Prof. Nishimura)

18 Taiwan team

BEM in Taiwan

2013 BEM Workshop in Taiwan

- Host 中興土木 相見歡 Keynote speaker

壽克堅 主任

Host

1983(English)
1988 (Russian)
1990 (reprinted)

Dean S L Crouch
Academician, NAE

臺灣數學與工程互動表

- Taiwan SIAM 扮演的角色
  - 建立數學與工程的連接橋樑
  - Mathematics與Engineering並重

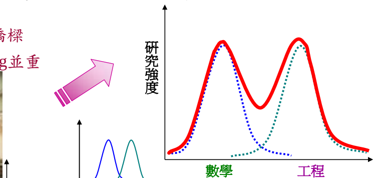

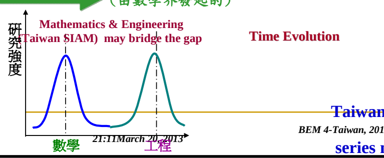

Taiwan BEM series meeting (由工程界發起的)

BEM in Taiwan

2014 BEM Workshop in Taiwan

- Host 中山應數 呂宗澤 西子灣等著您

Overview of numerical methods

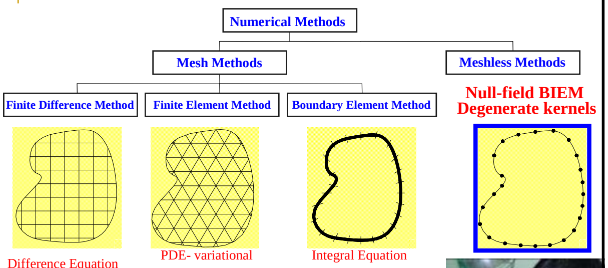

開刀  把脈  針灸 

數學 工程

大會共同主席:楊德良呂宗澤 陳正宗

Joint International Workshop on Trefftz Method VI and Method of Fundamental Solutions II
March 15-18, 2011, Kaohsiung, Taiwan

Alternatives to solve crack problems

Multi-domain BEM by Liggett (before 1984)
Special Green's function
Dislocation model
DDM by Crouch
Dual BEM (single-domain BEM since 1986)

Liggett book (1983)

- The singularities that occur when the base point and field point coincide are not integrable ???

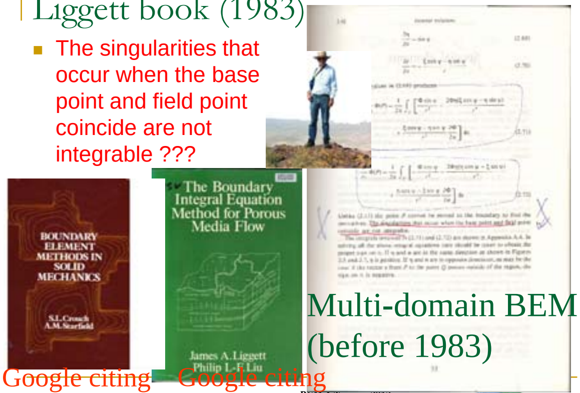

Multi-domain BEM (before 1983)

Google citing 963 Google citing 359

Citing records (updated Feb, 2013)

Rizzo, 1967 QAM

Hong and Chen, 1988 ASCE-EM

Chen and Hong, 1999 ASME, AMR

Crouch, 1976 IJNME

Portela and Aliabadi 1992, IJNME

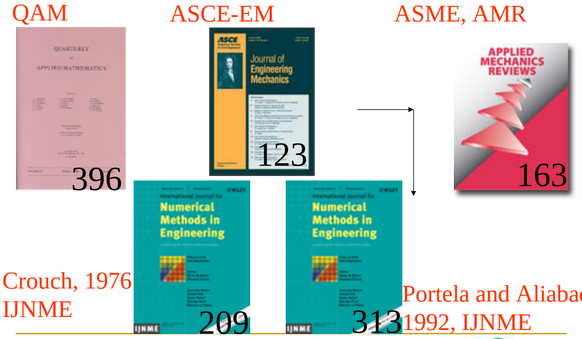

二00九年余德浩教授得獎有感

台灣海洋大學 陳正宗

Natural BEM

Hypersingular BIEM

Dual BEM

兩岸三地志一方
余然自得邊界元
祝家學說超奇異
陳功在臺尋對偶

BEM highly-cited papers

(Feb. 25, 2013)

Time	Author	Journal	Cited No.	Method
1967	Rizzo	QAM	396	BEM
1976	Crouch	IJNME	209	DDM
1988	Hong & Chen	ASCE-EM	123	Dual BEM
1992	Portela & Aliabadi	IJNME	313	Dual BEM
1997	Mukherjee couple	IJNME	181	BNM
1999	Chen & Hong	ASME-AMR	163	Dual BEM

Dual Integral Equations by Hong and Chen(1984-1986)

Singular integral equation → **Hypersingular integral equation**

Cauchy principal value → **Hadamard principal value**

(Mangler principal value)

Boundary element method → **Dual boundary element method**

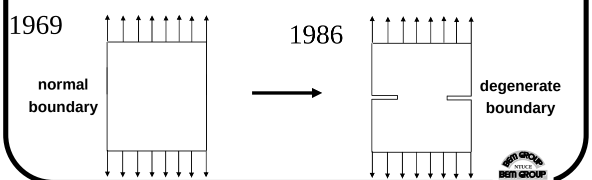

Degenerate boundary

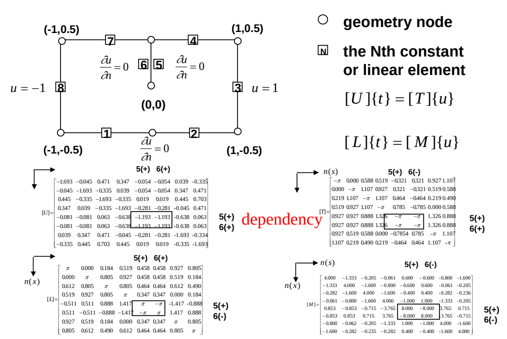

Nonuniqueness

Dual BEM, DDM and Dislocation theory

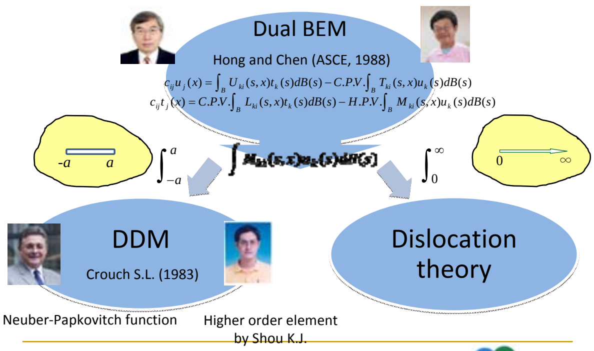

Successful experiences in Taiwan since 1986 (degenerate boundary)

crack (fracture)
incomplete partition (acoustics)
sheet pile (seepage)
breakwater (ocean engineering)
thin airfoil (aerodynamics)
comb drive (electromagnetics, MEMS)

Solid rocket motor (Army工蜂火箭)

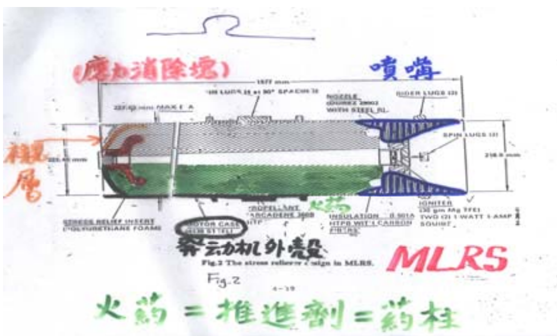

X-ray detection (三溫暖測試)

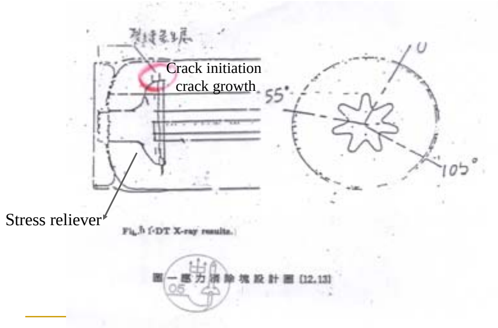

FEM simulation

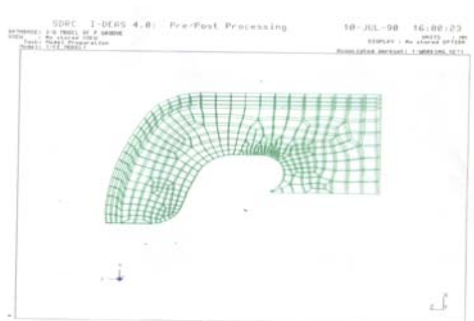

Stress analysis

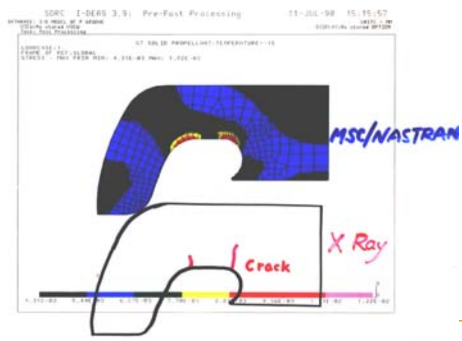

BEM simulation (Army)

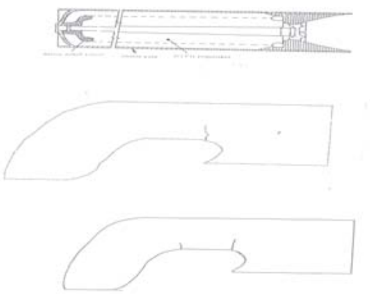

V-band structure (Tien-Gen missile)

FEM simulation

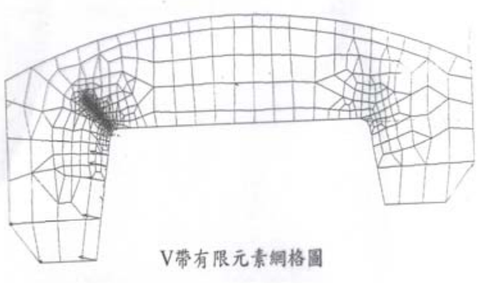

Application to V-band structure:

$E = 19950\ kgf/mm^2$, $\upsilon = 0.27$, $a = 0.125$ $\sigma = 3.63 kgf/mm^2$

Pari's law: $\frac{da}{dN} = C(\Delta K)^m$

$C = 4.624 \times 10^{-12}$, $m = 3.3$, $R = \frac{2}{3}$

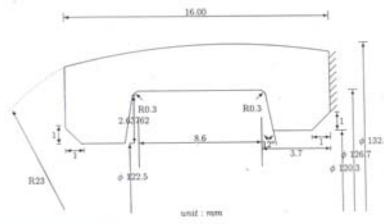

Seepage flow (Laplace equation)

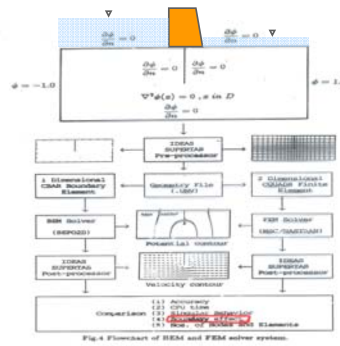

Sheet pile
Cutoff wall

Meshes of FEM and BEM

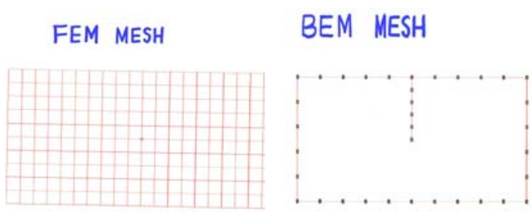

Free surface seepage flow using hypersingular formulation

FEM (iteration No.49) BEM(iteration No.13)

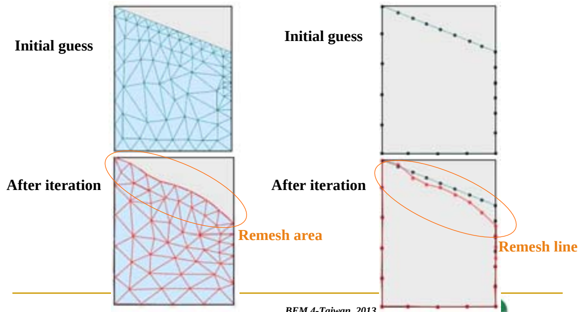

Incomplete partition in room acoustics (Helmholtz equation)

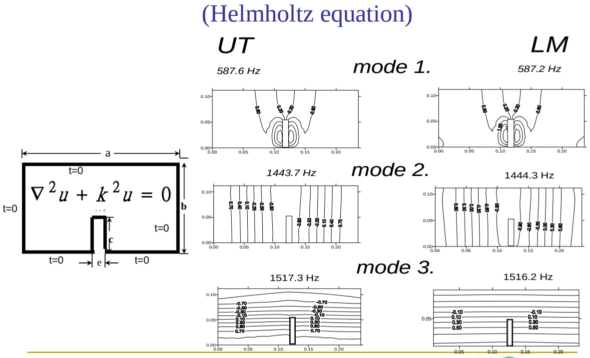

Water wave problem with breakwater (the modified Helmholtz equation)

$$\nabla^2 u(\tilde{x}) - \lambda^2 u(\tilde{x}) = 0$$

oblique incident water wave

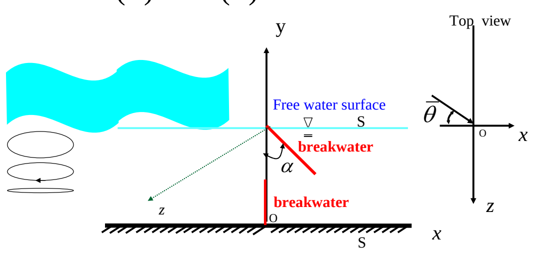

Reflection and Transmission

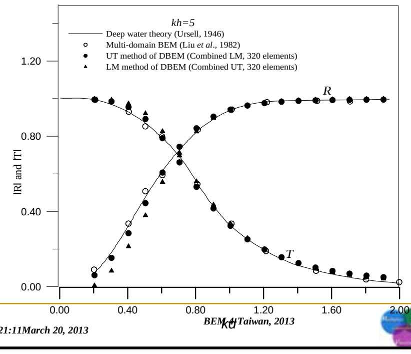

Cracked torsion bar

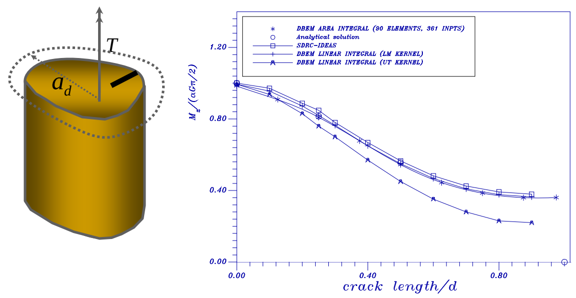

IEEE J MEMS

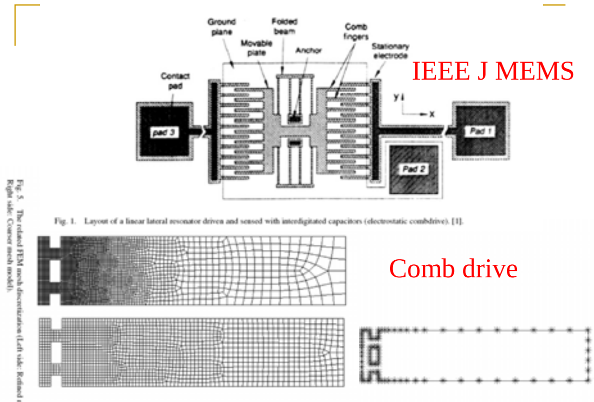

Comb drive

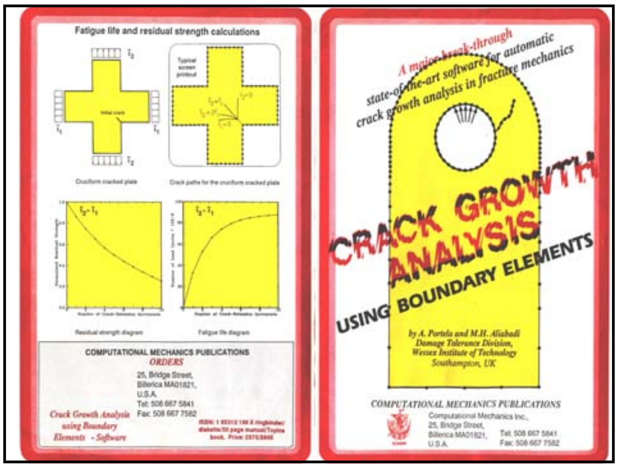
Fatigue life and residual strength calculations
COMPUTATIONAL MECHANICS PUBLICATIONS
ORDERS
25, Bridge Street,
Billerica MA01821,
U.S.A.
Tel: 508 667 5841
Fax: 508 667 7582
Crack Growth Analysis using Boundary Elements - Software
A major break-through state-of-the-art software for automatic crack growth analysis in fracture mechanics
CRACK GROWTH ANALYSIS
USING BOUNDARY ELEMENTS
by A. Portela and M.H. Aliabadi
Damage Tolerance Division,
Wessex Institute of Technology
Southampton, UK
COMPUTATIONAL MECHANICS PUBLICATIONS

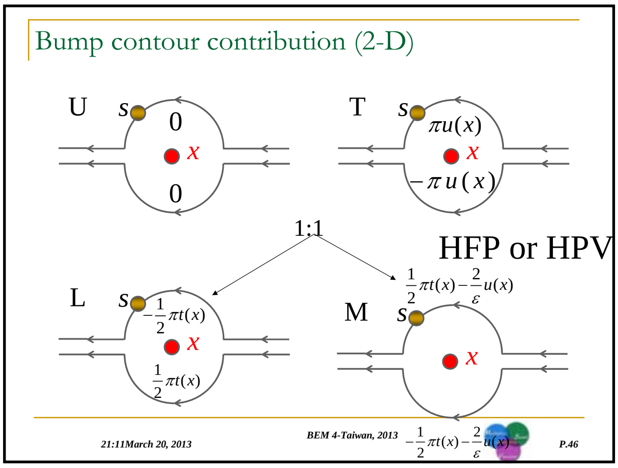
Bump contour contribution (2-D)
U
T
s
0
x
0
$\pi u(x)$
$-\pi u(x)$
1:1
HFP or HPV
$\frac{1}{2}\pi t(x)-\frac{2}{\varepsilon}u(x)$
L
M
$-\frac{1}{2}\pi t(x)$
$\frac{1}{2}\pi t(x)$
21:11March 20, 2013
BEM 4-Taiwan, 2013
$-\frac{1}{2}\pi t(x)-\frac{2}{\varepsilon}u(x)$
P.46

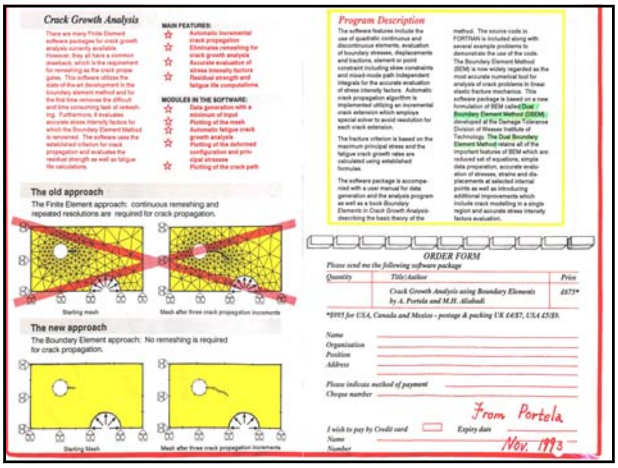
Crack Growth Analysis
MAIN FEATURES:
MODULES IN THE SOFTWARE:
The old approach
The Finite Element approach: continuous remeshing and repeated resolutions are required for crack propagation.
The new approach
The Boundary Element approach: No remeshing is required for crack propagation.
Program Description
ORDER FORM
From Portela
Nov. 1993

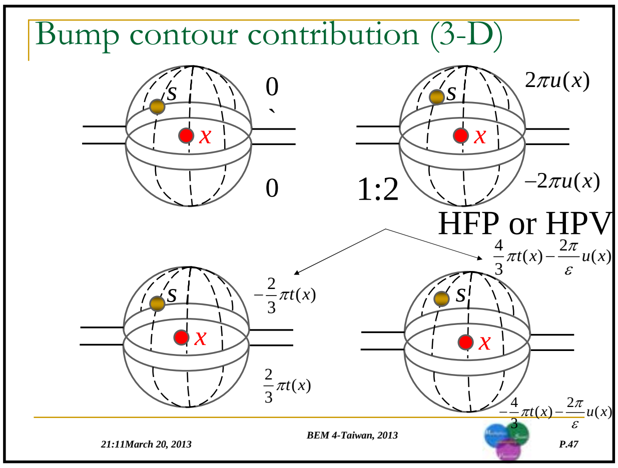
Bump contour contribution (3-D)
0
0
$2\pi u(x)$
$-2\pi u(x)$
1:2
HFP or HPV
$\frac{4}{3}\pi t(x)-\frac{2\pi}{\varepsilon}u(x)$
$-\frac{2}{3}\pi t(x)$
$\frac{2}{3}\pi t(x)$
$-\frac{4}{3}\pi t(x)-\frac{2\pi}{\varepsilon}u(x)$
21:11March 20, 2013
BEM 4-Taiwan, 2013
P.47

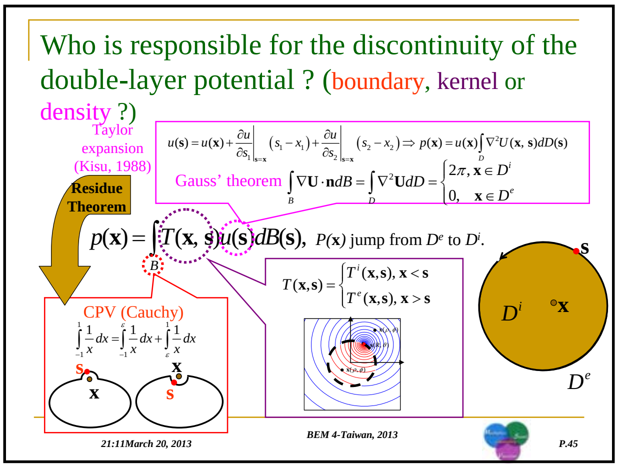
Who is responsible for the discontinuity of the double-layer potential ? (boundary, kernel or density ?)
Taylor expansion (Kisu, 1988)
$u(\mathbf{s})=u(\mathbf{x})+\frac{\partial u}{\partial s_1}\Big|_{\mathbf{s}=\mathbf{x}}(s_1-x_1)+\frac{\partial u}{\partial s_2}\Big|_{\mathbf{s}=\mathbf{x}}(s_2-x_2)\Rightarrow p(\mathbf{x})=u(\mathbf{x})\int_D \nabla^2 U(\mathbf{x},\mathbf{s})dD(\mathbf{s})$
Gauss' theorem $\int_B \nabla \mathbf{U}\cdot \mathbf{n} dB=\int_D \nabla^2 \mathbf{U} dD=\begin{cases}2\pi, \mathbf{x}\in D^i\\ 0, \mathbf{x}\in D^e\end{cases}$
Residue Theorem
$p(\mathbf{x})=\int_B T(\mathbf{x},\mathbf{s})u(\mathbf{s})dB(\mathbf{s})$, $P(\mathbf{x})$ jump from D^e to D^i.
$T(\mathbf{x},\mathbf{s})=\begin{cases}T^i(\mathbf{x},\mathbf{s}), \mathbf{x}<\mathbf{s}\\ T^e(\mathbf{x},\mathbf{s}), \mathbf{x}>\mathbf{s}\end{cases}$
CPV (Cauchy)
$\int_{-1}^{1}\frac{1}{x}dx=\int_{-1}^{-\varepsilon}\frac{1}{x}dx+\int_{\varepsilon}^{1}\frac{1}{x}dx$
D^i
D^e
21:11March 20, 2013
BEM 4-Taiwan, 2013
P.45

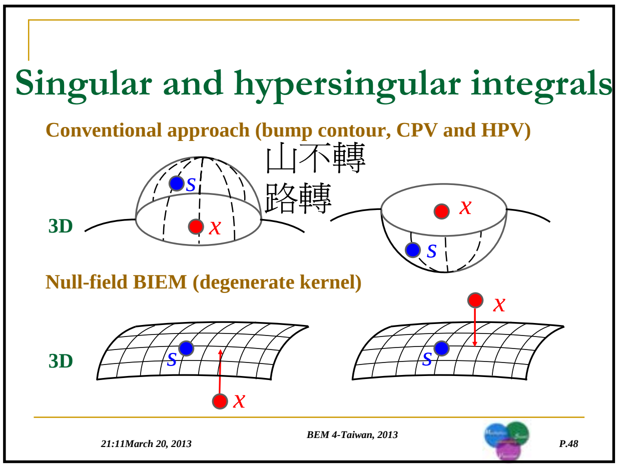
Singular and hypersingular integrals
Conventional approach (bump contour, CPV and HPV)
山不轉
路轉
3D
Null-field BIEM (degenerate kernel)
3D
21:11March 20, 2013
BEM 4-Taiwan, 2013
P.48

Singular and hypersingular integrals

Conventional approach (bump contour, CPV and HPV)

2D

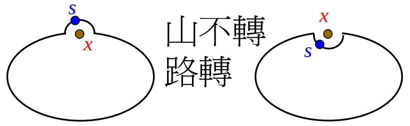

Null-field BIEM (degenerate kernel)

2D

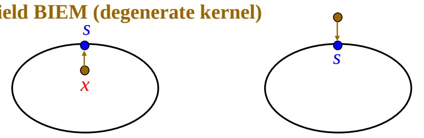

Degenerate kernel (Laplace 2D for a circle)

Expand fundamental solution by using degenerate kernel

$$U(s,x)=\begin{cases}\boxed{U^I(s,x)=\sum_{j=0}^{\infty}A_j(s)B_j(x),\quad |x|\le|s|,}\\ \boxed{U^E(s,x)=\sum_{j=0}^{\infty}A_j(x)B_j(s),\quad |x|>|s|,}\end{cases}$$

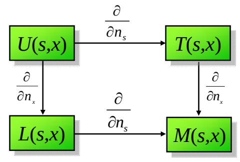

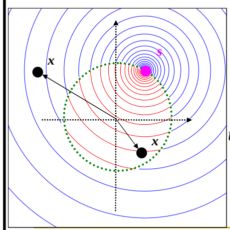

$$U(s,x)=\begin{cases}U^i(R,\theta;\rho,\phi)=\frac{1}{2\pi}\left[\ln R-\sum_{m=1}^{\infty}\frac{1}{m}\left(\frac{\rho}{R}\right)^m\cos m(\theta-\phi)\right], & R\ge\rho\\ U^e(R,\theta;\rho,\phi)=\frac{1}{2\pi}\left[\ln\rho-\sum_{m=1}^{\infty}\frac{1}{m}\left(\frac{R}{\rho}\right)^m\cos m(\theta-\phi)\right], & R<\rho\end{cases}$$

Key point-Addition theorem (degenerate kernel)

Degenerate kernel

$$U(s,x)=\begin{cases}\sum_{j=0}^{\infty}F_j(x)G_j(s), & \xi\ge\xi_s\\ \sum_{j=0}^{\infty}F_j(s)G_j(x), & \xi<\xi_s\end{cases}$$

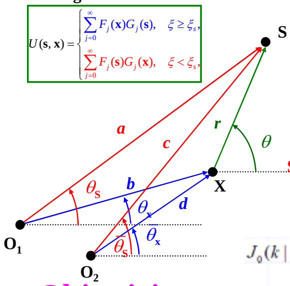

Objectivity

Addition theorem

$$e^{\alpha+\beta}=e^{\alpha}\cdot e^{\beta}$$

$$\sin(\alpha+\beta)=\sin\alpha\cos\beta+\cos\alpha\sin\beta$$

$$\cos(\alpha+\beta)=\cos\alpha\cos\beta-\sin\alpha\sin\beta$$

$$\vec{a}=\vec{b}+\vec{r}$$

$$J_0(k|\vec{a}|)=J_0(k|\vec{b}+\vec{r}|)$$

$$=\sum_{n=-\infty}^{\infty}(-1)^n J_n(k|\vec{b}|)J_n(k|\vec{r}|)e^{in(\theta-\theta_x)}$$

Subtraction theorem (Two-point function)

$$e^{\alpha-\beta}=e^{\alpha+(-\beta)}=e^{\alpha}e^{-\beta}=\frac{e^{\alpha}}{e^{\beta}}$$

$$\vec{r}=\vec{a}-\vec{b}=\vec{c}-\vec{d}$$

$$J_0(k|\vec{r}|)=J_0(k|\vec{c}-\vec{d}|)=J_0(k|\vec{c}+(-\vec{d})|)$$

$$=\sum_{n=-\infty}^{\infty}J_n(k|\vec{c}|)J_n(k|\vec{d}|)e^{in(\theta_s-\theta_x)}$$

Boundary integral equation and null-field boundary integral equation (3D)

Interior case **Exterior case**

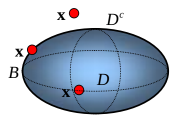

$$U(s,x)=ikh_0^{(1)}(kr)$$

$$T(s,x)=\frac{\partial U(s,x)}{\partial n_s}$$

$$t(s)=\frac{\partial u(s)}{\partial n_s}$$

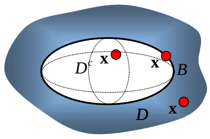

$$\boxed{4\pi u(x)=\int_B T(s,x)u(s)dB(s)-\int_B U(s,x)t(s)dB(s),\quad x\in D\cup B}$$

$$\boxed{2\pi u(x)=C.P.V.\int_B T(s,x)u(s)dB(s)-R.P.V.\int_B U(s,x)t(s)dB(s),\quad x\in B}$$

Degenerate (separable) form

$$\boxed{0=\int_B T(s,x)u(s)dB(s)-\int_B U(s,x)t(s)dB(s),\quad x\in D^c\cup B}$$

Degenerate (separable) form of fundamental solution (Laplace 1D)

$$U(s,x)=\begin{cases}\boxed{\sum_{i=1}^{2}F_i(x)G_i(s),\ x\ge s}\\ \boxed{\sum_{i=1}^{2}F_i(s)G_i(x),\ s>x}\end{cases}$$

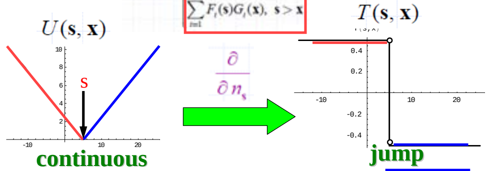

continuous **jump**

$$U(s,x)=\frac{1}{2}|x-s|=\begin{cases}\boxed{\frac{1}{2}(x-s),\ x\ge s}\\ \boxed{\frac{1}{2}(s-x),\ x<s}\end{cases}$$

$$T(s,x)=\begin{cases}\boxed{-\frac{1}{2},\ x\ge s}\\ \boxed{\frac{1}{2},\quad x<s}\end{cases}$$

Null-field BIEM

$$\boxed{\varphi(x)=\int_B K(s,x)\psi(s)dB(s)}$$

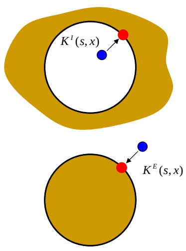

Degenerate kernel

$$K^I(s,x)=\sum_{j=0}^{\infty}A_j(s)B_j(x),\ |x|\le|s|,$$

$$K^E(s,x)=\sum_{j=0}^{\infty}A_j(x)B_j(s),\ |x|>|s|,$$

Fundamental solution

$$\frac{-iH_0^{(1)}(kr)}{4}$$

No principal value

CPV and HPV

Advantages of present approach

1. Mesh-free generation
2. Well-posed model
3. Principal value free
4. Elimination of boundary-layer effect
5. Exponential convergence

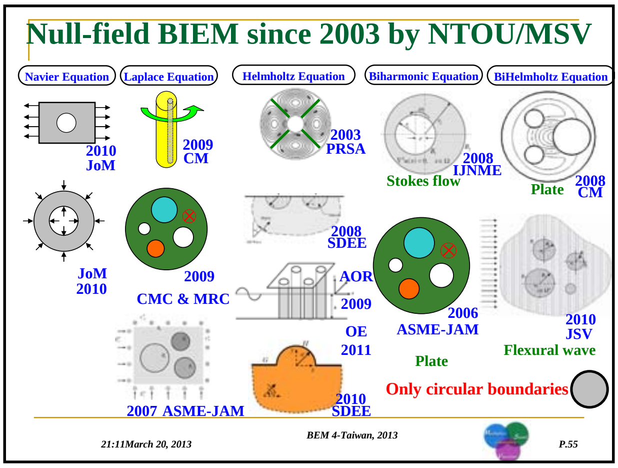
Null-field BIEM since 2003 by NTOU/MSV
Navier Equation
Laplace Equation
Helmholtz Equation
Biharmonic Equation
BiHelmholtz Equation
2010 JoM
2009 CM
2003 PRSA
2008 IJNME
Stokes flow
Plate
2008 CM
JoM 2010
2009
CMC & MRC
2008 SDEE
AOR 2009
OE 2011
2006 ASME-JAM
Plate
2010 JSV
Flexural wave
2007 ASME-JAM
2010 SDEE
Only circular boundaries
21:11March 20, 2013
BEM 4-Taiwan, 2013
P.55

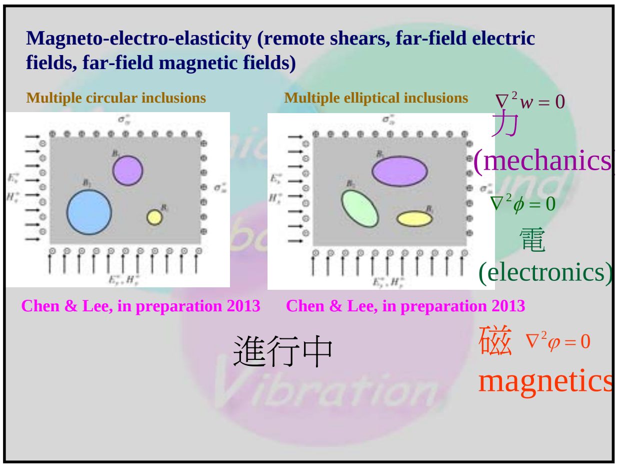
Magneto-electro-elasticity (remote shears, far-field electric fields, far-field magnetic fields)
Multiple circular inclusions
Multiple elliptical inclusions
$\nabla^2 w = 0$
力
(mechanics)
$\nabla^2 \phi = 0$
電
(electronics)
Chen & Lee, in preparation 2013
Chen & Lee, in preparation 2013
進行中
磁 $\nabla^2 \varphi = 0$
magnetics

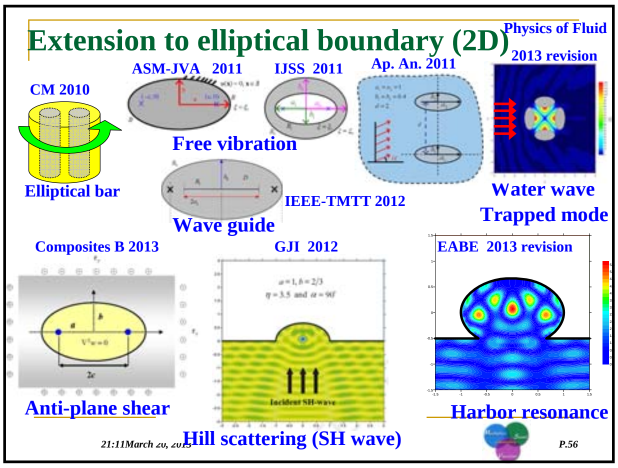
Extension to elliptical boundary (2D)
Physics of Fluid 2013 revision
ASM-JVA 2011
IJSS 2011
Ap. An. 2011
CM 2010
Free vibration
Elliptical bar
Water wave
Trapped mode
IEEE-TMTT 2012
Wave guide
Composites B 2013
GJI 2012
EABE 2013 revision
Anti-plane shear
Harbor resonance
Hill scattering (SH wave)
21:11March 20, 2013
P.56

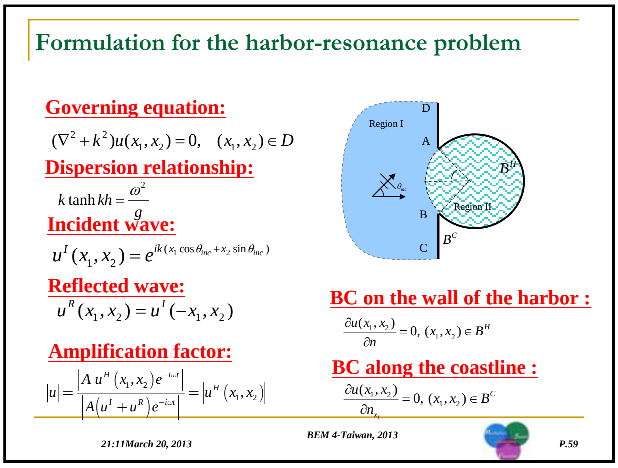
Formulation for the harbor-resonance problem
Governing equation:
$(\nabla^2 + k^2)u(x_1,x_2)=0, \quad (x_1,x_2)\in D$
Dispersion relationship:
$k \tanh kh = \frac{\omega^2}{g}$
Incident wave:
$u^I(x_1,x_2)=e^{ik(x_1\cos\theta_{inc}+x_2\sin\theta_{inc})}$
Reflected wave:
$u^R(x_1,x_2)=u^I(-x_1,x_2)$
Amplification factor:
$|u|=\frac{|A\,u^H(x_1,x_2)e^{-i\omega t}|}{|A(u^I+u^R)e^{-i\omega t}|}=|u^H(x_1,x_2)|$
Region I
Region II
BC on the wall of the harbor :
$\frac{\partial u(x_1,x_2)}{\partial n}=0, \ (x_1,x_2)\in B^H$
BC along the coastline :
$\frac{\partial u(x_1,x_2)}{\partial n_x}=0, \ (x_1,x_2)\in B^C$
21:11March 20, 2013
BEM 4-Taiwan, 2013
P.59

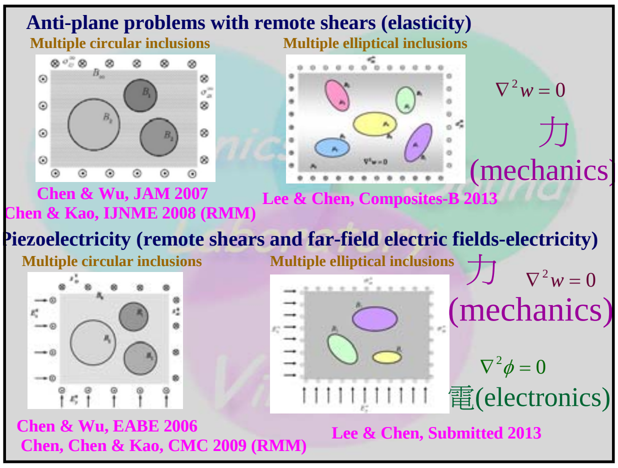
Anti-plane problems with remote shears (elasticity)
Multiple circular inclusions
Multiple elliptical inclusions
$\nabla^2 w = 0$
力
(mechanics)
Chen & Wu, JAM 2007
Chen & Kao, IJNME 2008 (RMM)
Lee & Chen, Composites-B 2013
Piezoelectricity (remote shears and far-field electric fields-electricity)
Multiple circular inclusions
Multiple elliptical inclusions
力 $\nabla^2 w = 0$
(mechanics)
$\nabla^2 \phi = 0$
電(electronics)
Chen & Wu, EABE 2006
Chen, Chen & Kao, CMC 2009 (RMM)
Lee & Chen, Submitted 2013

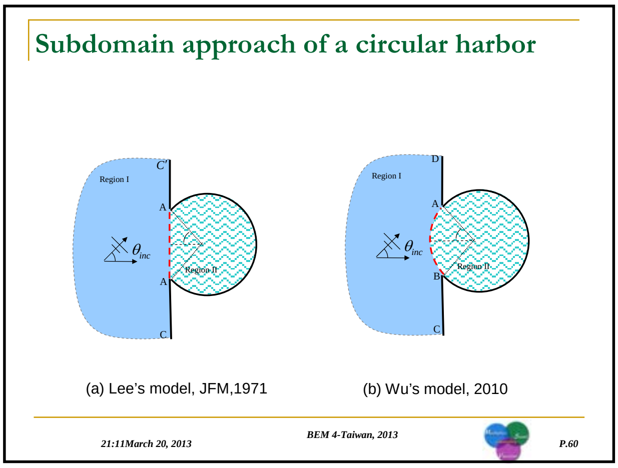
Subdomain approach of a circular harbor
Region I
Region II
(a) Lee's model, JFM,1971
(b) Wu's model, 2010
21:11March 20, 2013
BEM 4-Taiwan, 2013
P.60

Decomposition of the harbor-resonance problem

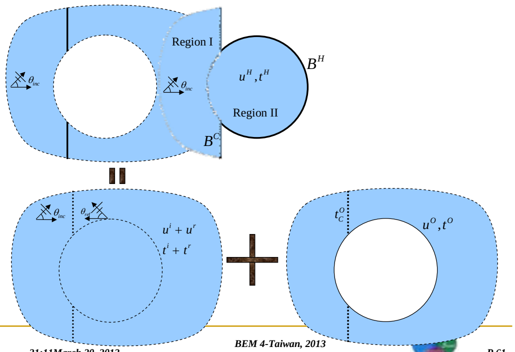

Response curve of the circular harbor with a 60° opening at the center of harbor

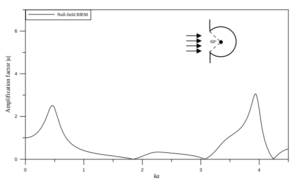

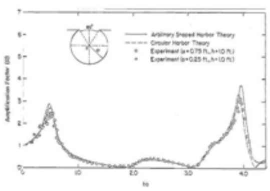

Present method (2010) J. J. Lee, JFM (1971)

Response curve of the circular harbor with a 60° opening at a location of $r_p = 0.7,\ \theta_p = 135^o$

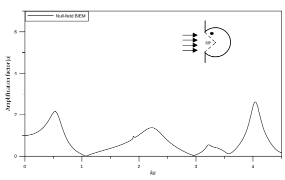

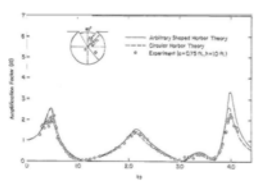

Present method (2010) J. J. Lee, JFM (1971)

Analog between the harbor resonance and the hill scattering

	Harbor resonance	Hill scattering
Medium	Water	Soil
Assumption	Constant water depth	Homogeneous soil
Linear model	Linearized water wavetheory Inviscid, Incompressible (ideal flow)	Linear elastic
Wave type	Gravity wave	SH wave
Governing equation	$(\nabla^2 + k^2)u(x) = 0$	$(\nabla^2 + k^2)u(x) = 0$
Boundary condition	Neumann Impermeable (harbor wall and coastline)	Neumann Traction free (ground surface)

Physics 異

Mathematics 同

Displacement amplitudes versus x/a

$\theta_{inc} = 0$ and $ka = \pi$

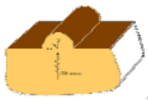

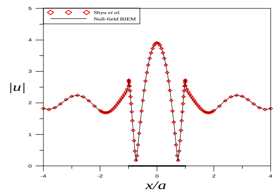

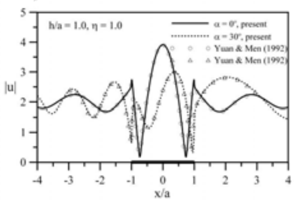

Present method (2010) Tsaur and Chang, GJI, 2009

Shyu *et al., 2009*

Displacement amplitudes versus x/a

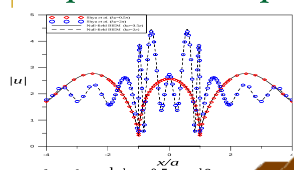

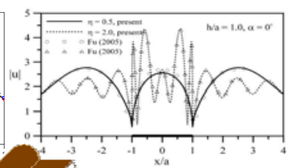

$\theta_{inc} = 0$ and $ka = 0.5\pi$ and 2π

Present method (2010), Shyu, *2009*

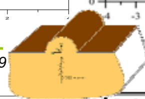

Tsaur and Chang, GJI, 2009

$\theta_{inc} = 0$ and $ka = 3\pi$

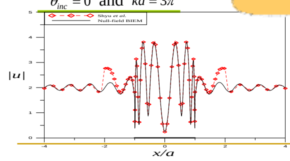

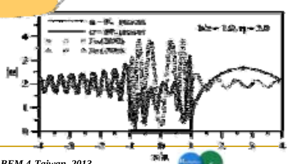

Harbor resonance

Hill scattering

Different physics problems, but is the same mathematical model

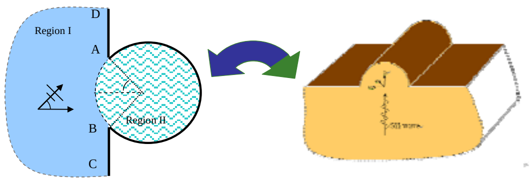

History of focusing effect (earthquake)

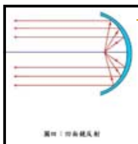

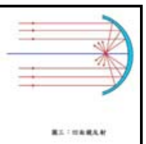

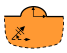

1963 Skopje earthquake

1967 Venezuela earthquake

1994 Northridge earthquake

1995 Kobe earthquake

2000 Davis et al., Science

Focusing effects

Harbor resonance (gravity wave)

Hill scattering (SH-wave)

circular

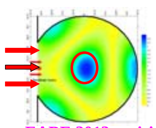

EABE 2013 revision

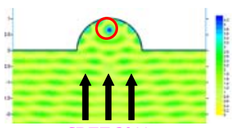

SDEE 2011

elliptical

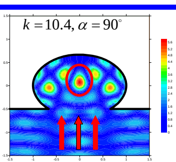

Joint International Workshop on Trefftz Method VI and Method of Fundamental Solutions II, 2011

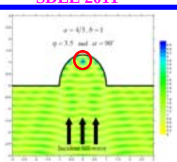

GJI 2012

Applications of the null-field BIEM to Geomechanics by NTOU/MSV

- **SDEE 2008**
  alluvial valley
- **SDEE 2011**
  semi-circular hill
- **GJI 2012**
  semi-elliptical hill
- **Unpublished 2013**
  concave and convex elliptic-arc topography

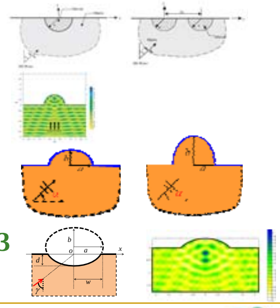

Conclusions

Part I

- Overview of BEM development in Taiwan

Part II

- Dual BEM in Taiwan (1984-2002)

Part III

- Null field BIEM (2003-2013)

The end (感謝壽克堅主任邀請)

Thanks for your kind attentions

Welcome to visit the web site of MSVLAB/NTOU

http://msvlab.hre.ntou.edu.tw/

Boundary Element Analysis of the Stress Concentration in 3D Anisotropic Bodies

邊界元素法分析三維異向體之應力集中

夏育群

國立成功大學航空太空工程系教授

Boundary Element Analysis of the Stress Concentration in 3D Anisotropic Bodies

Y.C. Shiah[1] and C.L. Tan[2]

[1]ycshiah@mail.ncku.edu.tw, Department of Aeronautics and Astronautics, National Cheng Kung University 701, Taiwan, R.O.C.

[2]ctan@mae.carleton.ca, Department of Mechanical and Aerospace Engineering, Carleton University Ottawa, Ontario, Canada K1S 5B6

Keywords: *Boundary Element Method, BEM, Green's function, 3D generally anisotropic bodies*

Abstract

In practice, a complete 3D BEM analysis for engineering problems usually requires millions of computations of the fundamental solutions. While the fundamental solutions for both 2D and 3D isotropic elasticity and those for 2D anisotropic elasticity have been well established, relatively slow progress has been made for the corresponding fundamental solutions of 3D anisotropic elasticity. This is mainly due to the lack of very explicit closed forms for expressing them.

The associated Green's functions for 3D anisotropic bodies were firstly derived in a seminal paper by Lifschitz and Rosenzweig in 1947 [1]. It was expressed as a line integral around a unit circle with the integrand containing the Christoffel matrix defined in terms of elastic constants. Since then, reformulations of the Green's functions into simpler analytical forms have been a focus of lots of researches in the past (see, e.g. Synge [2], Barnett [3], Ting and Lee [4], Nakamura and Tanuma [5], Wang [6], Sales and Gray [7], Pan and Yuan [8], Tonon et al. [9], Lee [10], Phan et al. [11], and Wang and Denda [12]). Instead of directly calculating the Green's functions, Wilson and Cruse [13] interpolated a database of the fundamental solutions generated in advance for a given material based on the solution of Lifschitz and Rozentsweig [1] in their BEM calculations. However, the difficulty may arise that, for highly anisotropic materials, a large number of pre-calculated points are required to attain accuracy. For avoiding such pre-calculations, the best strategy would be to compute the fundamental solutions directly at the exact positions of all involved field points. For this, Sales and Gray [7] employed the calculus of residues to transform the integrand of the line integral for the Green's function into a rational function. However, the main concern of the Sales–Gray algorithm lied in its numerical instability when multiple poles of the residue are present. This was, however, overcome by an extension of the work by Phan *et al* [11], employing the Radon transform along with the calculus of residues. Wang [6] derived an explicit algebraic expression for the displacement Green's function which involved contour integration over a rectangular parallelepiped and presented a strategy for determining its derivatives. Following this work, Tonon et al. [9] implemented the formulations in a BEM analysis, where distinct roots of the sextic equation were assumed. In the recent work by Wang and Denda [12], the Green's function for displacements in their BEM implementation was expressed in terms of a contour integral over a

semi-circle, whose analytical solution was obtained over triangular boundary elements with a piecewise linear interpolation function. As compared with the formulation presented by Wang [6], a relatively simpler explicit form for the 3D anisotropic Green's function was presented by Ting and Lee [4]. The closed-form solution is expressed primarily in terms of Stroh's eigenvalues and remains valid for repeated eigenvalues. By following the Fourier integral solutions developed by Barnett [3] and using the Cauchy residues theorem, Lee [10] further derived the explicit expressions for the derivatives of the 3D anisotropic Green's function in a high-order-tensor form. By extending the work of Ting and Lee [4], Lee [14] further derived the algebraic forms for the first-order derivatives, expressed in the spherical coordinates; however, no explicit expressions for the 2^{nd} order derivatives were presented. Very recently, their algebraic expressions for the 2^{nd} order derivatives were derived by Shiah and Tan [15] by following the same approach of Lee [14] and implemented in their BEM analysis of stresses inside anisotropic bodies.

Although the formulations derived by Lee [14] as well as those by Shiah and Tan [15] are remarkable for both accuracy and efficiency, great programming efforts will be involved due to their tedious algebraic forms. For improving the computational efficiency and conciseness of the formulations, Shiah et al. [16] used a double Fourier series, based on the formulations given by Ting and Lee [4], to represent the 3D anisotropic Green's function for displacements in terms of the spherical coordinates. Also, by directly taking differentiations, derivatives of the Green's function up to the 2^{nd}-order were presented. The formulations presented by Shiah et al. [16] are fully explicit and extraordinarily concise in form. The present work is to apply their revised formulations to study the stress concentrations in 3D anisotropic bodies by a few numerical examples. Also, for verifications, the results are compared with the finite element analyses by ANSYS.

References

[1] Lifshitz, I.M.; Rozenzweig, L.N.: Construction of the Green Tensor for the fundamental equation of elasticity theory in the case of unbounded elastically anisotropic medium, Zh. Eksp. Teor. Fiz., 17, 783-791, 1947.

[2] Synge, J.L.: The Hypercircle in Mathematical Physics, Cambridge University Press, Cambridge, 1957.

[3] Barnett, D.M.: The precise evaluation of derivatives of the anisotropic elastic Green's functions. Phys. Stat. Sol. (b) 49, 741–748, 1972.

[4] Ting, T.C.T.; Lee,V.G.: The three-dimensional elastostic Green's function for general anisotropic linear elastic solid. Q. J. Mech. Appl. Math., 50, 407-426, 1997.

[5] Nakamura, G.; Tanuma, K.: A formula for the fundamental solution of anisotropic elasticity. Q. J. Mech. Appl. Math., 50, 179-194, 1997.

[6] Wang, C.Y.: Elastic fields produced by a point source in solids of general anisotropy. J. Engng. Math., 32, 41-52, 1997.

[7] Sales, M.A.; Gray, L.J.: Evaluation of the anisotropic Green's function and its derivatives. Comp. & Struct., 69, 247-254, 1998.

[8] Pan, E.; Yuan, F.G.: Boundary element analysis of three dimensional cracks in anisotropic solids. Int. J. Numer. Methods Engng., 48, 211-237, 2000.

[9] Tonon, F.; Pan, E.; Amadei, B.: Green's functions and boundary element method formulation for 3D anisotropic media. Comp. & Struct., 79, 469-482, 2001.

[10] Lee,V.G.: Explicit expression of derivatives of elastic Green's functions for general anisotropic materials. Mech. Res. Comm., 30, 241–249, 2003.

[11] Phan, P.V.; Gray, L.J.; Kaplan, T.: On the residue calculus evaluation of the 3D anisotropic elastic Green's function. Comm. Numer. Methods Engng., 20, 335-341., 2004.

[12] Wang, C.Y.; Denda, M.: 3D BEM for general anisotropic elasticity. Int. J. Solids Struct., 44, 7073-7091., 2007.

[13] Wilson, R.B.; Cruse, T.A.: Efficient implementation of anisotropic three dimensional boundary integral equation stress analysis. Int. J. Numer. Methods Engng., 12, 1383-1397, 1978.

[14] Lee,V.G.: Derivatives of the three-dimensional Green's function for anisotropic materials. Int. J. Solids Struct., 46, 1471-1479, 2009.

[15] Shiah, Y.C.; Tan, C. L.: Higher-Order Green's Function Derivatives and BEM Evaluation of Stresses at Interior Points in a 3D Generally Anisotropic Solid, CMES-Computer Modeling in Engineering & Sciences, Vol. 78, pp. 95-108, 2011.

[16] Shiah Y.C.; Tan, C.L.; Wang, C.Y.: An Improved Numerical Evaluation Scheme of the Fundamental Solution and its Derivatives for 3D Anisotropic Elasticity Based on Fourier Series, CMES-Computer Modeling in Engineering & Sciences, Vol. 87, No. 1, pp. 1-22, 2012.

Boundary Element Analysis of the Stress Concentration in 3D Anisotropic Bodies

Y.C. Shiah[1] (夏育群) and C.L. Tan[2]

[1] Dept. of Aeronautics and Astronautics, National Cheng Kung University, Taiwan, R.O.C.

[2] Department of Mechanical & Aerospace Engineering, Carleton University, Ottawa, Canada

OUTLINE OF PRESENTATION

- Introduction
- The BIE & Green's functions
- Derivatives of the fundamental solutions
- Fourier series representations
- Examples
- Conclusions

INTRODUCTION

The Boundary Element Method (BEM)

- particularly well-suited for investigating stress concentrations in linear elastic mechanics
- well developed for isotropy and 2D anisotropy
- for **3D anisotropic elasticity**, the developments are relatively limited in number
  - ➢ Main reasons: time consuming and expensive to evaluate the non-explicit forms of the fundamental solutions.

INTRODUCTION *(contd.)*

❖ Fracture mechanics studies in 3D anisotropic elasticity using BEM include:

- V. Sladek and J. Sladek (1982)*
- E. Pan and F. G. Yuan (2000)
- J. Rungamornrat (2006)
- J. Rungamornrat and M.E. Mear (2008)
- A. Saez, M. P. Ariza and J. Dominguez (1997)**
- C.S.Chen, C.H. Chen and E. Pan (2009)**

**No numerical implementation*

***Transverse isotropy*

The Boundary Integral Equation (BIE)

For displacements at interior point *p*:

$$u_i(p) + \oiint_S u_i(Q) T^*_{ij}(p,Q)dS = \oiint_S t_i(Q) U_{ij}(p,Q)dS$$

For displacement derivatives/strains at

$$u_{i,k}(p) + \oiint_S u_j(Q) T^*_{ij,k}(p,Q)dS = \oiint_S t_j(Q) U_{ij,k}(p,Q)dS$$

Stresses

$$\sigma_{ij} = C_{ijmn}\left(u_{m,n} + u_{n,m}\right)/2$$

Fundamental Solutions *(contd.)*

- Lifschitz and Rozenzweig (1947): line integral around a unit circle
- ➢ Continuing works:

  Synge (1957), Barnett (1972), Ting and Lee (1997), Nakamura and Tanuma (1997), Sales and Gray (1998), Wilson and Cruse (1978), Pan and Yuan (2000), Tonon et al. (2001), Lee (2003), Phan et al. (2004), Wang (2007), Wang and Denda (2007), Lee (2009), Shiah and Tan (2011)

Fundamental Solutions (contd.)

- ◆ ***the challenge*** - improve on its explicitness; efficiency of numerical evaluation
- ◆ This talk presents an alternative means to compute the Green's function and its derivatives.

- Green's functions employed:
  - Solution by Ting &Lee (1997) - for displacements U_{ij}
  - Construct the fundamental solutions, including U_{ij}, $U_{ij,m}$, $U_{ij,mn}$ by the Fourier series

FUNDAMENTAL SOLUTIONS

$$U_{ij} = \frac{1}{8\pi^2 r}\int_0^{2\pi} Z_{ij}^{-1}(\mathrm{k}(\psi))\,\mathrm{d}\psi \quad \text{where } \mathbf{Z} \equiv Z_{ik}(\mathbf{k}) = C_{ijks}k_j k_s$$

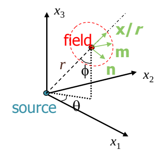

field point: $\mathbf{x}\ (x_1, x_2, x_3)$

$[\mathbf{n}, \mathbf{m}, \mathbf{x}/r]$ => right-handed triad

$\mathbf{n} = (\cos\phi\cos\theta, \cos\phi\sin\theta, -\sin\phi)$,

$\mathbf{m} = (-\sin\theta, \cos\theta, 0)$,

$\mathbf{y} \equiv \mathbf{x}/r$

Fundamental Solutions (contd.)

Introducing:

$$\mathbf{Q} \equiv Q_{ik} = C_{ijks}n_j n_s,\ \mathbf{R} \equiv R_{ik} = C_{ijks}n_j m_s,\ \mathbf{T} \equiv T_{ik} = C_{ijks}m_j m_s$$

$$\mathbf{\Gamma}(p) = \mathbf{Q} + p(\mathbf{R}+\mathbf{R}^T) + p^2\mathbf{T}$$

$$\mathbf{U}(\mathbf{x}) \equiv U_{ij} = \frac{1}{4\pi r}H_{ij} = \frac{1}{4\pi r}\frac{1}{|\mathbf{T}|}\sum_{n=0}^{4} q_n \hat{\mathbf{\Gamma}}^{(n)}$$

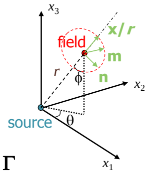

- $\hat{\mathbf{\Gamma}}$, with components, $\hat{\Gamma}^{(n)}$, is the adjoint of $\mathbf{\Gamma}$
- q_n are algebraic functions of p_v, the Stroh's eigenvalues

Fundamental Solutions (contd.)

by Ting, T.C.T.; Lee,V.G. (1997)

$$\mathbf{U}(\mathbf{x}) = \mathbf{H}[\mathbf{x}]/4\pi r \quad , \quad \mathbf{H}[\mathbf{x}] = \frac{1}{|\mathbf{T}|}\sum_{\mathbf{n}=0}^{4}\mathbf{q}_\mathbf{n}\hat{\mathbf{\Gamma}}^{(\mathbf{n})}$$

$$\mathbf{q}_\mathbf{n} = \begin{cases} \dfrac{-1}{2\beta_1\beta_2\beta_3}\left[\mathrm{Re}\left\{\displaystyle\sum_{\mathbf{t}=1}^{3}\frac{\mathbf{p}_\mathbf{t}^\mathbf{n}}{(\mathbf{p}_\mathbf{t}-\bar{\mathbf{p}}_{\mathbf{t}+1})(\mathbf{p}_\mathbf{t}-\bar{\mathbf{p}}_{\mathbf{t}+2})}\right\} - \delta_{\mathbf{n}2}\right] & \textbf{for } \mathbf{n} = \mathbf{0, 1, 2,} \\ \dfrac{1}{2\beta_1\beta_2\beta_3}\left[\mathrm{Re}\left\{\displaystyle\sum_{\mathbf{t}=1}^{3}\frac{\mathbf{p}_\mathbf{t}^{\mathbf{n}-2}\bar{\mathbf{p}}_{\mathbf{t}+1}\bar{\mathbf{p}}_{\mathbf{t}+2}}{(\mathbf{p}_\mathbf{t}-\bar{\mathbf{p}}_{\mathbf{t}+1})(\mathbf{p}_\mathbf{t}-\bar{\mathbf{p}}_{\mathbf{t}+2})}\right\}\right] & \textbf{for } \mathbf{n} = \mathbf{3, 4,} \end{cases}$$

Fundamental Solutions (contd.)

$$\mathbf{U}(\mathbf{x}) = \mathbf{H}[\mathbf{x}]/4\pi r \quad , \quad \mathbf{H}[\mathbf{x}] = \frac{1}{|\mathbf{T}|}\sum_{\mathbf{n}=0}^{4}\mathbf{q}_\mathbf{n}\hat{\mathbf{\Gamma}}^{(\mathbf{n})}$$

$$\hat{\Gamma}_{\mathbf{ij}}^{(\mathbf{n})} = \tilde{\Gamma}_{(i+1)(j+1)(i+2)(j+2)}^{(\mathbf{n})} - \tilde{\Gamma}_{(i+1)(j+2)(i+2)(j+1)}^{(\mathbf{n})}, \quad (\mathrm{i, j} = 1, 2, 3)$$

$$\tilde{\Gamma}_{\mathbf{pqrs}}^{(4)} = T_{\mathbf{pq}}T_{\mathbf{rs}},$$

$$\tilde{\Gamma}_{\mathbf{pqrs}}^{(3)} = V_{\mathbf{pq}}T_{\mathbf{rs}} + T_{\mathbf{pq}}V_{\mathbf{rs}},$$

$$\tilde{\Gamma}_{\mathbf{pqrs}}^{(2)} = T_{\mathbf{pq}}Q_{\mathbf{rs}} + T_{\mathbf{rs}}Q_{\mathbf{pq}} + V_{\mathbf{pq}}V_{\mathbf{rs}},$$

$$\tilde{\Gamma}_{\mathbf{pqrs}}^{(1)} = V_{\mathbf{pq}}Q_{\mathbf{rs}} + V_{\mathbf{rs}}Q_{\mathbf{pq}},$$

$$\tilde{\Gamma}_{\mathbf{pqrs}}^{(0)} = Q_{\mathbf{pq}}Q_{\mathbf{rs}}.$$

Fundamental Solutions (contd.)

$$U_{ij,l} = \frac{1}{4\pi^2 r^2}\left[-\pi\, y_l\, H_{ij} + C_{pqrs}\left(y_s M_{lqiprj} + y_q M_{sliprj}\right)\right]$$

$$M_{ijklmn} = \frac{2\pi i}{|\mathrm{T}|^2}\sum_{t=1}^{3}\frac{\Phi'_{ijklmn}(p_t) - 2\Phi_{ijklmn}(p_t)\times\left(\dfrac{1}{p_t - p_{t+1}} + \dfrac{1}{p_t - p_{t+2}}\right)}{(p_t - p_{t+1})^2(p_t - p_{t+2})^2}$$

$$\Phi_{ijklmn}(p) = \frac{\mathrm{B}_{ij}(p)\hat{\Gamma}_{kl}(p)\hat{\Gamma}_{mn}(p)}{(p-\bar{p}_1)^2(p-\bar{p}_2)^2(p-\bar{p}_3)^2},$$

$$\mathrm{B}_{ij}(p) = n_i n_j + \left(n_i m_j + m_i n_j\right)p + m_i m_j p^2$$

Fundamental Solutions *(contd.)*

$$U_{ij,mn} = \frac{1}{4\pi^2 r^3}\left\{\begin{array}{l} 2\pi y_m y_n H_{ij} \\ -2C_{pqrs}\left(y_n y_s M_{mqiprj} + y_n y_q M_{msiprj} + y_m y_s M_{msiprj}\right) \\ +C_{pqrs}C_{ghkl}\left[\begin{array}{l} y_s y_l\left(N_{mnqhigkprj} + N_{mnqhiprgkj}\right) \\ +y_s y_h\left(N_{mnqligkprj} + N_{mnqliprgkj}\right) \\ +y_q y_l\left(N_{hmnsrjigkp} + N_{hmnsiprklj}\right) \\ +y_q y_h\left(N_{lmnsrjigkp} + N_{lmnsiprgkj}\right) \end{array}\right] \end{array}\right\}$$

$y_1 = \sin\varphi\cos\theta$, $y_2 = \sin\varphi\sin\theta$, $y_3 = \cos\varphi$

Fourier series representation

$$\mathbf{U}(r,\theta,\phi) = \frac{\mathbf{H}[\theta,\phi]}{4\pi r}$$

H(θ, ø) periodic with an interval width 2π for both spherical angles; i.e.

$$H_{uv}(\theta,\phi+2\pi) = H_{uv}(\theta,\phi)$$

Represent **H**(*θ, ø*) by double Fourier series

$$H_{uv}(\theta,\phi) = \sum_{m=-\infty}^{\infty}\sum_{n=-\infty}^{\infty}\lambda_{uv}^{(m,n)}\, e^{i(m\theta+n\phi)}, \quad (u,v=1,2,3)$$

$$\lambda_{uv}^{(m,n)} = \frac{1}{4\pi^2}\int_{-\pi}^{\pi}\int_{-\pi}^{\pi} H_{uv}(\theta,\phi)\, e^{-i(m\theta+n\phi)}\, d\theta\, d\phi$$

Fourier series representation

- Gaussian quadrature:

$$\lambda_{uv}^{(m,n)} = \frac{1}{4}\sum_{p=1}^{k}\sum_{q=1}^{k} w_p w_q f_{uv}^{(m,n)}\left(\pi\xi_p, \pi\xi_q\right)$$

- Integrand

$$f_{uv}^{(m,n)}(\theta,\phi) = H_{uv}(\theta,\phi)\, e^{-i(m\theta+n\phi)}$$

Fourier series representation

Green's function is thus written as:

$$U_{uv}(r,\theta,\phi) = \frac{1}{4\pi r}\sum_{m=-\alpha}^{\alpha}\sum_{n=-\alpha}^{\alpha}\lambda_{uv}^{(m,n)}\, e^{i(m\theta+n\phi)}$$

- Coefficients $\lambda_{uv}^{(m,n)}$ need to be evaluated ONCE only for a given material (independent of the no. of field points).
- Typical values: α = 16; k = 60 for highly anisotropic materials.

1st Order Derivatives

$$U_{ij,l} = \frac{\partial U_{ij}}{\partial r}\frac{\partial r}{\partial x_l} + \frac{\partial U_{ij}}{\partial \theta}\frac{\partial \theta}{\partial x_l} + \frac{\partial U_{ij}}{\partial \phi}\frac{\partial \phi}{\partial x_l}$$

$$U_{ij,l} = \frac{1}{4\pi r^2}\left\{\begin{array}{ll} \displaystyle\sum_{m=-\alpha}^{\alpha}\sum_{n=-\alpha}^{\alpha}\lambda_{ij}^{(m,n)} e^{i(m\theta+n\phi)}\left[\begin{array}{l} -\cos\theta\left(\sin\phi - i\,n\cos\phi\right) \\ -i\,m\sin\theta/\sin\phi \end{array}\right] & \text{for } l=1 \\ \displaystyle\sum_{m=-\alpha}^{\alpha}\sum_{n=-\alpha}^{\alpha}\lambda_{ij}^{(m,n)} e^{i(m\theta+n\phi)}\left[\begin{array}{l} -\sin\theta\left(\sin\phi - i\,n\cos\phi\right) \\ +i\,m\cos\theta/\sin\phi \end{array}\right] & \text{for } l=2 \\ \displaystyle\sum_{m=-\alpha}^{\alpha}\sum_{n=-\alpha}^{\alpha}\lambda_{ij}^{(m,n)} e^{i(m\theta+n\phi)}\left[-\left(\cos\phi + i\,n\sin\phi\right)\right] & \text{for } l=3 \end{array}\right.$$

2nd Order Derivatives

$$U_{ij,lk} = \frac{\partial U_{ij,l}}{\partial r}\frac{\partial r}{\partial x_k} + \frac{\partial U_{ij,l}}{\partial \theta}\frac{\partial \theta}{\partial x_k} + \frac{\partial U_{ij,l}}{\partial \phi}\frac{\partial \phi}{\partial x_k}$$

e.g.

$$U_{ij,11} = \frac{1}{4\pi r^3}\sum_{m=-\alpha}^{\alpha}\sum_{n=-\alpha}^{\alpha}\lambda_{ij}^{(m,n)} e^{i(m\theta+n\phi)}\left\{\begin{array}{l} 2\sin\phi\cos\theta\left(\begin{array}{l}\cos\theta\left(\sin\phi - i\,n\cos\phi\right) \\ +i\,m\sin\theta/\sin\phi\end{array}\right) \\ -\dfrac{\sin\theta}{\sin\phi}\left[\begin{array}{l}\left(\sin\theta - i\,m\cos\theta\right)\left(\sin\phi - i\,n\cos\phi\right) \\ -i\,m\left(\cos\theta + i\,m\sin\theta\right)/\sin\phi\end{array}\right] \\ +\cos\phi\cos\theta\left[\begin{array}{l} -\cos\theta\left(\begin{array}{l}\left(\cos\phi + i\,n\sin\phi\right) \\ +i\,n\left(\sin\phi - i\,n\cos\phi\right)\end{array}\right) \\ +i\,m\sin\theta\left(\cos\phi - i\,n\sin\phi\right)/\sin^2\phi \end{array}\right] \end{array}\right\}$$

Examples: *Nb crystal cylinder*

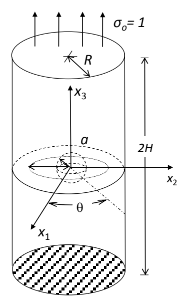

Consider a/R=0.4 , 0.5 $H=2R$

C^*_{11}= 246 GPa; C^*_{12}= 134 GPa; C^*_{44}= 28.7 GPa.

Material axes rotated CCW with respect to x_1, x_2 and x_3, by 15º, 30º and 45º, respectively

$$\mathbf{C} = \begin{pmatrix} 218.76 & 153.52 & 141.72 & -10.01 & 0.40 & 7.21 \\ 153.52 & 209.89 & 150.59 & -2.21 & 0.96 & -0.18 \\ 141.72 & 150.59 & 221.69 & 12.22 & -1.36 & -7.04 \\ -10.01 & -2.21 & 12.22 & 45.29 & -7.04 & 0.96 \\ 0.40 & 0.96 & -1.36 & -7.04 & 36.42 & -10.01 \\ 7.21 & -0.18 & -7.04 & 0.96 & -10.01 & 48.22 \end{pmatrix}$$

Examples: *Nb crystal cylinder*

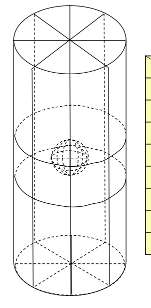

8 elements with 228 nodes

$\delta = \sqrt{u_1^2 + u_2^2 + u_3^2}$ (*10^{-9}) at r/R =0.75

	a/R=0.4			a/R=0.5		
θ	FEM	BEM	|% Diff.|	FEM	BEM	|% Diff.|
0^0	0.1104	0.1078	2.39	0.1240	0.1213	2.15
45^0	0.1236	0.1209	2.16	0.1390	0.1363	1.91
90^0	0.1362	0.1335	1.99	0.1529	0.1502	1.74
135^0	0.1381	0.1351	2.15	0.1562	0.1531	2.01
180^0	0.1203	0.1175	2.30	0.1349	0.1322	2.03
225^0	0.1040	0.1011	2.80	0.1161	0.1131	2.58
270^0	0.1033	0.1003	2.91	0.1167	0.1133	2.92

Determination of SIF's

- Use of special crack front elements
- Shape functions with the appropriate near field variations
- Work in 3D isotropy and transverse isotropy:
  e.g. - M.L. Luigi and S. Rizutti (1987)
  - S.B. Liu and C.L. Tan (1995)
  - A. Saez, MP. Ariza and J. Dominguez (1997)

Determination of SIF's (contd.)

- Traction formula:

$$(K_I)_A = (t_3^*)_A \sqrt{\pi l}$$
$$(K_{II})_A = (t_1^*)_A \sqrt{\pi l}$$
$$(K_{III})_A = (t_2^*)_A \sqrt{\pi l}$$

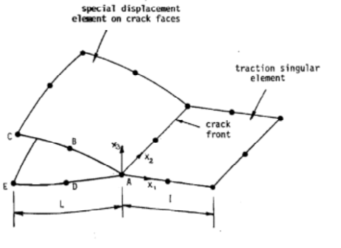

EXAMPLES

- ***Example 1: Penny shaped crack in a transversely isotropic infinite medium*** (*Graphite epoxy: C_{11}=13.92 MPa, C_{12}=6.92 MPa, C_{13}=6.44 MPa, C_{33}=160.7 MPa, C_{44}=7.07 MPa*)

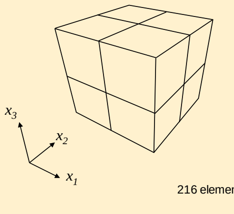

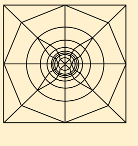

216 elements, 604 nodes

Example 1: Results

Analytical solution: Case (1) - For remote tension $\sigma_{33} = \sigma_o$, in isotropy and tranverse isotropy,

$$K_I / \sigma_o \sqrt{\pi a} = 0.637$$

BEM Solution: $K_I / \sigma_o \sqrt{\pi a}$ = 0.633 (isotropy); 0.638 (trans. isotropy).

Analytical solution: Case (2) - For remote shear $\sigma_{23} = \tau_o$ at the top and bottom faces,

Isotropy: $[K_{II} / \tau_o \sqrt{\pi a} = 0.7490 \sin\theta, \ K_{III} / \tau_o \sqrt{\pi a} = 0.5243 \cos\theta\ ]$

Transverse isotropy: $[K_{II} / \tau_o \sqrt{\pi a} = 0.8115 \sin\theta, \ K_{III} / \tau_o \sqrt{\pi a} = 0.4617 \cos\theta]$

Example 1 *(contd.)*

Case 2:

Angle θ deg.	Isotropic Medium K_{II}^{*}	Isotropic Medium K_{III}^{*}	Graphite Epoxy K_{II}^{*}	Graphite Epoxy K_{III}^{*}
0	0	0.5190 (0.5243)	0	0.4555 (0.4617)
30	0.3734 (0.3745)	0.4494 (0.4540)	0.4053 ().4057)	0.3943 (0.3999)
60	0.6467 (0.6486)	0.2594 (0.2621)	0.7016 (0.7028)	0.2280 (0.2309)
90	0.7471 (0.7490)	0	0.8102 (0.8115)	0

$$K_{II}^{*} = K_{II} / \tau_o \sqrt{\pi a} \;,\; K_{III}^{*} = K_{III} / \tau_o \sqrt{\pi a}$$

Example 2: Cylindrical bar (Zn crystal) with a penny shaped crack under remote tension; material axes rotated 60° clockwise about the x_1-axis.

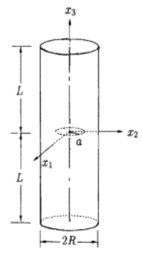

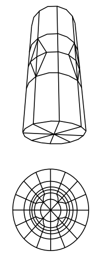

BEM: 240 elements
660 nodes

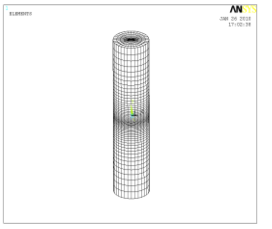

FEM: 59136 elements, 122226 nodes

Example 2 *(contd.)*

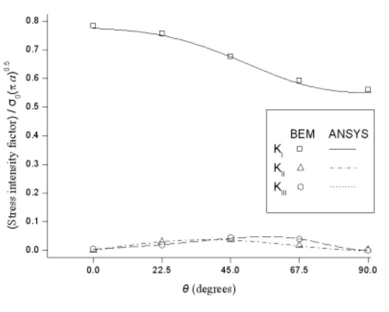

Example of bi-crystals

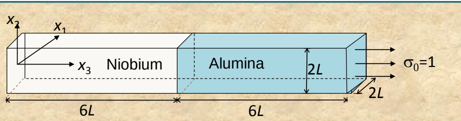

Niobium

Alumina

$$\mathbf{C} = \begin{pmatrix} 246 & 134 & 134 & 0 & 0 & 0 \\ 134 & 246 & 134 & 0 & 0 & 0 \\ 134 & 134 & 246 & 0 & 0 & 0 \\ 0 & 0 & 0 & 28.7 & 0 & 0 \\ 0 & 0 & 0 & 0 & 28.7 & 0 \\ 0 & 0 & 0 & 0 & 0 & 28.7 \end{pmatrix} \text{GPa} \;;\; \mathbf{C} = \begin{pmatrix} 465 & 124 & 117 & 101 & 0 & 0 \\ 124 & 465 & 117 & -101 & 0 & 0 \\ 117 & 117 & 563 & 0 & 0 & 0 \\ 101 & -101 & 0 & 233 & 0 & 0 \\ 0 & 0 & 0 & 0 & 233 & 101 \\ 0 & 0 & 0 & 0 & 101 & 170.5 \end{pmatrix} \text{GPa}$$

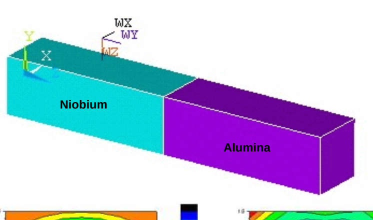

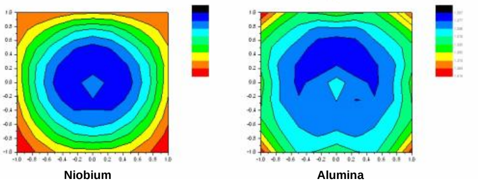

Niobium Alumina

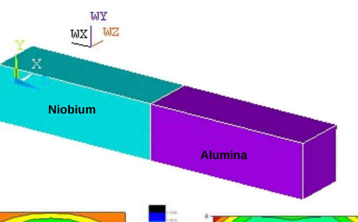

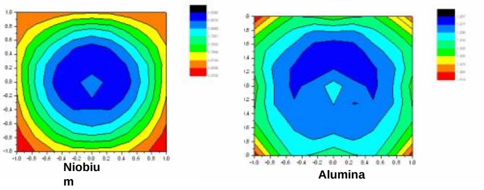

Niobiu
m

Alumina

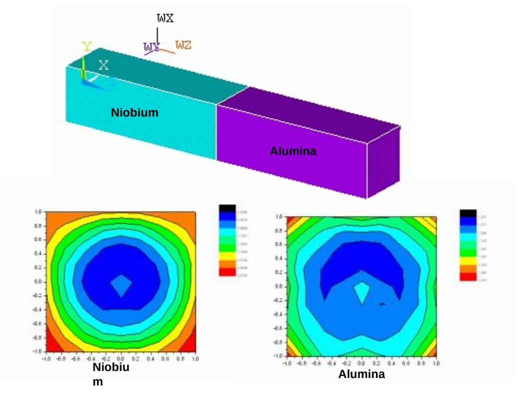

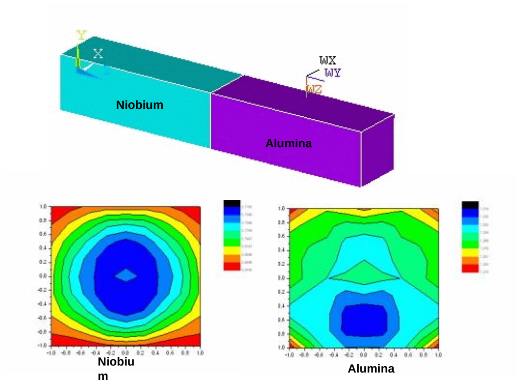

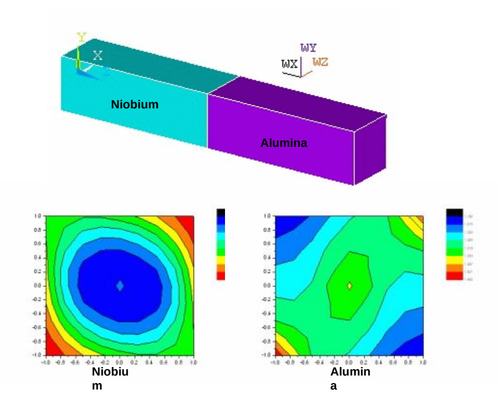

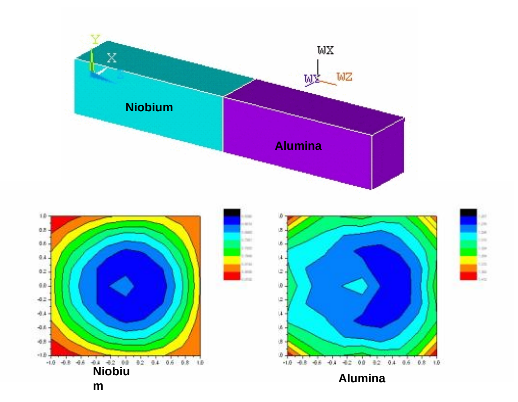

CONCLUSIONS

- The Fourier series forms of the fundamental solutions for 3D anisotropic bodies are very explicit in form and efficient in computation.
- Programming of the formulations requires very minor efforts.
- Implementation in the BEM makes this method more advantageous in practical applications.

Thank you for your interest!

THANK YOU!

Analysis of Rock Fracture Mechanics Using the BEM

邊界元素法應用於岩石之破壞力學性質分析

陳昭旭

國立成功大學資源工程系教授

Analysis of Rock Fracture Mechanics Using the BEM

Chao-Shi Chen*

*chencs@mail.ncku.edu.tw, Department of Resources Engineering,

National Cheng Kung University, Tainan 70101, Taiwan

This paper introduced a numerical technique based on the boundary element method (BEM) for the analysis of linear elastic fracture mechanics (LEFM) problems on stress intensity factor, SIF, and modeling crack propagation path involving anisotropic rocks. The most important feature of this analysis is that it is a single domain method, and yet it is very accurate, efficient and versatile, i.e. material properties in the medium can be anisotropic as well as isotropic. Problem domain can be finite, infinite or semi-infinite. The crack can be of multiple, branched or internal type with a straight shape. Furthermore, cases of the fracture toughness and bi-materials can also be analyzed.

Key words: *Stress intensity factor, SIF, single-domain Boundary Element Method, BEM, crack propagation, anisotropic rock.*

1 Introduction

Defects are commonly originated from the free surface. They are inherent to the structural materials or are developed during manufacturing and fabrication. Thus, study of surface cracks is fundamental to fracture analysis of the involved structure. Regardless of how a surface crack is initiated or introduced in a component, accurate prediction of the fracture conditions is very important in solid mechanics. There are 3 basic modes of crack tip deformation in the fracture process: mode I (tension, opening), mode II (in-plane shear, sliding), and mode III (out-of-plane shear, tearing), which presents the displacements of the crack surfaces of a local element containing the crack tip. Any deformation of the crack surface can be obtained from superposition of these basic deformation modes. Cracks within the earth crust may be either shear fractures of the type or tension fractures. Tension fractures are opening mode cracks. Shear fractures are more complicated and often form as a mixed mode crack. Mixed mode cracking means that 2 or 3 of the above modes are active during failure. Commonly opening mode failure is combined with one of the other two modes. The fracture mechanical safety of a solid elastic structure can be designed depended on these SIFs [1]. Therefore, evaluation of SIFs along the crack tip in linear elastic fracture mechanics has been considerably investigated. However, accurate calculation of SIFs for crack surface is still an important computational issue in fracture mechanics.

Whittaker et al. [2] classified the experimental sample types to determine the SIFs, and concluded the following various methods to determine the SIF: (i) analytical methods (i.e. complex stress function, weight function, stress concentration, integral transformation), (ii) numerical methods (i.e. finite element, finite difference, finite volume, boundary element, boundary collocation), (iii) experimental methods (i.e. photo-elastic, compliance, acoustic emission), and (iv) estimative methods (i.e. superposition). Numerical techniques in fracture mechanics have become indispensable tools for solving all kinds of science and engineering problems. The evaluation of the SIFs may have direct practical applications in obtaining the safety factor of the elastic structures in engineering design. Due to the varied engineering conditions in this research area, it is imperative to develop new numerical methods or to explore alternative techniques for the purpose of solving the complicated problems and to improve the efficiency and accuracy of existing or new numerical methods.

Recently, the two most popular techniques in computational continuum mechanics, namely finite element method (FEM) and boundary element method (BEM), are used in the analysis of stress of strain for practical engineering problems. The BEM is firmly established in many engineering disciplines as an effective alternative computational tool the FEM. The BEM has proven to be a powerful numerical technique that has some advantages over the domain-based method such as finite element method. The BEM is a numerical computational method of solving linear partial differential equations which have been formulated as integral equations. It can be applied in many areas of engineering and science including fluid mechanics, acoustics, electromagnetics, plasticity, and fracture mechanics. The BEM is used in the fracture analysis of structures and rocks, because of the complex shape and continuously changing path of the propagating crack. The main attraction of BEM is reduction in the dimensionality of the problem: for two-dimensional problems, only the line boundary of the domain needs to be discretized into elements. The simpler modeling of the body means that regions of high stress concentration can be modeled in more detail as necessary high concentration of elements is confined to one less dimension. Another important feature of the boundary element formulation is that it provides a continuous modeling of the interior since no discretization of the interior is required; this leads to a high resolution of internal stresses and displacements.

The critical value of the SIFs is defined as the fracture toughness when the crack propagation initiates. In addition, the fracture toughness can be defined as a measure of the ability of a material to resist the growth of a preexisting crack under stress. Thus, rock fracture toughness is the most fundamental parameter in fracture mechanics, and can be obtained by experimental procedures if the SIFs are known for a given body under a certain type and magnitude of loading. In the laboratory, there are many testing methods suggested by the International Society for Rock Mechanics (ISRM) for determining the mode I fracture toughness of isotropic rocks, such as chevron bend (CB) specimen method, short rod (SR) specimen method, cracked chevron notched Brazilian disk (CCNBD) method, and cracked straight through Brazilian disk (CSTBD) method (Ouchterlony, 1988). Disadvantages of these methods include complicated loading fixtures, complex sample preparation, limitations due to the isotropic behavior of rocks, and limited only to mode I conditions. Recently, most investigations in linear elastic fracture mechanics have focused on fracture toughness determination for mixed-mode. In engineering, we often need to consider the problems of mixed-mode crack. However, no suggested method has been accepted as the standard by the ISRM, even though a broad range of testing methods has been used to evaluate the fracture toughness parameters under mixed-mode loading. The fracture of brittle materials occurs at a shear stress approximately equal to the tensile fracture stress. Hence, it is important from an engineering point of view to study the combined mode I or mixed-mode as appeared in [3-9]. Therefore consideration of mixed-mode fracture becomes significant and necessary in fracture mechanics investigation.

The boundary element method (BEM) has gotten extensive application to engineering because of reduced order, discretization error only on the boundary and low computational complexity. For plane problem, using the source point serving as origin, the tangent and normal direction of integral element to establish local coordinate system, analytical solutions are obtained for all integrals of linear element. Therefore, analytical solutions for the variables in the region calculated can be acquired; and it guarantees the accuracy and continuity of the variables of region near the border. This study concentrates on the development of the single-domain BEM using the FORTRAN programming language, which is then applied to anisotropic rock of fracture mechanics problems.

2 Methodology

2.1 Single-domain Boundary Integral Equation

The traditional displacement boundary integral equation for linear elasticity can be expressed as

$$C_{ij}(s_k)u_j(s_k)+\int_{\Gamma}T_{ij}(z_k,s_k)u_j(z_k)d\Gamma(z_k) = \int_{\Gamma}U_{ij}(z_k,s_k)t_j(z_k)d\Gamma(z_k) \tag{1}$$

where i, j, k=1, 2; T_{ij} and U_{ij} are the Green's functions of traction and displacement; u_j and t_j are the boundary displacements and tractions; C_{ij} are quantities that depend on the geometry of the boundary and are equal to $\delta_{ij}/2$ for a smooth boundary; z_k and s_k are the field and source points on the boundary Γ of the domain.

Discretization of Equation (1) gives a linear system of algebraic equations, which can be solved for the unknown displacements u_j and tractions t_j on the boundary. However, for a cracked elastic medium, Equation (1) is not sufficient for solving all the unknowns along the outer boundary of the problem as well as along the two sides of the crack surfaces because of the geometric singularity associated with the crack surface.

In the single-domain BEM formulation of Pan [10] for cracked anisotropic media, the displacement integral equation is collocated only on the outer boundary and the traction integral equation only on one side of crack surface. The displacement integral equation applied to the outer boundary results in the following form ($s_{k,B} \in \Gamma_B$ only, Figure 1)

$$\begin{aligned} &C_{ij}(s_{k,B})+u_j(s_{k,B})+\int_{\Gamma_B}T_{ij}(z_{k,B},s_{k,B})u_j(z_{k,B})d\Gamma(z_{k,B}) \\ &+\int_{\Gamma_C}T_{ij}(z_{k,C},s_{k,B})[u_j(z_{k,C+})-u_j(z_{k,C-})]d\Gamma(z_{k,C}) \\ &=\int_{\Gamma_B}U_{ij}(z_{k,B},s_{k,B})t_j(z_{k,B})d\Gamma(z_{k,B}) \end{aligned} \tag{2}$$

where Γ_C has the same outward normal as Γ_{C+}. Here, the subscripts B and C denote the outer boundary and the crack surface, respectively.

The traction integral equation (for sk being a smooth point on the crack) applied to one side of the crack surface is ($s_{k,C} \in \Gamma_{C+}$ only)

$$\begin{aligned} &0.5t_j(s_{k,C})+n_m(s_{k,C})\int_{\Gamma_B}C_{lmik}T_{ij,k}(s_{k,C},z_{k,B})u_j(z_{k,B})d\Gamma(z_{k,B}) \\ &+n_m(s_{k,C})\int_{\Gamma_C}C_{lmik}T_{ij,k}(s_{k,C},z_{k,C})[u_j(z_{k,C+})-u_j(z_{k,C-})]d\Gamma(z_{k,C}) \\ &=n_m(s_{k,C})\int_{\Gamma_B}C_{lmik}U_{ij,k}\times(s_{k,C},z_{k,B})t_j(z_{k.B})d\Gamma(z_{k,B}) \end{aligned} \tag{3}$$

where C_{lmik} is the 4th-order stiffness tensor; n_m is the unit outward normal to the contour path; the gradient tensors $T_{ij,k}$ and $U_{ij,k}$ denote differentiation with respect to s_k .

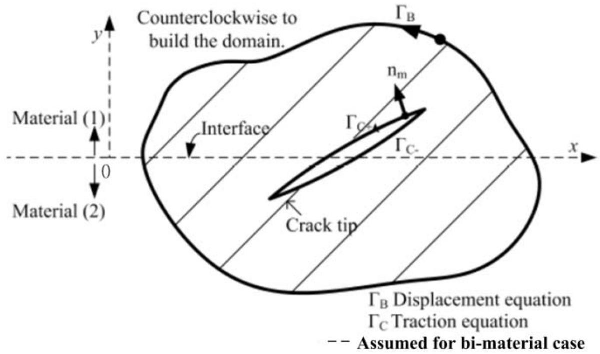

Figure 1 Geometry of a two-dimensional cracked domain.

The internal stresses $\sigma(z_k)$ are determined by the equation (4) and following expression

$$\begin{aligned} &\sigma_{lm}(z_k)+\int_{\Gamma_B}C_{lmik}T_{ij,k}(s_{k,C},z_{k,B})u_j(z_{k,B})d\Gamma(z_{k,B}) \\ &+\int_{\Gamma_C}C_{lmik}T_{ij,k}(s_{k,C},z_{k,C})\left[u_j(z_{k,C+})-u_j(z_{k,C-})\right]d\Gamma(z_{k,C}) \\ &=\int_{\Gamma_B}C_{lmik}U_{ij,k}(s_{k,C},z_{k,B})t_j d\Gamma(z_{k,B}) \end{aligned} \tag{4}$$

For given solutions (related to the body force of gravity, rotational forces, and the far-field stresses), the boundary integral equations (2) and (3) can be discretized and solved numerically for the unknown boundary displacements (or displacement discontinuities on the cracked surface) and tractions. In solving these equations, the hyper-singular integral term in (3) can be handled using an accurate and efficient Gauss quadrature formula, which is similar to the traditional weighted Gauss quadrature but has a different weight [11].

Previously, fracture mechanics problems in isotropic or anisotropic case (or bi-materials case) were mostly handled by the multiple-domain BEM in which each side of the crack surface is put into different domains and artificial boundaries are introduced to connect the crack surface to the un-cracked boundary (shown in Figure 2). For the bi-material case, discretization along the interface is also required if one uses the Kelvin-type (infinite domain) Green's functions. But we present a single-domain BEM formulation in which neither the artificial boundary nor the discretization along the un-cracked interface is necessary (as shown in Figure1).

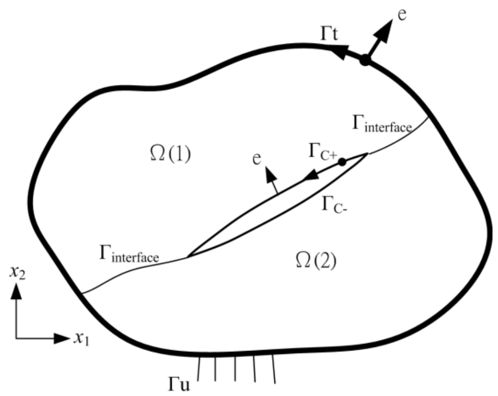

Figure 2 Geometry of a 2-D cracked domain (multiple-domain BEM).

2.2 Calculation of Stress Intensity Factors

The mixed mode stress intensity factors (SIFs) for anisotropic media can be determined by using the extrapolation method of the relative crack opening displacement (COD), combined with a set of the shape functions. The relative COD is defined as [10]

$$\Delta u_i = \sum_{k=1}^{3} \phi_k \Delta u_i^k \qquad (5)$$

where the subscript i denotes COD component and the superscript k (1,2,3) denotes the CODs at nodes $\xi = -\frac{2}{3}, 0, \frac{2}{3}$, respectively. The shape functions f_k are those introduced by [10]

$$\begin{aligned} f_1 &= \frac{3\sqrt{3}}{8}\sqrt{\xi+1}[5-8(\xi+1)+3(\xi+1)^2], \\ f_2 &= \frac{1}{4}\sqrt{\xi+1}[-5+18(\xi+1)+9(\xi+1)^2] \qquad (6) \\ f_3 &= \frac{3\sqrt{3}}{8\sqrt{5}}\sqrt{\xi+1}[1-4(\xi+1)+3(\xi+1)^2] \end{aligned}$$

For this case, the relation of the CODs at a distance r behind the crack-tip and the SIFs can be found as [10, 12, 13]

$$\begin{aligned} \Delta u_1 &= 2\sqrt{\frac{2r}{\pi}}(H_{11}K_I + H_{12}K_{II}) \\ \Delta u_2 &= 2\sqrt{\frac{2r}{\pi}}(H_{21}K_I + H_{22}K_{II}) \end{aligned} \qquad (7)$$

where

$$\begin{aligned} H_{11} &= \mathrm{Im}\left(\frac{\mu_2 P_{11} - \mu_2 P_{12}}{\mu_1 - \mu_2}\right);\ H_{12} = \mathrm{Im}\left(\frac{P_{11} - P_{12}}{\mu_1 - \mu_2}\right) \\ H_{21} &= \mathrm{Im}\left(\frac{\mu_2 P_{21} - \mu_2 P_{22}}{\mu_1 - \mu_2}\right);\ H_{22} = \mathrm{Im}\left(\frac{P_{21} - P_{22}}{\mu_1 - \mu_2}\right) \end{aligned} \qquad (8)$$

Substituting the CODs into the equation (5) and equation (7), we obtain a set of algebraic equations which the SIFs KI and KII can be solved. A sign convention for the corresponding SIFs is shown in Figure 3. Using the relative COD, the sign of SIFs can then be determined.

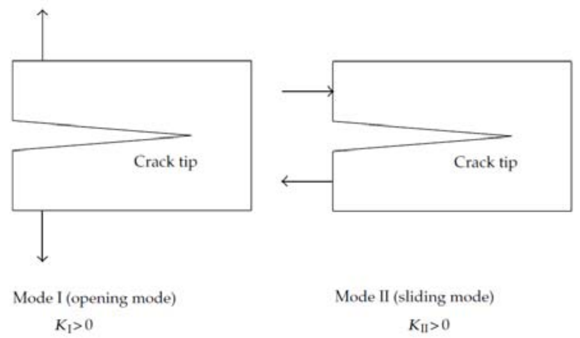

Figure 3 Sign convention used for determining SIFs in mode I and mode II.

2.3 Calculation of Fracture Toughness

In this paper, we consider a thin circular disc of radius R and thickness t with a central crack of length 2*a*, loaded by a pair of concentrated and diametral compressive loads W (Figure 4), the normalized SIFs defined as F_I and F_{II} are equal to

$$F_I = K_I/K_0;\ F_{II} = K_{II}/K_0 \qquad (9)$$

$$K_0 = \frac{W}{\pi R t}\sqrt{\pi a} \qquad (10)$$

where K_I and K_{II} are the SIFs of mode I and II.

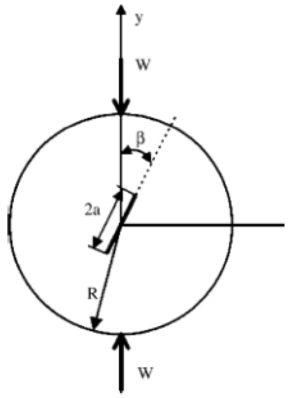

Figure 4 Geometry of cracked Brazilian disc

Substituting the normalized SIFs (F_I, F_{II}) at the crack tip into Equation (9), we get the critical values of SIFs (K_{IC}, K_{IIC}) which are defined as the Fracture Toughness.

In fracture mechanics, there are three criteria commonly used to predict the crack initiation angle: the maximum tensile stress criterion, or σ-criterion [14]; the maximum energy release rate criterion, or G-criterion [15] and the minimum strain energy density criterion, or S-criterion [16]. Among them, the σ-criterion has been found to predict well the directions of crack initiation compared to the experimental results for polymethylmethacrylate [17, 18] and brittle clay [19]. Because of its simplicity, the σ-criterion seems to be the most popular criterion in mixed mode I-II fracture studies [2]. Therefore, the σ-criterion was used in this paper to determine the crack initiation angle for anisotropic plates to predict the crack propagation.

For anisotropic materials, the general form of the elastic stress field near the crack tip in the local Cartesian coordinates $x'' - y''$ in Figure 5 can be expressed in terms of the two stress intensity factors K_I and K_{II} as follows [12]

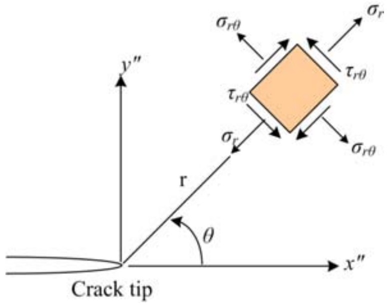

Figure 5 Crack tip coordinate system and stress components.

$$\sigma_{x''} = \frac{K_I}{\sqrt{2\pi r}} \mathrm{Re}\left[\frac{\mu_1\mu_2}{\mu_1 - \mu_2}\left(\frac{\mu_2}{\sqrt{\cos\theta + \mu_2 \sin\theta}} - \frac{\mu_1}{\sqrt{\cos\theta + \mu_1 \sin\theta}}\right)\right] + \frac{K_{II}}{\sqrt{2\pi r}} \mathrm{Re}\left[\frac{1}{\mu_1 - \mu_2}\left(\frac{\mu_2^2}{\sqrt{\cos\theta + \mu_2 \sin\theta}} - \frac{\mu_1^2}{\sqrt{\cos\theta + \mu_1 \sin\theta}}\right)\right]$$

$$\sigma_{y''} = \frac{K_I}{\sqrt{2\pi r}} \mathrm{Re}\left[\frac{1}{\mu_1 - \mu_2}\left(\frac{\mu_1}{\sqrt{\cos\theta + \mu_2 \sin\theta}} - \frac{\mu_2}{\sqrt{\cos\theta + \mu_1 \sin\theta}}\right)\right] + \frac{K_{II}}{\sqrt{2\pi r}} \mathrm{Re}\left[\frac{1}{\mu_1 - \mu_2}\left(\frac{1}{\sqrt{\cos\theta + \mu_2 \sin\theta}} - \frac{1}{\sqrt{\cos\theta + \mu_1 \sin\theta}}\right)\right]$$

$$\tau_{x''y''} = \frac{K_I}{\sqrt{2\pi r}} \mathrm{Re}\left[\frac{\mu_1\mu_2}{\mu_1 - \mu_2}\left(\frac{1}{\sqrt{\cos\theta + \mu_1 \sin\theta}} - \frac{1}{\sqrt{\cos\theta + \mu_2 \sin\theta}}\right)\right] + \frac{K_{II}}{\sqrt{2\pi r}} \mathrm{Re}\left[\frac{1}{\mu_1 - \mu_2}\left(\frac{\mu_1}{\sqrt{\cos\theta + \mu_1 \sin\theta}} - \frac{\mu_2}{\sqrt{\cos\theta + \mu_2 \sin\theta}}\right)\right] \quad (11)$$

Using coordinate transformation, the stress fields near the crack tip in the polar coordinates (r, θ) in Figure 5 is as follows

$$\begin{aligned} \sigma_\theta &= \frac{\sigma_{x''} + \sigma_{y''}}{2} - \frac{\sigma_{x''} - \sigma_{y''}}{2}\cos 2\theta - \tau_{x''y''}\sin 2\theta \\ \tau_\theta &= -\frac{\sigma_{x''} - \sigma_{y''}}{2}\sin 2\theta + \tau_{x''y''}\cos 2\theta \end{aligned} \quad (12)$$

If the maximum σ-criterion is used, the angle of crack initiation, θ_0, must satisfy

$$\frac{\partial\sigma_\theta}{\partial\theta} = 0 \ \ (\text{or } \tau_{r\theta} = 0) \text{ and } \frac{\partial^2\sigma_\theta}{\partial\theta^2} < 0 \quad (13)$$

A numerical procedure was applied to find the angle θ_0 when σ_θ is a maximum for known values of the material elastic constants, the anisotropic orientation angle ψ and the crack geometry.

Since the proposed BEM formulation is simple and can be used for any kind of crack geometry, it is straightforward to extend to analyze the crack propagation in anisotropic materials. The process of crack propagation in anisotropic homogeneous material under mixed mode I-II loading is simulated by incremental crack extension with a piecewise linear discretization. For each incremental analysis, the crack extension is conveniently modeled by a new boundary element. A computer program has been developed to automatically generate new data required for sequentially analyzing the changing boundary configuration. Based on the calculation of the SIFs and crack initiation angle for each increment, the procedure of crack propagation can be simulated. The steps in the crack propagation process are summarized as follows (Figure 6)

(i) compute the SIFs using the proposed BEM formulation;

(ii) determine the angle of crack initiation based on the maximum circumferential stress criterion;

(iii) extend the crack by a linear element of length selected by the user along the direction determined in step (ii);

(iv) automatically generate the new BEM mesh;

(v) repeat all of the above steps until the crack is near the outer boundary.

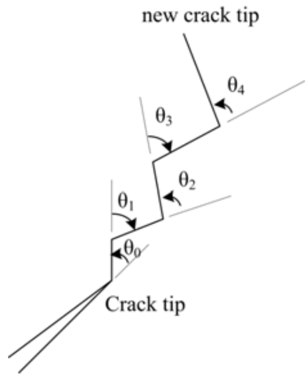

Figure 6 Process of crack propagation by increasing the number of linear elements

3 BEM in fracture mechanics applications

We concentrate on the development of the single-domain BEM using the FORTRAN programming language, which is then applied to anisotropic rock of fracture mechanics problems. In this section, the following numerical examples are presented to verify the computer program and to show the efficiency and versatility of the present BEM method for problems related to fractures in anisotropic rock.

3.1 Stress intensity factors

Example 1: Isotropic Cracked Brazilian Disc

The geometry of the problem is that of a thin circular disc of radius R and thickness t with a central crack of length 2*a*, loaded with a pair of concentrated and diametral compressive load W, as shown in Figure 4. Two cases are analyzed: (1) a/R = 0.5, the crack angle β varies between 0 and π/2, and (2) β = 45°, a/R varies between 0.1 and 0.7. The two normalized SIFs, F_I and F_{II}, calculated with the BEM program for these two cases, are compared with those obtained numerically by Atkinson et al. [4] and Chen et al. [6]. The results are shown in Tables 1 and 2. In general, a good agreement is found among these three methods.

Table 1 Normalized SIFs for a central slant in an isotropic Brazilian disc subjected to a concentrated load (a/R = 0.5.)

β(rad.)	Atkinson et al. [4]		Chen et al. [6]		This study	
	F_I	F_{II}	F_I	F_{II}	F_I	F_{II}
0	1.387	0	1.339	0	1.343	0
π/16	0.970	-1.340	0.960	-1.275	0.952	-1.281
2π/16	0.030	-2.113	0.074	-2.061	0.056	-2.052
3π/16	-0.946	-2.300	-0.903	-2.275	-0.915	-2.262
π/4	-1.784	-2.132	-1.737	-2.103	-1.749	-2.098
5π/16	-2.446	-1.728	-2.377	-1.711	-2.395	-1.714
6π/16	-2.885	-1.188	-2.826	-1.197	-2.851	-1.202
7π/16	-3.127	-0.604	-3.092	-0.614	-3.123	-0.617
π/2	-3.208	0	-3.180	0	-3.213	0

Table 2 Normalized SIFs for a central slant in an isotropic Brazilian disc subjected to a concentrated load (β = 45°)

a/R	Atkinson et al. [4]		Chen et al. [6]		This study	
	F_I	F_{II}	F_I	F_{II}	F_I	F_{II}
0.1	-1.035	-2.010	-1.020	-1.968	-1.018	-1.965
0.2	-1.139	-2.035	-1.116	-1.995	-1.116	-1.992
0.3	-1.306	-2.069	-1.272	-2.036	-1.277	-2.029
0.4	-1.528	-2.100	-1.484	-2.069	-1.492	-2.065
0.5	-1.784	-2.132	-1.737	-2.103	-1.749	-2.098
0.6	-2.048	-2.200	-2.020	-2.148	-2.039	-2.139
0.7	N.A.	N.A.	-2.337	-2.213	-2.364	-2.224

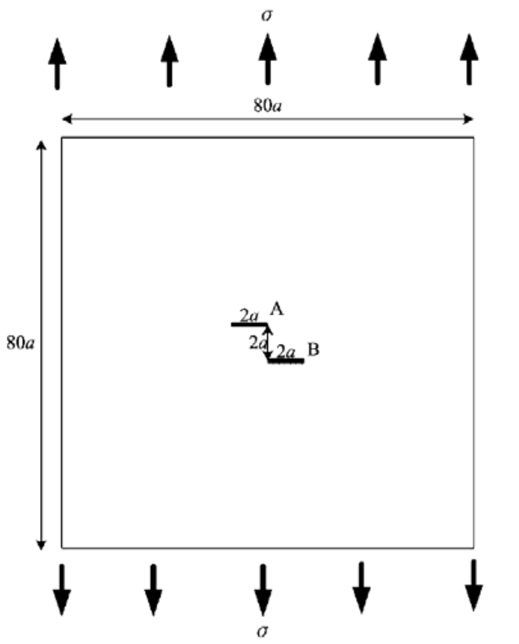

Figure 7 Square plate with two parallel cracks.

Example 2: Two parallel cracks in the finite plate with an offset under a uniform tension.

The geometry is that of a square plate and is shown in Figure 7. For the comparison, crack length is taken as $2a=2$. The stress intensity factors at cracks tip A and B are listed in Table I together with those from Dwyer [20], who used an edge function method and the results from Rooke and Cartwright [21] for an infinite body. It is obvious from Table 3 that these are very close to those obtained by the other researchers.

Table 3 Comparison of normalized SIFs for two parallel cracks with an offset in the finite plate.

tip	Dwyer [20]		Rooke and Cartwright [21]		This study	
	F_I	F_{II}	F_I	F_{II}	F_I	F_{II}
A	1.725	-0.197	1.770	-0.216	1.738	-0.1992
B	1.866	-0.0693	1.860	-0.0813	1.868	-0.0801

Example 3: Horizontal Crack in Material #1. (Bi-material case)

A horizontal crack under uniform pressure P is shown in Figure 8. The crack, whose length is 2a, is located distance d from the interface. The Poisson's ratios for materials #1 and #2 are $\nu_{\#1} = \nu_{\#2} = 0.3$, and the ratio of the shear modulus $G_{\#2}/G_{\#1}$ varies. A plane stress condition is assumed. The results are given in Table 4 for various values of the shear modulus ratio. They are compared to the results of Isida and Noguchi [22], who used a body force integral equation method, and those of Ryoji and Sang-Bong [23], who used a multi-domain BEM formulation. As it can be seen in this table that the results are in agreement.

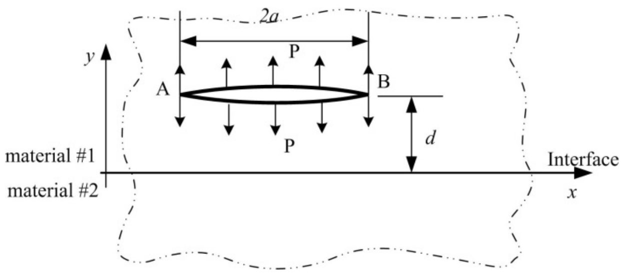

Figure 8 A horizontal crack under uniform pressure in material #1 of an infinite bi-material.

Table 4 Comparison of SIFs (horizontal crack)

d/2*a*	$G_{\#2}/G_{\#1}$	Isida and Noguchi [22]		Ryoji and Sang-Bong [23]		This study	
		F_I	F_{II}	F_I	F_{II}	F_I	F_{II}
0.05	0.25	1.468	0.286	1.468	0.292	1.476	0.285
0.5	0.25	1.197	0.074	1.197	0.072	1.198	0.071
0.05	2.0	0.872	-0.087	0.869	-0.085	0.871	-0.088
0.5	2.0	0.935	-0.024	0.934	-0.023	0.936	-0.023

3.2 Effect of degree of anisotropy on SIFs

After accuracy checking, we then treat more challenging problems involving anisotropic plate to run our BEM program for determining SIFs.

Table 5 Three sets of dimensionless elastic constants (ν=0.25).

	E/E'	E/G'
Condition I	1/3 1/2 1 2 3	2.5
Condition II	1	0.5 1.5 2.5 3.5 4.5
Condition II	1	2.5

	ν'
Condition I	0.25
Condition II	0.25
Condition II	0.05 0.15 0.25 0.35 0.45

Example 1: Anisotropic case

In order to evaluate the influence of material anisotropy on the SIFs, consider the rectangular plate of Figure 9. The material is transversely isotropic with the plane of transverse isotropy inclined at an angle ψ with respect to the x-axis. The material has five independent elastic constants (E, E', ν, ν', and G') in the local coordinate system: E and E' are the Young's modulus in the plane of transverse isotropy and in a direction normal to it, respectively; ν and ν' are the Poisson's ratios characterizing the lateral strain response in the plane of transverse isotropy to a stress acting parallel and normal to it, respectively; and G' is the shear moduli in the planes normal to the plane of transverse isotropy. In this example, the anisotropic orientation, ψ varies from 0° to 180°.

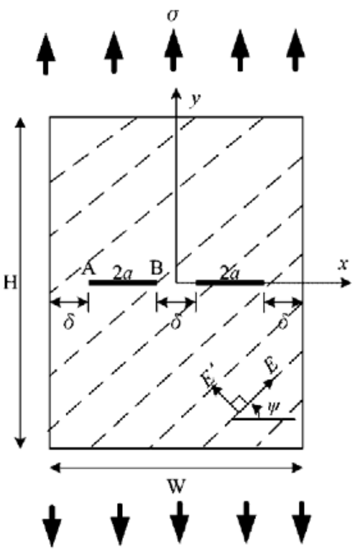

Figure 9 Two collinear cracks in the finite plate under uniaxial tension and orientation of the planes of anisotropy, ψ varies from 0° to 180°.

Three sets of dimensionless elastic constants are considered and are defined as conditions I, II, and III in Table 5. The numerical results are plotted in Figures 10–12 for condition I, II, and III, respectively. The inner tip B results for the isotropic case (E/E'=1, E/G'=2.5, and ν'=0.25) are also shown for comparison as solid lines in Figures 10–12. Analysis of Figures 10–12 reveals several major trends can be underlined as follows.

(1) For conditions I and II, the orientation of the planes of plate anisotropy with respect to the horizontal plane has a strong influence on the value of the inner tip SIFs. The influence is small for condition III. This means that the effect of E/E' and E/G' on the SIFs is more important than that of ν'.

(2) The variation of the SIFs with the anisotropic orientation, ψ is periodic with a 90° period.

(3) There is a greater variation in the SIFs with the orientation angle, ψ for materials having a high degree of anisotropy (E/E'=3 or 1/3; E/G'=0.5 or 4.5).

(4) Figure 10 indicates that the maximum absolute values of the SIFs occur when the loading is parallel to the plane of transverse isotropy (ψ=90°).

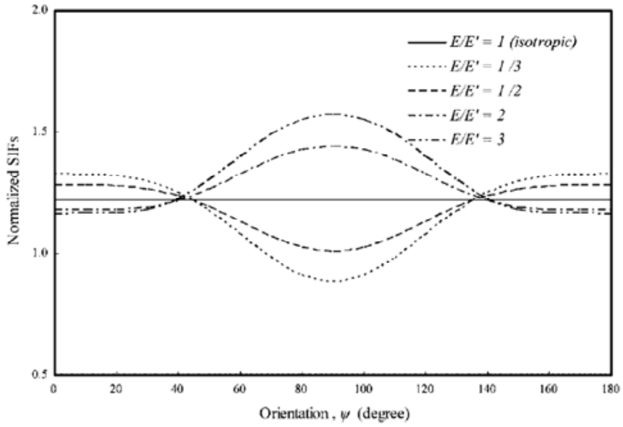

Figure 10 Variation of F_I with the material orientation angle ψ for condition I (β=0°, E/G'=2.5, ν'=0.25).

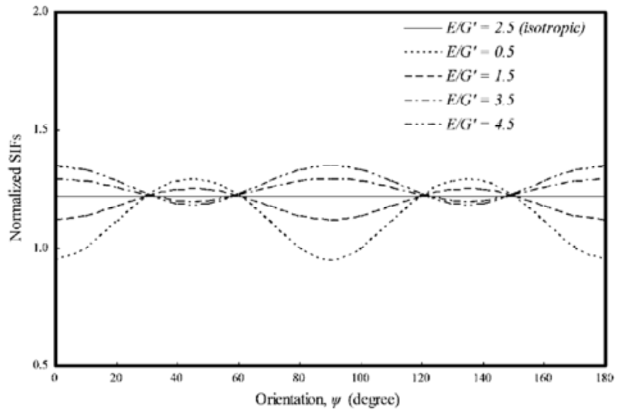

Figure 11 Variation of F_I with the material orientation angle ψ for condition II (β=0°, E/E'=1, ν'=0.25).

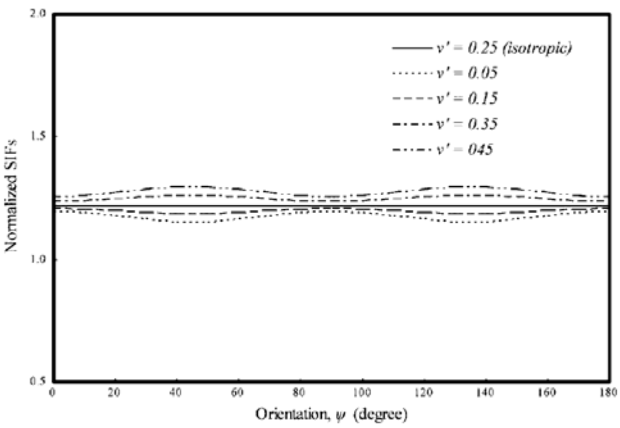

Figure 12 Variation of F_I with the material orientation angle ψ for condition III (β=0°, E/E'=1, E/G'=2.5).

Example 2: Effect of crack angle β when ψ=0°

The variation of the SIFs with the crack angle β for conditions I, II, and III is considered in this example by taking, ψ=0°, and β to vary from 0° to 90° as shown in Figure 13. The variations of the inner tip SIFs with the crack angle β are shown in Figures 14–16 for conditions I, II, and III, respectively.

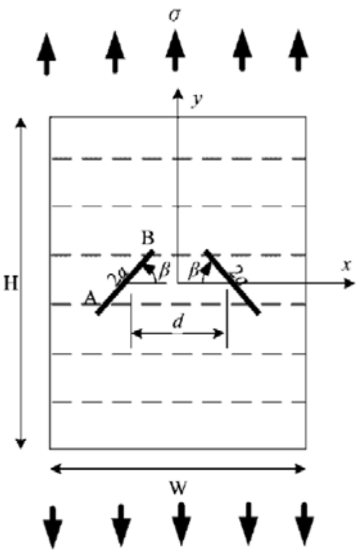

Figure 13 Two inclined cracks in a finite plate under uniaxial tension and orientation of the planes of anisotropy, ψ=0°, and β to vary from 0° to 90°.

For all conditions, the mode I SIF reaches a positive maximum value when the cracks are perpendicular to the applied load (i.e. β=0°) and the distance between two inner tips is closer. On the contrary, the mode I SIF decreases smoothly to be a minimum value when the crack is parallel to the load (i.e. β=90°). The mode II SIF vanishes when the crack angle β=0° or 90° and reaches a maximum absolute value when the crack is oriented at about β=30° to β=45°. Comparison with condition I to condition III we found that E/G' has the greatest effect on the mode I SIFs, and E/E' has the next greatest, and that the influence of ν' is almost negligible.

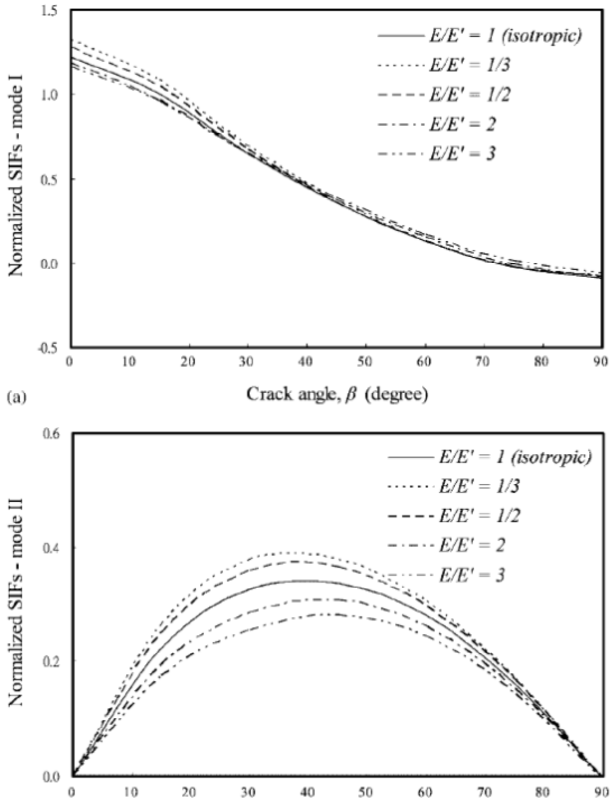

Figure 14 Variation of F_I in (a) and F_{II} in (b) with the crack angle β for condition I (β=0°, E/G'=2.5, ν'=0.25).

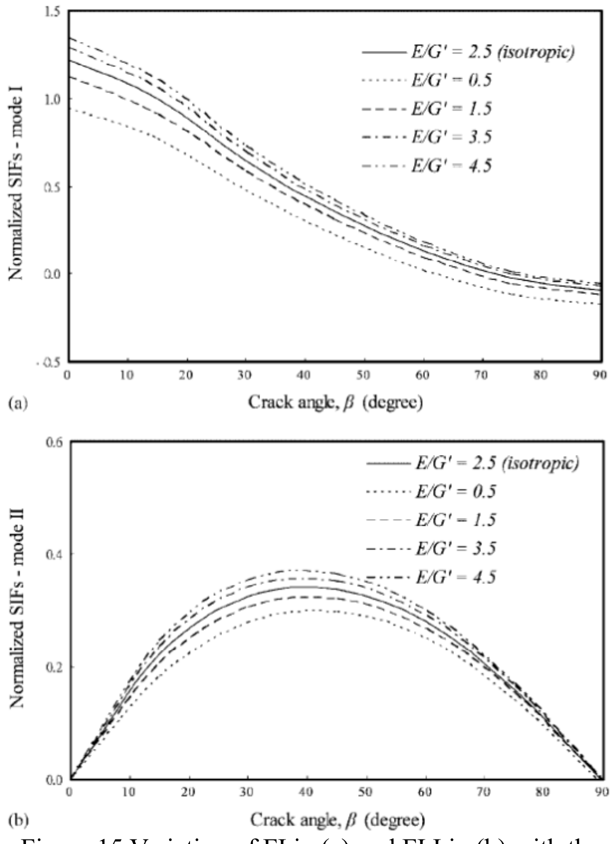

Figure 15 Variation of FI in (a) and FI I in (b) with the crack angle β for condition II (β=0°, E/E'=1, ν'=0.25).

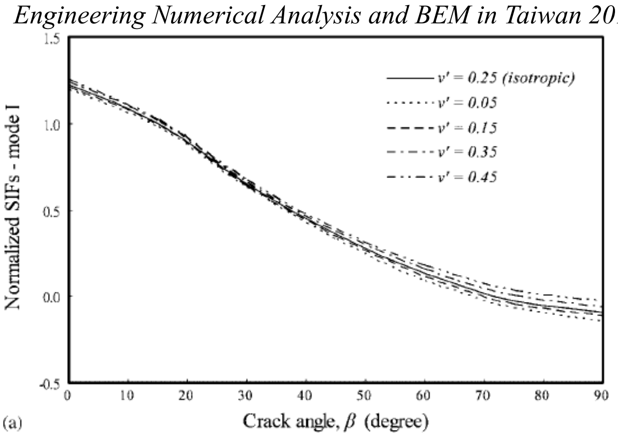

(a)

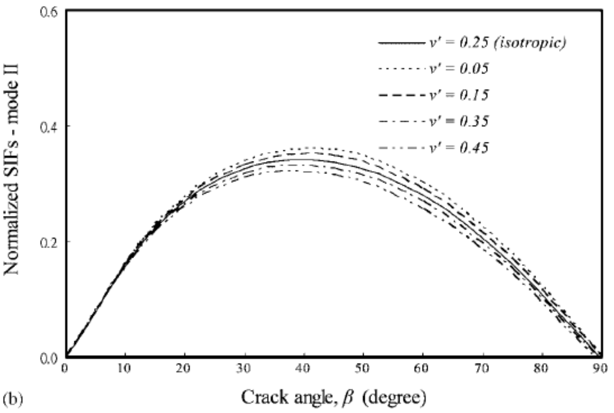

(b)

Figure 16 Variation of FI in (a) and FI I in (b) with the crack angle β for condition III (β=0°, E/E'=1, E/G'=2.5).

3.3 Crack Propagation Path Simulation

Example 1: On Anisotropic Material

To demonstrate the proposed BEM procedure when predicting crack propagation in the anisotropic materials under mixed-mode I-II loading, the propagation path in a CSTBD specimen is numerically predicted and compared with the actual laboratory observations. In these experiments, a crack initially inclined with respect to the applied stress is allowed to grow under concentrated diametrical loading. The Brazilian tests on CSTBD specimens with a diameter of 7.4 cm, a thickness of 1 cm, and a crack length of 2.2 cm are conducted to observe the actual propagation paths and are compared with the numerical predictions.

Details of the experimental procedure can be found in the paper by Ke et al. [24]. The five elastic constants of anisotropic marble are E = 78.302 GPa, E' = 67.681 GPa, ν = 0.267, ν'= 0.185, G = 30.735 GPa, and G' = 25.336 GPa, respectively. The ratios of E/E' and E/G' are 1.156 and 3.091, respectively. Since the value of E/E' = 1.156, this marble can be classified as a slightly anisotropic rock. Two specimens with the material inclination angle ψ = 45°, defined as the AM-4, and DM-4, have crack angles β = 0° and β = 45° respectively. After Brazilian tests with cracked specimens, the paths of crack propagation for AM-4 and DM-4 are shown in Figures 17 and 19, respectively. It can be observed that the crack propagates nearly perpendicular to the crack surface in the initial stage and then rapidly approaches toward the loading point. The proposed BEM procedure is also used to simulate crack propagation in the CSTBD specimens. The outer boundary and crack surface are discretized with 28 continuous and 20 discontinuous quadratic elements, respectively. Figures 18 and 20 are the comparisons of crack propagation paths between experimental observations and numerical predictions in AM4 and DM-4, respectively. Again, the proposed BEM procedure accurately simulates the crack propagation in these anisotropic specimens. According to the simulations of foregoing examples, it can be concluded that the proposed BEM is capable of predicting the crack propagation in anisotropic rocks.

Figure 17 Photograph of specimen AM-4 after failure (ψ = 0° and β = 45°).

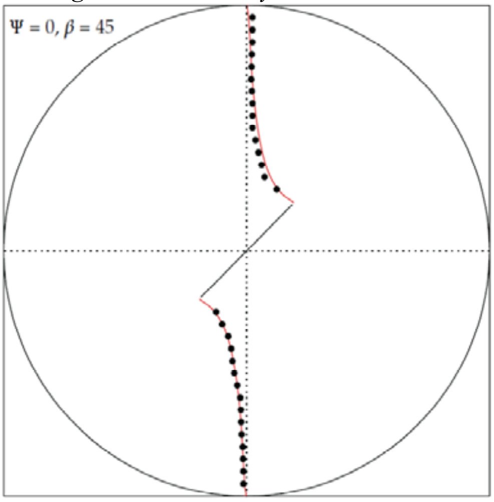

Figure 18 Propagation of a crack at the center of a CSTBD specimen with ψ = 0° and β = 45°. Comparison between experimental observations and numerical predictions for specimen AM-4.

Figure 19 Photograph of specimen DM-4 after failure (ψ = 45° and β = 45°).

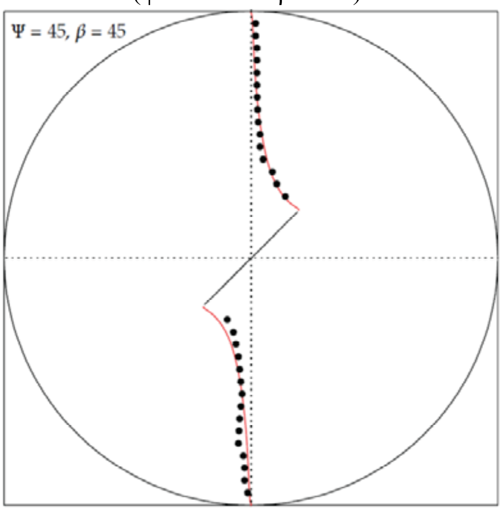

Figure 20 Propagation of a crack at the center of a CSTBD specimen with ψ = 45° and β = 45°. Comparison between experimental observations and numerical predictions for specimen DM-4.

Example 2: On Anisotropic Bi-material

In these experiments, a crack initially inclined with respect to the applied stress is allowed to grow under concentrated diametrical loading (as shown in Figure 21). The anisotropic elastic properties for rocks of types (1) and (2) are given in Table 6. The ratios of E/E' and E/G' are 1.635 and 4.301, respectively. Since the value of E/E' = 1.635, this rock of type (1) can be classified as a slightly anisotropic rock. Two specimens with the material inclination angle ψ = 45°∘ and 0°, defined as the SSD-1 and SSD-2, have crack angles β = 45° and 90°, respectively. After Brazilian tests with cracked bi-material specimens, the paths of crack propagation for SSD-1 and SSD-2 are shown in Figures 22(a) and 23(a), respectively. It can be observed that the crack propagates nearly perpendicular to the crack surface in the initial stage and then rapidly approaches toward the loading point. The proposed BEM procedure is also used to simulate crack propagation in the CSTBD specimens. Figures 22(b) and 23(b) are the comparisons examples; it can be concluded that the proposed BEM is capable of predicting the crack propagation in anisotropic bi-material rocks.

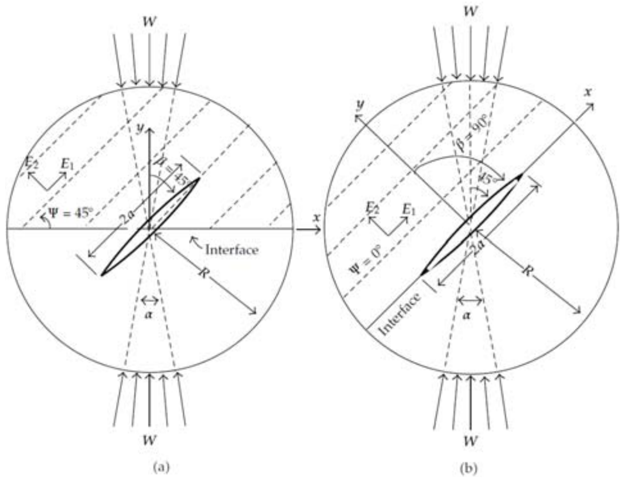

Figure 21 Geometry of a cracked straight through Brazilian disc (CSTBD) specimen of anisotropic Bi-material rock under diametrical loading.

Table 6 Elastic properties for rocks of type (1) and (2)

Rock types	E (GPa)	E' (GPa)	ν	ν'	G (GPa)	G' (GPa)	E/E'	E/G'
(1)	28.04	17.15	0.15	0.12	12.19	6.52	1.635	4.301
(2)	38.95	----	0.254	----	15.530	----	----	----

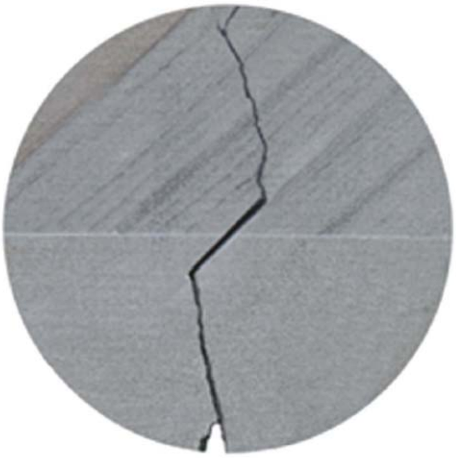

(a)

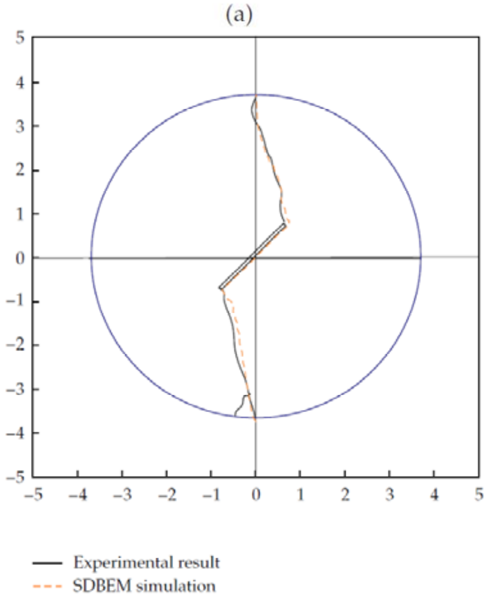

(b)

Figure 22 Comparison between experimental observations and numerical predictions for specimen SSD-1: (a) photograph of specimen SSD-1 after failure $\psi = 45°$ and $\beta = 45°$ and (b) propagation of a crack at the center of a CSTBD specimen with $\psi = 45°$ and $\beta = 45°$.

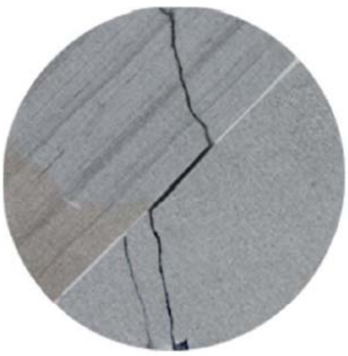

(a)

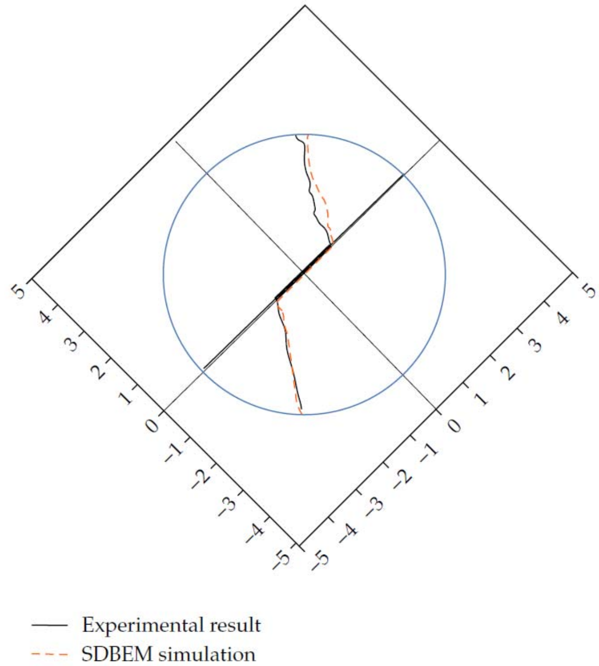

(b)

Figure 23 Comparison between experimental observations and numerical predictions for specimen SSD-2: (a) photograph of specimen SSD-2 after failure $\psi = 0°$ and $\beta = 90°$ and (b) propagation of an interfacial crack at the center of a CSTBD specimen with $\psi = 0°$ and $\beta = 90°$.

3.4 Fracture Toughness of Anisotropic Rock

From the experimental investigations carried out the following parameters were obtained: unit weight $\gamma = 16.59 KN/m^3$, water content $\omega = 0.11\%$, uniaxial compression strength $q_u = 76.43$ MPa for $\psi = 0°$, and $q_u = 22.93$ MPa for $\psi = 90°$. The elastic constants of the marble were determined by conducting Brazilian tests with gluing a 45° strain gage rosette on the center of each disc. Details of the procedure can be found in the paper by Chen et al. [6]. The five elastic constants of anisotropic marble are E = 78.302GPa, E'= 67.681GPa, ν = 0.267, ν' = 0.185, G = 30.735GPa, and G' = 25.336 GPa, respectively. The ratios of E/E', and E/G' are 1.156 and 3.091, respectively. Since the value of E/E' = 1.156, this marble can be classified as a slightly anisotropic rock.

Using a thin line saw with a thickness of 0.05 cm to cut down the V-shaped convex parts, the Cracked Straight Through Brazilian Disc (CSTBD) specimens were made. After preparation, the CSTBD specimens had a crack with a thickness of about 0.05cm and a ratio between the crack length and the disc radius a/R of about 0.3. A total of 39 CSTBD specimens were prepared with different values of the dip angle of the planes of rock anisotropy ψ = 0°, 15°, 30°, 45°, 60°, 75°, and 90° with different values of the angle β between the crack and loaded diameter. The test specimen characteristics are listed in Table 7. All specimens were brought to failure under a line load at a slow deformation rate of 0.5mm/min. by using a 100t MTS loading system. The testing requires only recording of the maximum load. The procedure used to determine the fracture toughness of the marble in mode I (K_{IC}), mode II (K_{IIC}) and mixed-mode (K_I, K_{II}) was as follows

(i) Determine the elastic properties of the marble;

(ii) Use the BEM to calculate the normalized SIFs (F_I and F_{II}). The input geometry (ψ, β, and a/R) should obviously be the same as that in the experiments;

(iii) Conduct diametral loading of a CSTBD specimen with a certain crack angle β and record the failure load; and

(iv) Calculate the fracture toughness using Equations (9) and (10).

The results of the BEM analysis are shown in Figures 24 to 30.These seven figures can then be used to determine the angle β_I corresponding to pure mode I (K_{II} = 0) and the angle β_{II} corresponding to pure mode II (K_I = 0). Furthermore, in order to determine the fracture toughness under mixed-mode loading, we select the angles β_M = 10°, 20°, 30°, 45° and 60° for ψ = 0°, 15°, 30°, 45°, 60°, 75°, and 90° to evaluate the mixed-mode fracture toughness. From the failure loads recorded by laboratory testing of discs oriented with an initial crack inclined at β_I , β_{II} or β_M, the critical SIF or fracture toughness in mode I (K_{IC}), mode II (K_{IIC}) and that in mixed-mode I–II (K_I and K_{II}) could be determined.

The values of the failure load W_f and the fracture toughness for the marble are reported in Table 8 when ψ = 0°, 15°, 30°, 45°, 60°, 75°, and 90°. The negative sign of K_{IC} and K_{IIC} in Table 8 is associated with the adopted sign convention of the mode I and mode II SIF.

From the theoretical analysis, it can be established that pure mode I type fracture occurs when β_I is about 0° and pure mode II type fracture occurs when β_{II} is about 25° to 28° for seven different material orientation angles. Table 8 lists the maximum failure load, mixed mode fracture at different crack inclination angles (β) and material orientation angles (ψ). It can be found that the absolute values of both K_{IC} and K_{IIC} decrease as increases and the values of the tensile strength [25] of anisotropic marble also decrease as increases (see Table 9).

It means that the pure mode I, pure mode II fracture toughness depend on the mechanical properties of rocks. In addition, we can find that the mode I fracture toughness (K_I or K_{IC}) is usually smaller than the mode II fracture toughness (K_{II} or K_{IIC}) when the crack inclination angle (β) is less than 60°. Therefore, KI reaches K_{IC} before K_{II} reaches K_{IIC}, which inevitably leads to mode I fracture. If β is larger than 60°, i.e. K_{II} reaches K_{IIC} before K_I reaches K_{IC}, it should leads to mode II fracture. The experimental results indicate that the mixed mode fracture toughness depends on the rock properties, crack inclination angle and anisotropic orientation.

3.5 **Fracture Criterion**

Based on the experimental results for anisotropic marble, a regression analysis was conducted to obtain the fracture criterion. In general, two types of fracture criterion curves, i.e. elliptic and quadratic curves, were considered. The experiment results were distributed over the first and the second quadrant, but the elliptic equation form $(K_I/K_{IC})^\alpha + (K_{II}/K_{IIC})^\alpha = 1$ is only suitable for the first quadrant.

Therefore, the quadratic equation form K_{II}/K_{IIC} =

$a(K_I/K_{IC})^2 + b(K_I/K_{IC}) + c$ is well suitable for applying to the experimental results. Figure 31 shows the fracture criterion of anisotropic marble. The equation of the fracture criterion of a quadratic fit which was found suitable for anisotropic marble is given as

$$K_{II}/K_{IIC} = -0.21(K_I/K_{IC})^2 - 0.59(K_I/K_{IC}) + 0.74 \qquad (14)$$

If Eq. (14) is satisfied, the point (K_I/K_{IC}, K_{II}/K_{IIC}) plots above the fracture envelope and crack initiation will occur. Otherwise, no crack initiation will occur when the point is below the fracture envelope.

4 Conclusions

A formulation of the BEM, based on the relative displacements near the crack tip, is utilized to determine the mixed-mode SIFs of anisotropic rocks. Numerical examples for the determination of the mixed-mode SIFs for a CSTBD specimen are presented for isotropic and anisotropic media. The numerical results obtained by the proposed method are in good agreement with those reported by previously published results. In addition, the SIFs for various crack geometry and loading type such as multiple cracks under far-field tensile stress and a cracked body hanging by its own weight are also determined by the proposed BEM formulation. The numerical results obtained by this study are in agreement with those reported by previously published results.

This paper presents the development of BEM procedure based on the maximum circumferential stress criterion for predicting the crack initiation directions and propagation paths in isotropic and anisotropic materials under mixed-mode loading. Good agreements are found between crack initiation and propagation predicted with the BEM and experimental observations reported by previous researchers of isotropic materials. Numerical simulations of crack initiation and propagation in CSTBD specimens of the anisotropic rock are also found to compare well with experimental results.

Calculation of the SIFs is conducted for several situations, like cracks along or off an interface. Numerical results show that the proposed method is very accurate even with relatively coarse mesh discretization. In addition, the proposed BEM program is not only very accurate but also very fast. The calculation time for each example is typically 30s by BEM code with a Personal Computer, PC (Intel Pentium 4, 2.4 GHz CPU, 1GB RAM).

References

[1] J. Toribio, V. Kharin: The reliability of the fracture mechanics approach to environmentally assisted cracking: 2. Engineering safe design, Mater. Design, 18(2), pp.95-101, 1997.

[2] B.N. Whittaker, R.N. Singh, Gexin Sun: Rock Fracture Mechanics: Principles, Design and Applications, Academic Press, Amsterdam, The Netherlands, 1992.

[3] H. Awaji, S. Sato: Combined mode fracture toughness measurement by the disk test, Trans. ASME, J. Eng. Mater. Tech. 100(4), pp.175–182, 1978.

[4] C. Atkinson, R. E. Smelser, J. Sanchez: Combined mode fracture via the cracked Brazilian disk test, Int. J. Fracture, 18(4), pp. 279–291, 1982.

[5] I.L. Lim, I. W. Johnston, S. K. Choi, J. N. Boland: Fracture testing of a soft rock with semi-circular specimens under three-point bending. Part 2: Mixed-mode. Int. J. Rock Mech. Min. Sci. 31(3), pp.185–197, 1994.

[6] C.S. Chen, E. Pan, B. Amadei: Fracture mechanics analysis of cracked discs of anisotropic rock using the boundary element method, Int. J. Rock Mech. Min. Sci. 35(2), pp. 195–218, 1998.

[7] N. A. Al-Shayea: Crack propagation trajectories for rocks under mixed mode I-II fracture, Engineering Geology, 81(1), pp.84–97, 2005.

[8] E. Pan, F.G. Yuan: Boundary element analysis of three-dimensional cracks in anisotropic solids, Int. J. Numer. Meth. Engng., 48, pp.211-237, 2000.

[9] V. Lazarus, J.B. Leblond, S.E. Mouchrif: Crack front rotation and segmentation in mixed mode I+III or I+II+III. Part I: Calculation of stress intensity factors, J. Mech. Physics Solids, 49, pp.1399-1420, 2001.

[10] E. Pan: A general boundary element analysis of 2-D linear elastic fracture mechanics, Int. J. Fracture, 88(1), pp. 41–59, 1997.

[11] G. Tsamasphyros, G. Dimou: Gauss quadrature rules for finite part integrals, Int. J. Numer. Meth. Engng., 30(1), pp.13–26, 1990.

[12] G.C. Sih, P.C. Paris, G.R. Irwin: On cracks in rectilinearly anisotropic bodies, Int. J. Fracture, 3, pp.189 – 203, 1965.

[13] P. Sollero, M.H. Aliabadi: Fracture mechanics analysis of anisotropic plates by the boundary element method, Int. J. Fracture, 64(4), pp. 269 – 284, 1993.

[14] F. Erdogan, G.C. Sih: On the crack extension in plates under loading and transverse shear, J. Basic Engng. 58, pp. 519–527, 1963.

[15] K. Palaniswamy, W.G. Knauss: Propagation of a crack under general, in-plane tension, Int. J. Fracture Mech., 8(1), pp.114–117, 1972.

[16] G.C. Sih: Strain-energy-density factor applied to mixed mode crack problems, Int. J. Fracture, 10(3), pp.305–321,

1974.

[17] C.W. Woo, L.H. Ling: On angle crack initiation under biaxial loading, J. Strain Anal. Eng. Design, 19(1), pp. 51–59, 1984.

[18] H.A. Richard: Examination of brittle fracture criteria for overlapping mode I and mode II loading applied to cracks, In Application of Fracture Mechanics to Materials and Structures, G. C. Sih et al., Ed., pp. 309–316, Martinus Nijhoff, 1984.

[19] L.E. Vallejo: The brittle and ductile behavior of a material containing a crack under mixed-mode loading, In Proceedings of the 28th U.S. Symposium on Rock Mechanics, University of Arizona, Tucson, Ariz, USA, 1987.

[20] J.F. Dwyer: Edge function analysis of crack interaction in anisotropic materials. Eng. Fracture Mech., 56(2), pp.233–248, 1997.

[21] D.P. Rooke, D.J. Cartwright: Compendium of stress intensity factor. Her majesty's stationary office, London, 1974.

[22] M. Isida, H. Noguchi: Plane problems of arbitrarily oriented cracks in bonded dissimilar materials, Tran. Japan Soc. Mech. Eng., 49, pp. 36–45, 1983.

[23] Y. Ryoji, C. Sang-Bong: Efficient boundary element analysis of stress intensity factors for interface cracks in dissimilar materials, Eng. Fracture Mech., 34(1), pp.179–188, 1989.

[24] C.C. Ke, C.S. Chen, C.H. Tu: Determination of fracture toughness of anisotropic rocks by boundary element method, Rock Mech. Rock Eng., 41(4), pp.509–538, 2008.

[25] S.C. Hsu: Determination of tensile strength of anisotropic rocks. M.S. Thesis, National Cheng Kung University, pp. 108, 2000. (In Chinese)

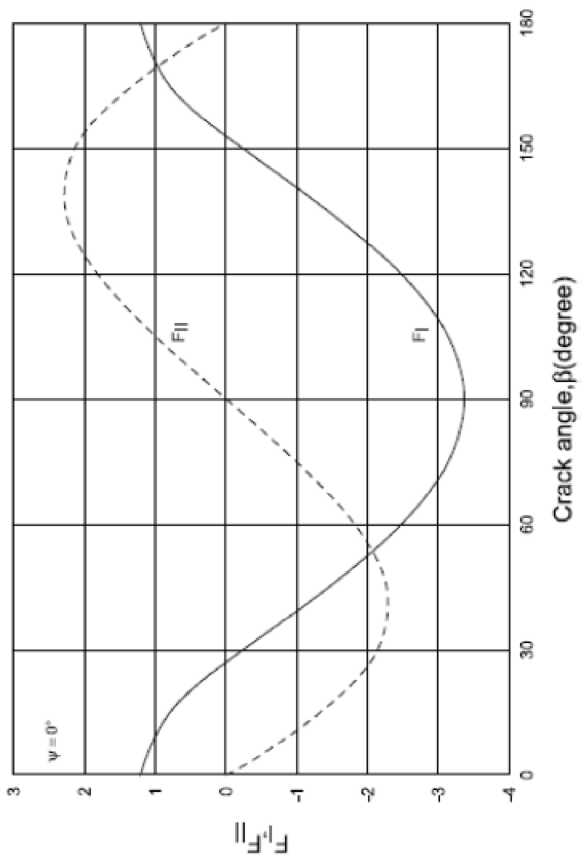

Figure 24 ψ=0°, β=0~180°

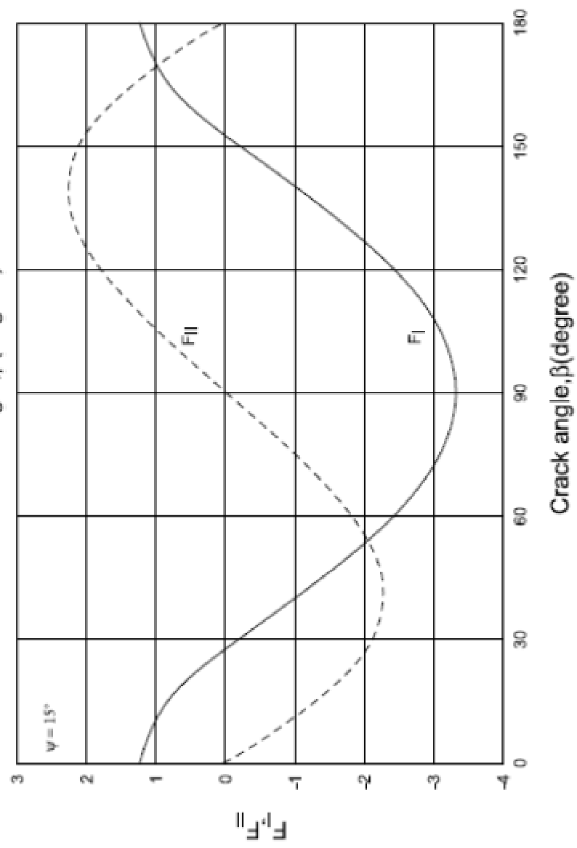

Figure 25 ψ=15°, β=0~180°

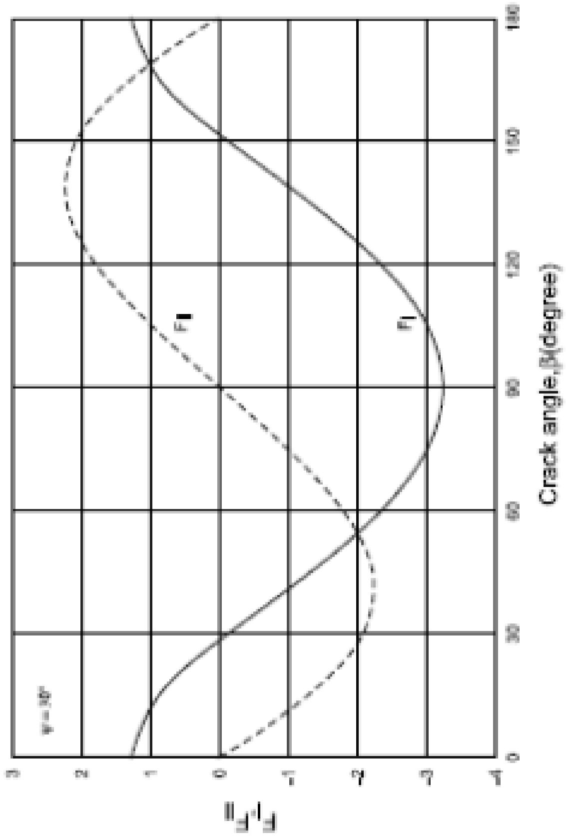

Figure 26 ψ=30°, β=0~180°

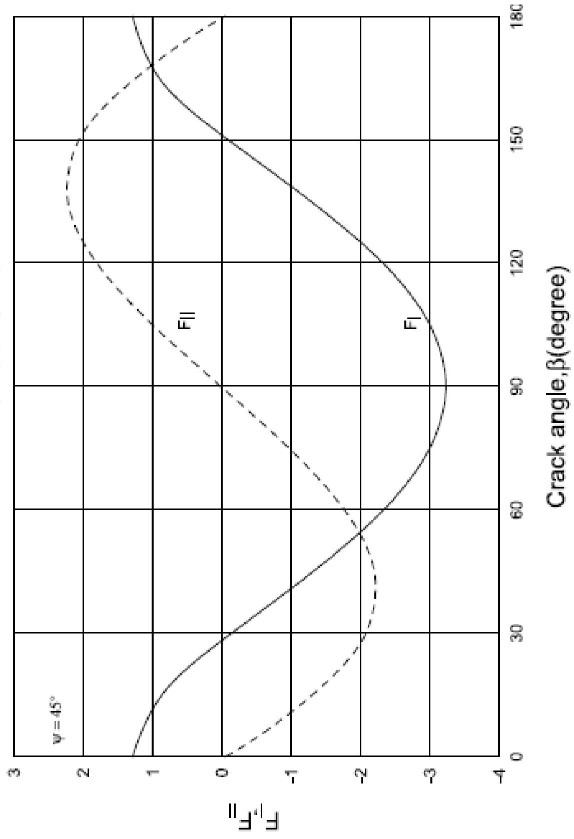

Figure 27 ψ=45°, β=0~180°

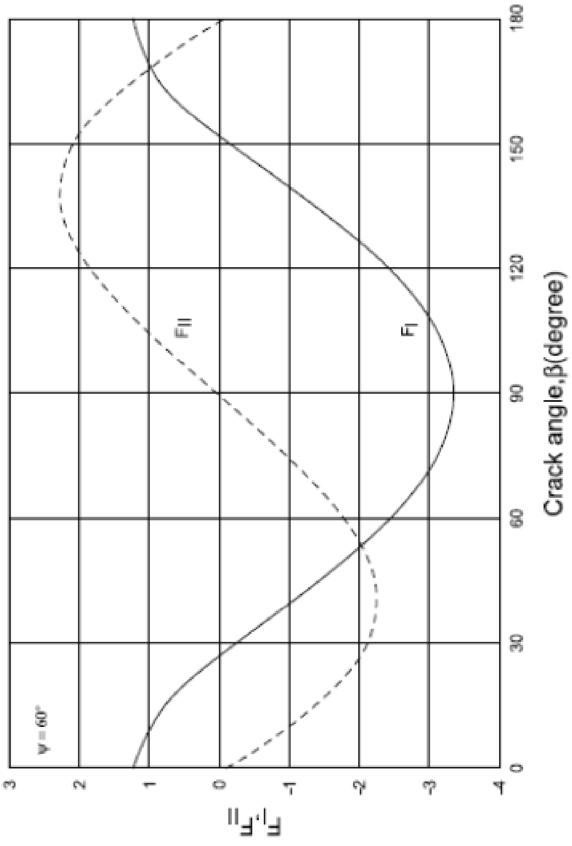

Figure 28 ψ=60°, β=0~180°

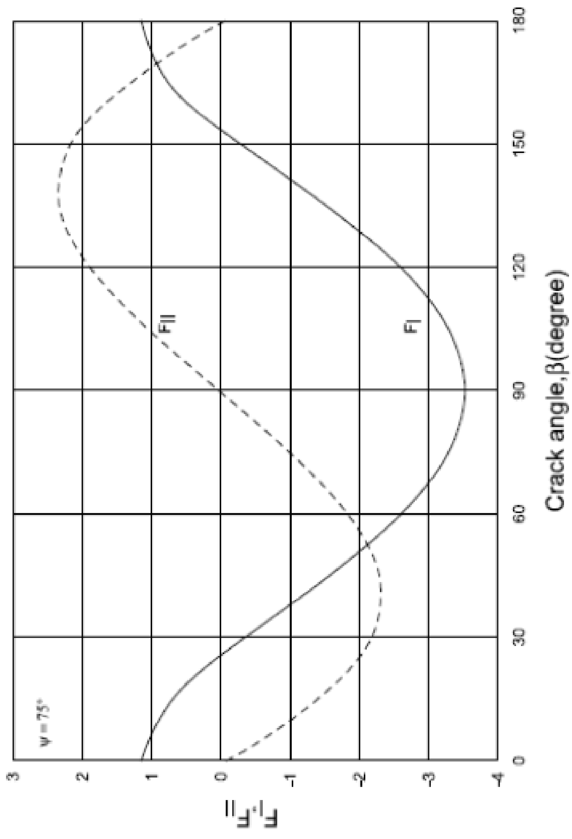

Figure 29 ψ=75°, β=0~180°

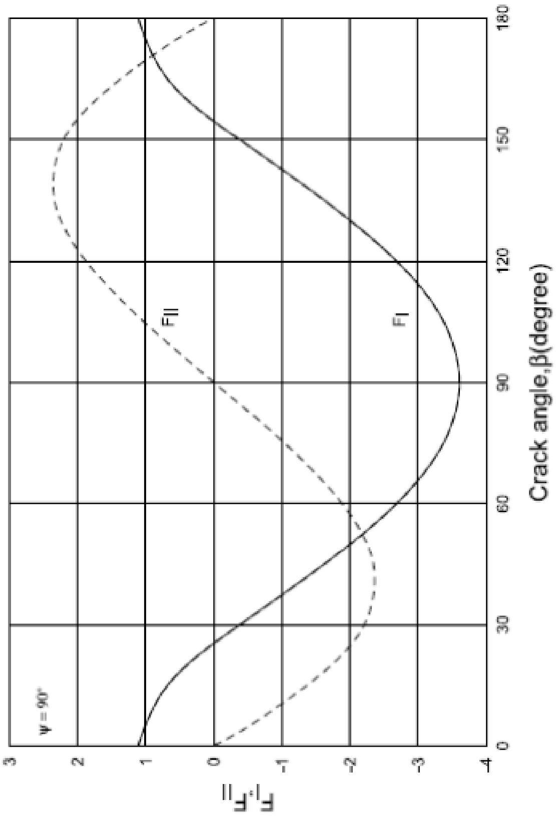

Figure 30 ψ=90°, β=0~180°

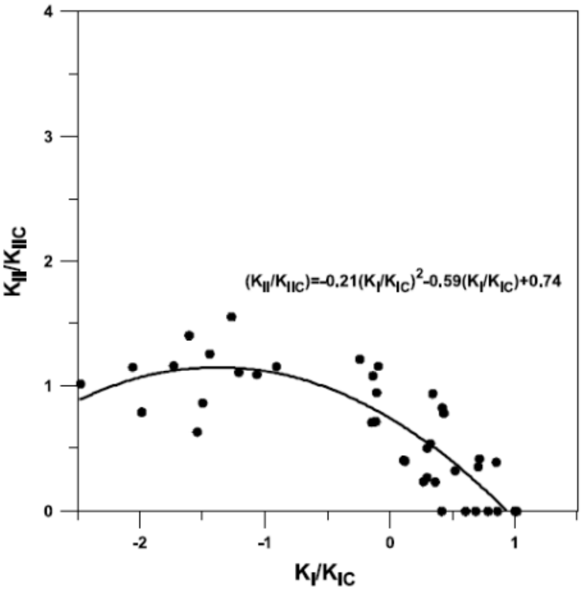

Figure 31 Mixed mode fracture criterion of anisotropic marble

Table 7 the ratios K_I/K_{IC} and K_{II}/K_{IIC}

ψ	0°	15°	30°	45°	60°	75°	90°
K_I/K_{IC}	1.000	1.015	0.861	0.785	0.687	0.605	0.414
	0.362	0.851	0.717	0.706	0.297	0.268	0.522
	0.431	0.325	0.419	0.298	0.122	0.109	0.343
	-0.145	-0.113	-0.094	-0.106	-0.137	-0.241	-0.422
	-1.442	-1.210	-0.909	-1.065	-1.731	-1.498	-1.606
	-1.987	-1.543	-2.059				-2.476
K_{II}/K_{IIC}	0	0.000	0.000	0.000	0.000	0.000	0.000
	0.233	0.390	0.417	0.354	0.267	0.235	0.321
	0.783	0.540	0.826	0.503	0.398	0.405	0.939
	0.177	0.718	1.161	0.947	1.080	1.216	1.474
	1.259	1.109	1.158	1.091	1.165	0.864	1.406
	0.791	0.635	1.152				1.016

Table 8 Measured failure load W_f and calculated values of K_I, K_{II}, K_{IC} and K_{IIC}

No.	ψ	β	t(cm)	a/R	$W_f(KN)$	K_I or $K_{IC}(\mathrm{MPa}\sqrt{m})$	K_{II} or $K_{IIC}(\mathrm{MPa}\sqrt{m})$	Remark
A-1	0°	0.5°	1.052	0.297	5.43	1.000	–	I
A-2		27.8°	1.308	0.300	7.27	–	−1.846	II
AM-1		10°	1.168	0.302	2.56	0.362	−0.431	I–II
AM-2		20°	1.434	0.299	7.74	0.431	−1.446	I–II
AM-3		30°	1.128	0.297	4.33	−0.145	−1.313	I–II
AM-4		45°	1.160	0.297	4.15	−1.442	−2.325	I–II
AM-5		60°	1.126	0.299	5.64	−1.987	−1.460	I–II
B-1	15°	0.4°	1.002	0.305	5.05	1.015	–	I
B-2		27.5°	1.010	0.297	5.78	–	−1.853	II
BM-1		10°	1.182	0.300	6.00	0.864	−0.723	I–II
BM-2		20°	1.414	0.303	5.33	0.330	−1.001	I–II
BM-3		30°	1.150	0.297	4.52	−0.115	−1.330	I–II
BM-4		45°	1.174	0.297	3.73	−1.228	−2.055	I–II
BM-5		60°	1.068	0.297	4.32	−1.566	−1.177	I–II
C-1	30°	0.2°	1.090	0.297	4.59	0.861	–	I
C-2		28.3°	1.040	0.297	3.8	–	−1.181	II
CM-1		10°	1.250	0.300	4.36	0.617	−0.493	I–II
CM-2		20°	1.350	0.297	5.11	0.361	−0.975	I–II
CM-3		30°	1.100	0.298	4.53	−0.081	−1.371	I–II
CM-4		45°	1.194	0.297	2.57	−0.783	−1.368	I–II
CM-5		60°	1.136	0.297	5.39	−1.773	−1.361	I–II
D-1	45°	179.5°	1.268	0.297	4.84	0.785	–	I
D-2		28.1°	1.334	0.298	5.44	–	−1.316	II
DM-1		10°	1.292	0.297	4.10	0.554	−0.466	I–II
DM-2		20°	1.500	0.297	3.81	0.234	−0.662	I–II
DM-3		30°	1.106	0.297	4.15	−0.083	−1.246	I–II
DM-4		45°	1.100	0.298	2.50	−0.836	−1.436	I–II
DM-5		60°	1.320	0.299	4.23	−1.200	−0.909	I–II
E-1	60°	179.2°	1.230	0.297	4.29	0.687	–	I
E-2		25.3°	1.188	0.297	2.81	–	−0.738	II
EM-1		10°	1.169	0.297	1.47	0.204	−0.197	I–II
EM-2		20°	1.350	0.299	1.47	0.084	−0.294	I–II
EM-3		30°	1.212	0.304	2.81	−0.094	−0.797	I–II
EM-4		45°	1.188	0.297	2.23	−0.748	−1.196	I–II
EM-5		60°	1.122	0.303	3.37	−1.189	−0.860	I–II
F-1	75°	179.2°	1.240	0.300	4.07	0.605		I
F-2		25.8°	1.174	0.297	2.66	–	−0.735	II
FM-1		10°	1.283	0.297	1.40	0.162	−0.173	I–II
FM-2		20°	1.310	0.297	1.41	0.066	−0.298	I–II
FM-3		30°	1.022	0.297	2.62	−0.146	−0.894	I–II
FM-4		45°	1.166	0.299	2.02	−0.767	−1.142	I–II
FM-5		60°	1.062	0.299	2.3	−0.906	−0.635	I–II
G-1	90°	0.4°	1.252	0.297	2.92	0.414	–	I
G-2		25.1°	1.266	0.297	2.75	–	−0.700	II
GM-1		10°	1.266	0.297	1.87	0.216	−0.225	I–II
GM-2		20°	1.488	0.299	3.53	0.142	−0.657	I–II
GM-3		30°	1.338	0.304	3.85	−0.183	−1.032	I–II
GM-4		45°	1.150	0.297	1.68	−0.665	−0.984	I–II
GM-5		60°	1.196	0.309	2.78	−1.025	−0.711	I–II

* I is the pure mode I fracture toughness; II is the pure mode II fracture toughness and I–II is the mixed mode fracture toughness.

Table 9 Comparison between fracture toughness and tensile strength [25] of anisotropic marble

ψ	$K_{IC}(\mathrm{MPa}\sqrt{m})$	$K_{IIC}(\mathrm{MPa}\sqrt{m})$	$\sigma_t(\mathrm{MPa})$
0	1.000	−1.846	40.250
15	1.015	−1.853	37.020
30	0.861	−1.278	32.277
45	0.785	−1.232	24.753
60	0.687	−0.738	18.613
75	0.605	−0.735	17.845
90	0.414	−0.699	16.555

Simulation of Seismic Signals Induced by Landslide by Numerical Coupling of PFC and FLAC

研究顆粒流與連體數值耦合方法模擬山崩產生之震動訊號

馮正一

國立中興大學水土保持學系教授

以顆粒流與連體數值方法耦合模擬山崩產生之震動訊號

馮正一[1*] 林群富[2] 蔡佩勳[3]

[1]國立中興大學水土保持學系教授*tonyfeng@nchu.edu.tw [2]國立中興大學水土保持學系碩士班 [3]朝陽科技大學營建工程系副教授

關鍵詞: PFC、HHT、FLAC、小林村、時頻分析。

摘要

本研究首先以二維顆粒流程式(PFC)模擬小林村崩塌，將 5 個監測點所得到之垂直力量震動訊號，以 Hilbert-Huang transform (HHT)分析，繪製成時頻圖，並與距離小林村 11.4 公里之甲仙寬頻地震站(SGSB)所記錄之震動訊號做比較，比對崩塌之延續時間。進一步地本研究以顆粒流程式(PFC)與連體程式(FLAC)耦合方法，以小林村崩塌為案例，建立山崩流動過程之數值模型，求取數個監測點位的震動訊號。本研究以 PFC 模擬山崩產生的岩塊散開滑動與流動過程，當岩塊撞擊有限差分數值模型(FLAC)構成的連體網格時，兩程式在各個時階內交換力量與位移。獲得監測點位的震動訊號後，我們再利用 Hilbert-Huang transform (HHT)分析得振動訊號之時頻圖，以探討該震動訊號之頻率特徵，並再次與甲仙寬頻地震站之記錄比較。我們未來的研究將再進行各項參數案例分析，繼續探討各參數對山崩震動訊號之影響。

Simulations of seismic signals induced by landslides by numerical coupling of PFC and FLAC

Zheng-yi Feng [1*] Chun-Fu Lin [2] Pei-hsun Tsai

Professor, Dept. of Soil and Water Conservation, National Chung Hsing University, Taichung 402, Taiwan

*tonyfeng@nchu.edu.tw

Graduate student, Dept. of Soil and Water Conservation, National Chung Hsing University, Taichung 402, Taiwan

Associate Professor, Department of Construction Engineering, Chaoyang University of Technology, Taichung 413, Taiwan

Key words: *PFC, FLAC, Xiaolin, Hilbert-Huang Transform, Time-frequency analysis*

ABSTRACT We first used the Particle Flow Code (PFC) to simulate the rock avalanche process of Xiaolin landslide. The vibrational signals of the vertical force components at five locations were analyzed using Hilbert-Huang transform (HHT) to obtained time-frequency spectrograms. The simulated results were compared for the duration of landslide and frequency content with the seismic signals recorded during the landslide from the Jiaxian broadband seismic station, SGSB, which is 11.4 km away from Xiaolin village. Further we developed a two-dimensional numerical coupling

approach using the Particle Flow Code (PFC) and Fast Lagrangian Analysis of Continua (FLAC) code to again simulate the rock avalanche process of Xiaolin landslide to monitor the seismic signals for some locations. The sliding of the rock fragments was simulated by the PFC particles. When the rock fragments impact on the top boundary of FLAC, forces and displacements will be interacted between the two codes. We again applied Hilbert-Huang transform for monitored seismic signals to obtain the time-frequency spectrograms for examining the characteristics of the frequency content. The simulated results were again compared with the seismic signals recorded at SGSB broadband station. For further research we plan to carry out various parametrical studies to discuss the factors that influence the seismic signals of landslides.

Engineering Numerical Analysis and BEM in Taiwan 2013
2013台灣工程計算力學暨邊界元素法研討會

Simulations of seismic signals induced by landslides by numerical coupling of PFC and FLAC

以顆粒流與連體數值方法耦合模擬山崩產生之震動訊號

Presenter: Zheng-Yi Feng

Department of Soil and Water Conservation, National Chung Hsing University

簡報者：馮正一

國立中興大學 水土保持學系

共同作者 Co-authors

馮正一 [1*]

[1]國立中興大學水土保持學系教授 *tonyfeng@nchu.edu.tw

Zheng-yi Feng, Professor, Dept. of Soil and Water Conservation, National Chung Hsing University, Taichung 402, Taiwan

林群富[2]

[2]國立中興大學水土保持學系碩士班

Chun-Fu Lin, Graduate student, Dept. of Soil and Water Conservation, National Chung Hsing University, Taichung 402, Taiwan

蔡佩勳[3]

[3]朝陽科技大學營建工程系副教授

Pei-hsun Tsai, Associate Professor, Department of Construction Engineering, Chaoyang University of Technology, Taichung 413, Taiwan

摘 要

- 二維顆粒流程式(PFC)模擬小林村崩塌，求得監測點之垂直力量震動訊號
- 震動訊號以Hilbert-Huang transform (HHT)分析，繪製成時頻圖，探討該震動訊號之頻率特徵
- 以顆粒流程式(PFC)與連體程式(FLAC)耦合方法，以小林村崩塌爲案例，建立山崩流動過程之數值模型
- 與距離小林村11.4公里之甲仙寬頻地震站(SGSB)所記錄之震動訊號做比較

關鍵詞： PFC、HHT、FLAC、小林村、時頻分析。

Abstract

- We used the Particle Flow Code (PFC) to simulate the rock avalanche process of Xiaolin landslide.
- The vibrational signals were analyzed using Hilbert-Huang transform (HHT) to obtained time-frequency spectrograms.
- The simulated results were compared for the duration of landslide and frequency content with the seismic signals recorded during the landslide from the Jiaxian broadband seismic station, SGSB, which is 11.4 km away from Xiaolin village.
- We coupled the Particle Flow Code (PFC) and Fast Lagrangian Analysis of Continua (FLAC) code to again simulate the rock avalanche process of Xiaolin landslide.

Key words: *PFC, FLAC, Xiaolin, Hilbert-Huang Transform, Time-frequency analysis*

Causes of the Xiaolin landslide

- Structural factors, weathering, and gravitational slope deformation were the underlying causes of the landslide.
- Triggered by intensive rainfall.

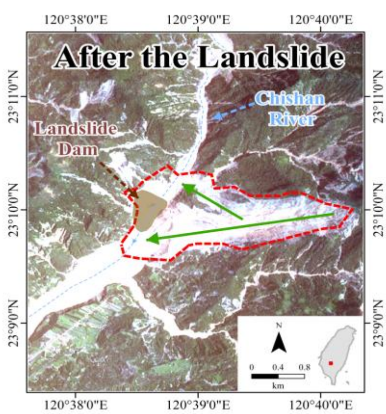

Zheng-Yi Feng (2011)

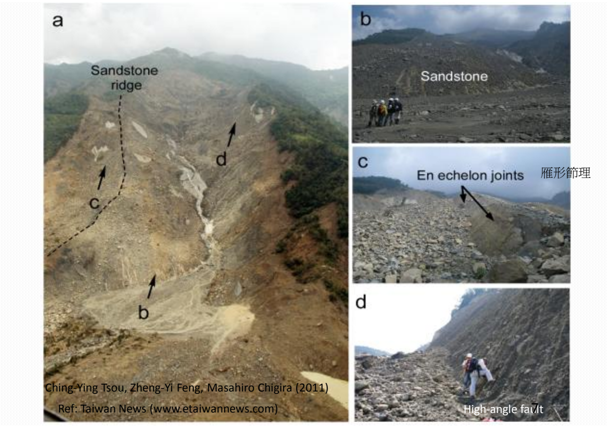

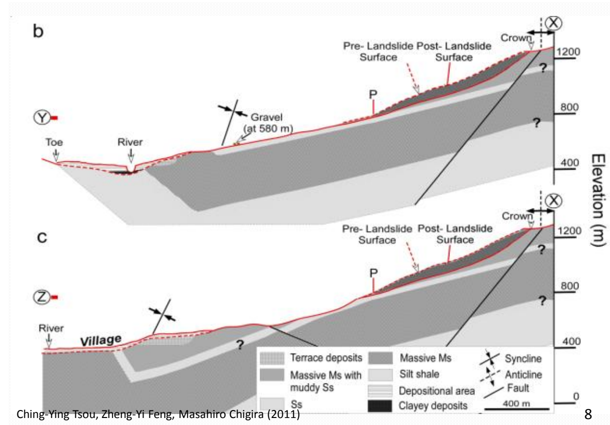

Seismic signals due to landslide

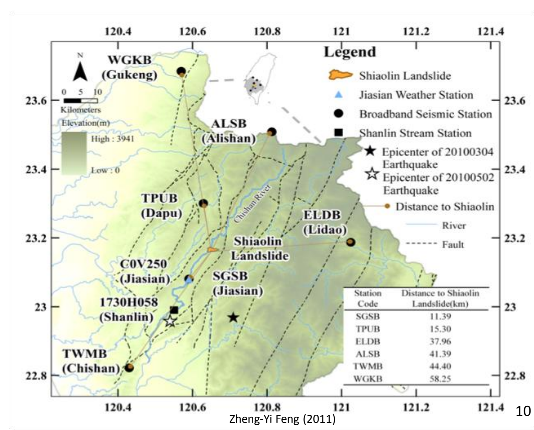

Station Code	Distance to Shiaolin Landslide(km)
SGSB	11.39
TPUB	15.30
ELDB	37.96
ALSB	41.39
TWMB	44.40
WGKB	58.25

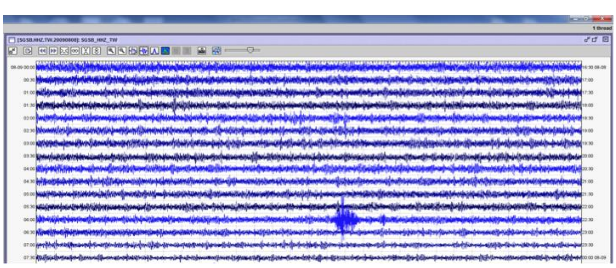

Seismic signal caused by the landslide at SGSB station

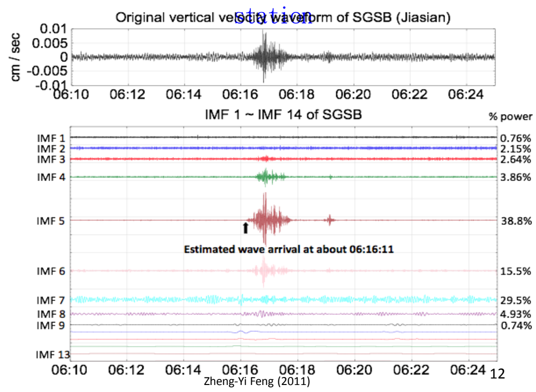

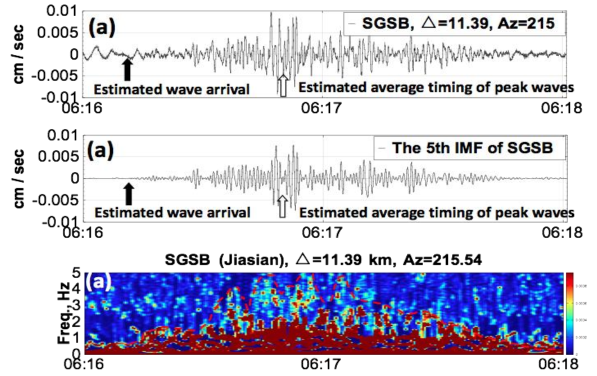

Zheng-Yi Feng (2011)

Seismic signal at TWMB station

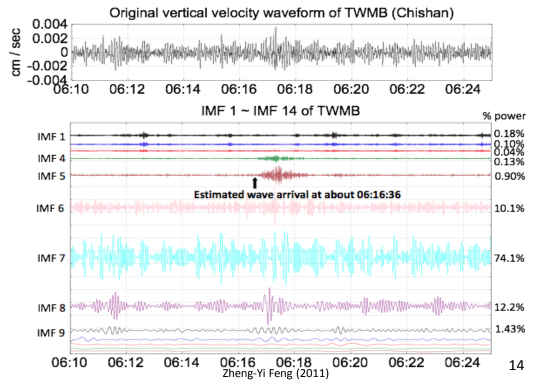

Zheng-Yi Feng (2011)

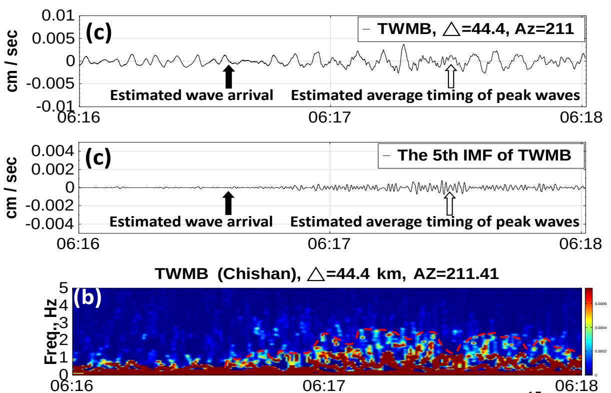

Zheng-Yi Feng (2011)

Key points of the LS vibration

- The surface-wave velocities in the region is estimated.
- The main frequency contents of the seismic waves caused by the Xiaolin landslide were in the range of 0.5 to 1.5 Hz.

PFC simulation y-force time-frequency analysis

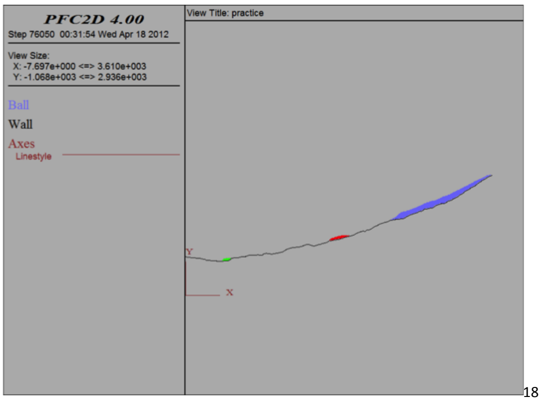

Fig. 6

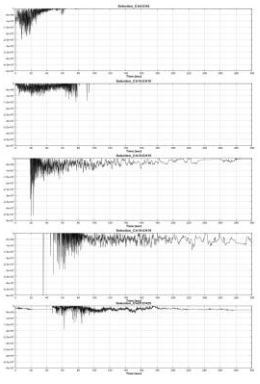

Fig. 7

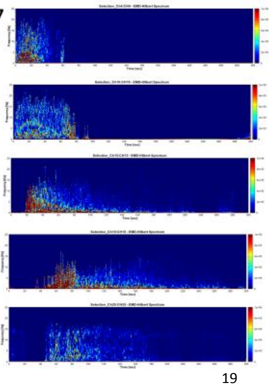

A two-dimensional numerical coupling approach using the PFC and FLAC

A preliminary result

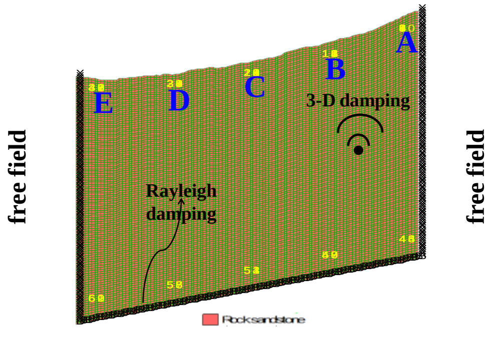

Unbalance force

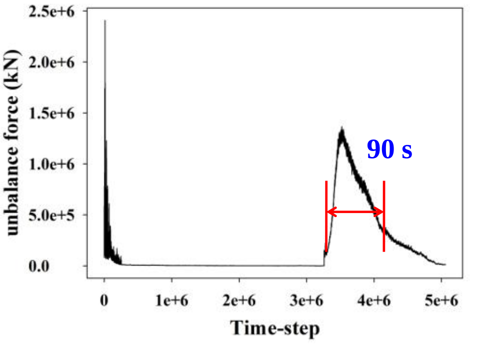

Before the Landslide

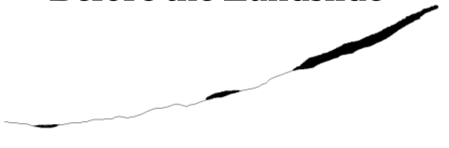

After the Landslide

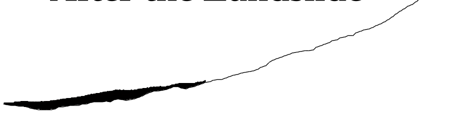

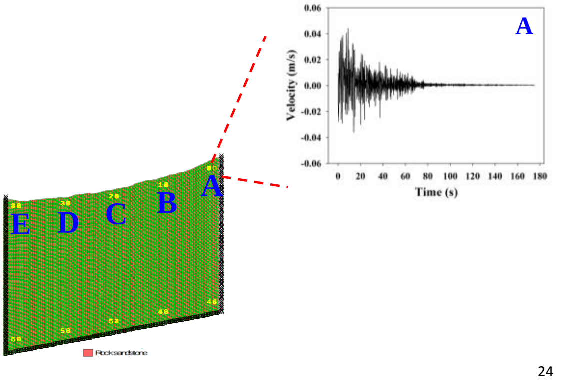

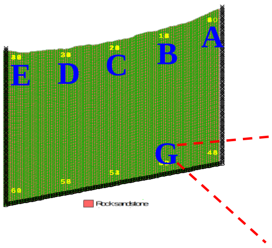

The signals are very small at the bottom of the model.

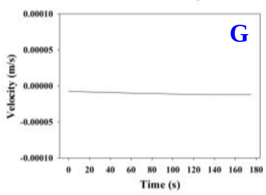

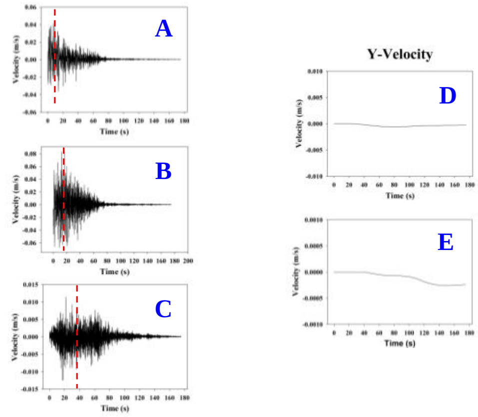

● **When quiet boundary was used, the domain kept falling. Why?**

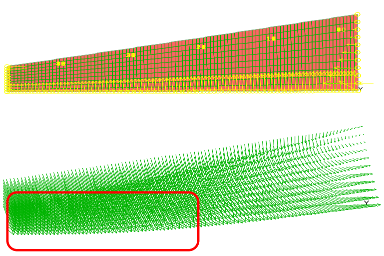

How shall we cope with？

- **Enlarge the domain?**
- **Use "free field"?**
- **Use Rayleigh damping?**
- **Use 3-D damping?**

References

- Zheng-Yi Feng (2011) The seismic signatures of the 2009 Shiaolin landslide in Taiwan, Nat. Hazards Earth Syst. Sci., 11, 1559-1569, doi:10.5194/nhess-11-1559-2011, 25 May 2011.
- Feng, Z.-Y. (2012) "The seismic signatures of the surge wave from the 2009 Xiaolin landslide-dam breach in Taiwan", Hydrological Processes, Vol. 26, Issue 9, pp.1342-1351, 30 April 2012, doi: 10.1002/hyp.8239
- Ching-Ying Tsou, Zheng-Yi Feng, Masahiro Chigira (2011) "Catastrophic landslide induced by Typhoon Morakot, Shiaolin, Taiwan", Geomorphology, Volume 127, Issues 3-4, 15, April 2011, Pages 166-178, 2011. doi:10.1016/j.geomorph.2010.12.013
- Lin, C. H., Kumagai, H., Ando, M., and Shin, T. C.: Detection of landslides and submarine slumps using broadband seismic networks, Geophys. Res. Lett., 37, L22309, doi:10.1029/2010gl044685, 2010.

Thank you very much for your attention.

Zheng-yi Feng, Ph.D., P.E.

Department of Soil and Water Conservation
National Chung Hsing University
tonyfeng@nchu.edu.tw

Applications in Computational Wind Engineering

計算風工程之應用

方富民

國立中興大學土木工程系教授

Applications in Computational Wind Engineering

Fuh-Min Fang

fmfang@nchu.edu.tw, Department of Civil Engineering, National Chung Hsing University, Taichung, Taiwan 40227

Key words: *Computational Wind Engineering, Finite volume Method, Large-eddy simulation*

Developments in computational wind engineering are introduced. Subjects of interest include the numerical predictions of wind effects (surrounding flow fields and wind loads) and the corresponding dynamic responses of structures.

The introduction starts with the description of Computational Wind Engineering (CWE) and how it is distinguished from Computational Fluid Dynamics (CFD). Compared with analytical and experimental methods, which are commonly used in the analyses of wind engineering problems, the merits and drawbacks of CWE applications are described. In addition, problems encountered in the execution of numerical calculations are illustrated.

Examples of numerical predictions in certain selected wind engineering problems are presented thereafter. The unsteady flow fields of several selected topics of bluff-body aerodynamics are demonstrated. Cases subject to building researches are two- and three-dimensional flows around a square or rectangular cylinder with a uniform or boundary-later type of approaching flow. Moreover, the result of the numerical simulation on a plume dispersion problem is also presented.

The numerical prediction of problems involving fluid-induced vibration is another subject of interest. To reflect the effect of interaction, the numerical calculations are performed by solving two sets of dynamic equations (respectively for the turbulent flows and the structure dynamics) alternatively. The dynamic simulations of two typical examples, one for an elastic fence in a boundary layer flow and the other for a uniform flow past a suspended bridge deck with a trapezoidal cross-section, are shown. Based on the time-series numerical results, furthermore, the aeroelastic behavior of the vibrating structure under wind action is investigated extensively.

Finally, the scope regarding local CWE development is stated. Future extensions on the CWE applications in certain possible aspects, together with the associated technical problems to be solved, are discussed. Accordingly, the immediate tasks for the local researchers are also illustrated.

References

[1] C.C. Chen, F.M. Fang, Y.C. Li, L.M. Huang, C.Y. Chung: Fluid forces on a square cylinder in oscillating flows with non-zero mean velocities, Int. J. Numer. Meth. FL., 60, pp.79-93, 2009.

[2] F.M. Fang, Y.C. Li, C.C. Liang, J.H. Chen: Numerical predictions on the dynamic response of a suspended bridge with a trapezoidal cross-section, J. Chin Inst. Eng., 28(2), pp.281-291, 2005.

[3] F.M. Fang, J.M. Ueng, J.C. Chen: Numerical investigations on the along-wind response of a vibrating fence under wind action, Wind Struct., 5(2-4), pp.329-336, 2002.

[4] F.M. Fang, W.D. Hsieh, S.W. Jong, J.J. She: Turbulent boundary layer characteristics along the centerline of a contracting wall, J. Hydraul. Eng., ASCE, 123, pp.560-565, 1997.

[5] F.M. Fang, C. Farell: Turbulent boundary layer characteristics along the centerline of a contracting wall, J. Wind Eng. Ind. Aerod., 61, pp.131-151, 1996.

Applications in Computational Wind Engineering

Fuh-Min Fang

Department of Civil Engineering
National Chung Hsing University

Computational Wind Engineering (CWE)

- search for solutions of wind-engineering problems
- more practical

Outline

- About CWE
- Comparisons with experimental and analytical methods
- Procedure of CWE
- Examples of recent works

Typical Methods

- Analytical
- Experimental
- Numerical

Computational Fluid Dynamics (CFD)

- cover all kinds of fluid dynamic problems
- emphases on numerical techniques, solution algorithm, turbulence modeling, etc.

Comparison I

	Analytical	**Numerical**
Governing Equations	ODE/PDE	modified equations
Boundary Treatment	harder	easier
Solution Achievement	harder	easier
Solutions	continuous	discrete

Comparison II

	Experimental	Numerical
Cost	higher	lower
Solution Outcome	partial, local	all-time, whole field
Complex Boundary	easier	harder
Solution Reliablity	good	getting better

CWE Examples

- 2-D cylinders (horizontal)
- 2-D cylinder (vertical)
- 2-D dual cylinders (tandem)
- 2-D dual cylinders (side-by-side)
- 3-D square prism
- Concentration/temperature fields
- Responses of a suspended bridge (interactive)

Procedure of CWE

- Domain selection
- Governing equations
- Boundary specifications
- Equation modifications
- Execution

Goals of CWE

- A parallel tool of analysis
- Numerical wind tunnel

Typical Applications in CWE

- Buildings

  surrounding flow
  surface pressure
  wind loads
  dynamic responses

- Suspended bridges

  wind effects
  dynamic responses

Future Improvements

- Hardware

  speed, capacity of computers

- Software

  Accuracy — numerical methods
  turbulence modeling

  Efficiency — parallel processing
  multi-block computation

Comment (1)

Due to significant improvements of computer hardware and software, the applications of numerical methods become more and more convenient in the analyses of fluid & structural dynamics.

Comment (2)

In addition to model experiments, CWE can be a parallel tool to analyze wind-engineering problems.

Comments (3)

Besides the analyses of wind and structural dynamics, CWE can also be applied in problems involved concentration and temperature variations.

Comments (4)

By performing an alternative solution procedure, the effect of interaction between a vibrating structure and its surrounding flow can be correctly simulated by CWE methods.

Comment (5)

Improvements on CWE are still needed to promote the resulting accuracy and the computational efficiency.

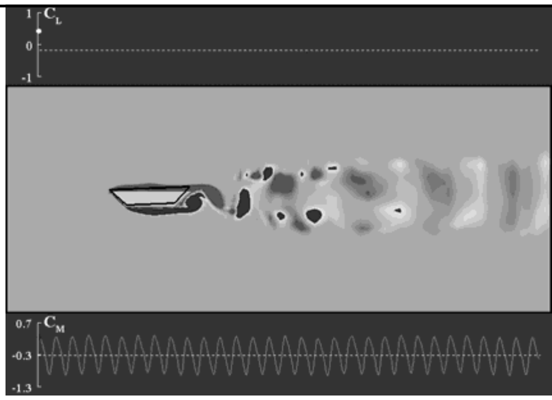

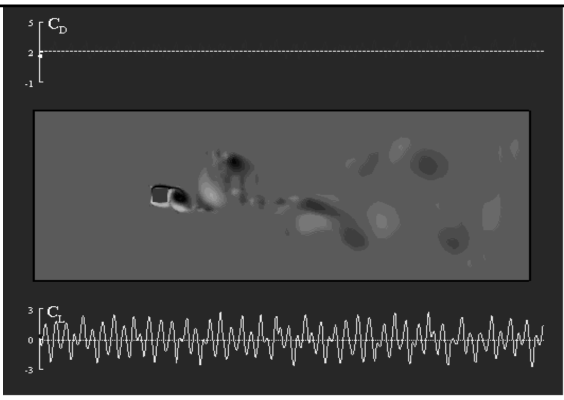

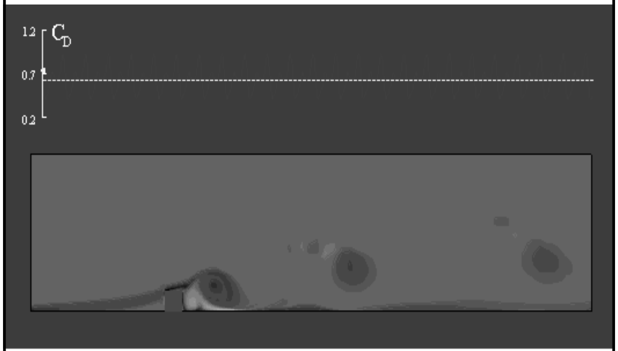

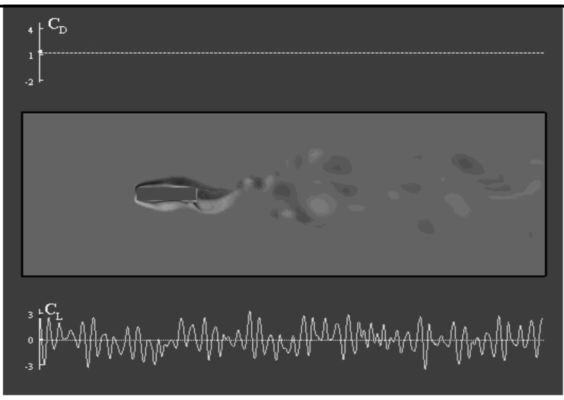

D/B=1

D/B=7

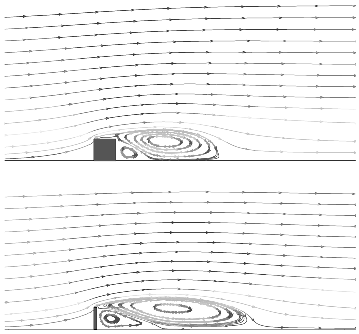

Mean Flow Field (vertical plane)

B/D=1

B/D=4

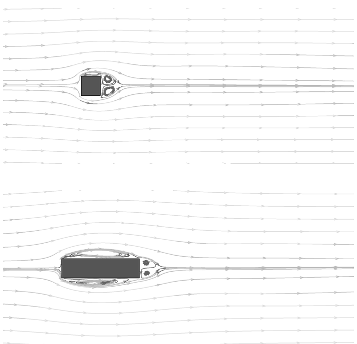

Mean Flow Field (horizontal plane)

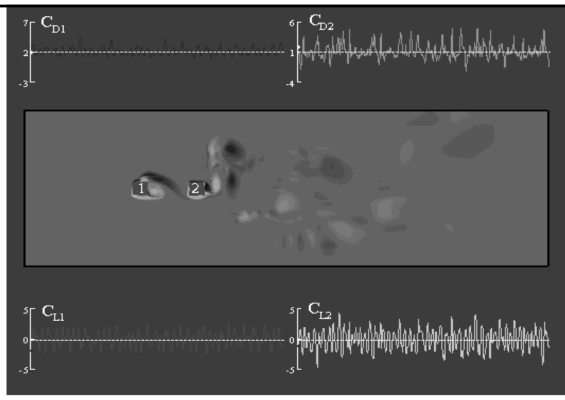

S/D=2

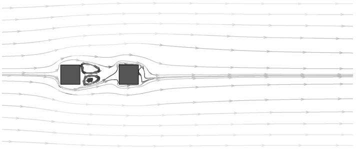

S/D=4

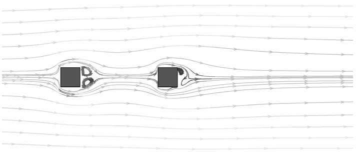

Mean Flow Field (tandem)

Results of 3-D square Prism

- Horizontal plane
- Vertical plane

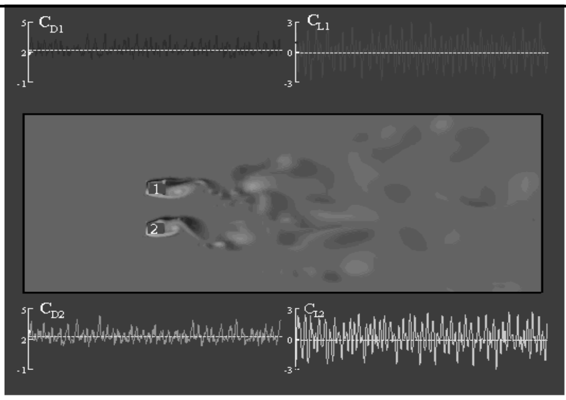

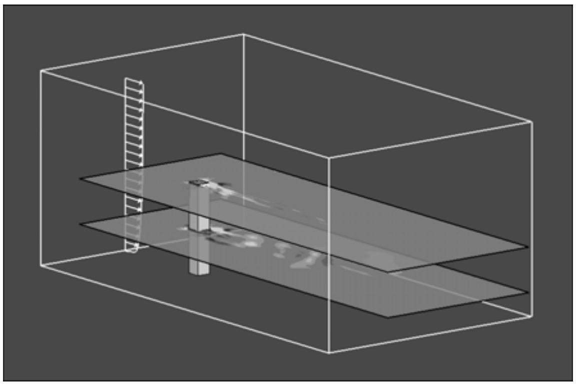

W/D=2

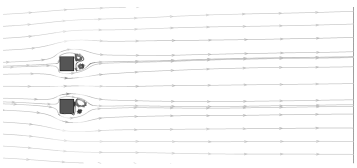

W/D=4

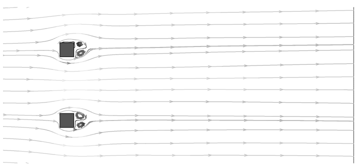

Mean Flow Field (side-by-side)

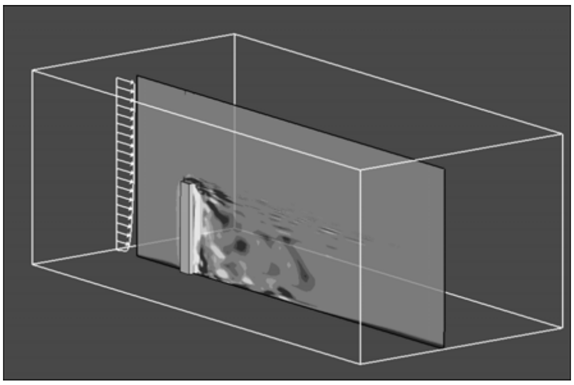

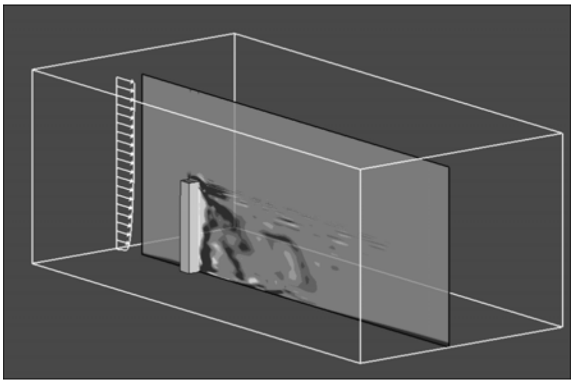

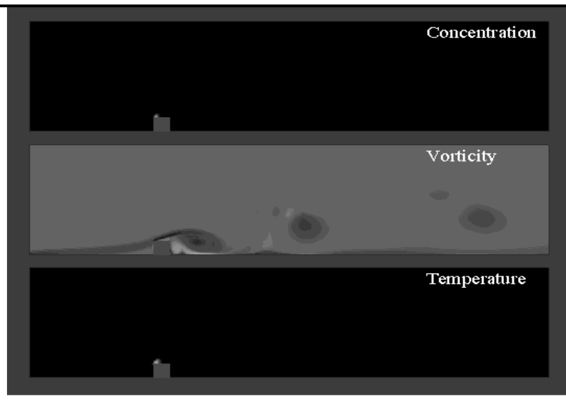

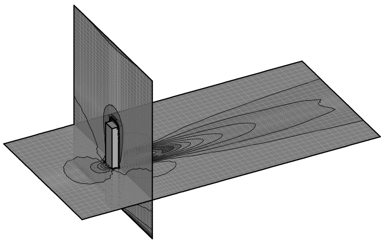

Iso-speed contours of mean flow

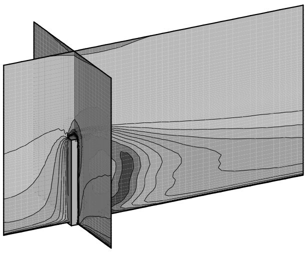

Iso-speed contours of mean flow

Indentation Fracture with coupling of DEM and FDM

耦合分離元素與有限差分法模擬貫切破壞

陳立憲

國立台北科技大學土木工程系副教授

耦合分離元素法與有限差分法模擬貫切破壞

陳立憲*, 王紹宇†, 江明軒†

*lhchen@ntut.edu.tw, 國立台北科技大學土木工程系副教授
†國立台北科技大學土木工程系碩士

關鍵字：*分離元素法、有限差分法、貫切破壞、變形不連續*

1 摘要

本研究使用分離元素法軟體 PFC2D 與有限差分法軟體 FLAC 兩二維數值軟體進行貫切破壞之數值耦合運算，利用耦合概念加速分析之運算速度，兩軟體之連結透過力與速度之交換傳遞。先以單壓試驗(Uniaxial Compression Test)；及巴西試驗(Brazilian Test)校驗耦合機制之適確性後，方應用於貫切試驗之解析。

2 說明

邇來台灣地區利用機械式開挖所遭遇之地質狀況愈趨困難、複雜且工程尺度規模增大，是故對於隧道機械式開挖之安全性與效率備受重視，而將隧道全斷面鑽掘機開挖(TBM)應用於雪山隧道開挖所遭遇到的問題，包括遭遇高強度岩石四稜砂岩以及充滿破碎帶與水脈的環境，導致 TBM 之開挖效率大幅降低，關於此類極近域應力場之接觸行為問題相關研究甚為缺乏，因此若能將極近域應力場之行為以及機械式開挖刀楔與岩石之接觸行為機制釐清，將對於開挖效率與機械設計提供依據。

本研究以數值模擬工具進行分析，利用數值耦合之方式進行岩石正向貫切試驗，並比對貫切試驗理論模式與試驗結果，冀望能提升隧道工程與地下管道之安全性與施工效率。

本研究利用由 Itasca Consulting Group 於 1995 出版之數值軟體 PFC2D (*Particle Flow Code in 2 Dimensions*)與 FLAC (*Fast Lagrangian Analysis of Continua*)進行耦合模擬分析，而本研究採用數值耦合之概念運用於岩石之正向貫切試驗，先利用單壓試驗與巴西試驗之模擬，並與單一數值軟體模擬之結果(PFC2D)及文獻資料進行比對，驗證數值耦合之可行性後，將之實際應用於貫切試驗，再將貫切試驗之模擬結果與理論解進行比對，初探此一數值模擬概念之行為特徵。

參考文獻

[1] Alehossein, H., Detournay, E. and Huang, H., (2000), Analytical model for the indentation of rocks by blunt tools, Rock Mechanics and Rock Engineering, vol. 33, no. 4, pp. 267-284.

[2] Johnson, K. L., (1970), “The correlation of indentation experiments,” J. Mech. Phys. Solids, pp. 115-126.

[3] Potyondy, D., Cundall, P., (2004), “A bonded-particle model for rock,” Int. J. Rock Mech. Min. Sci., vol. 41, pp. 1329-1364.

[4] Wanne, T., Johansson, E. and Potyondy, D., (2004), “Final coupled 3D thermo-mechanical modeling, Preliminary particle-mechanical modeling.” S. K. B. Rapport, R-04-03.

Indentation Fracture with Coupling of DEM and FDM

Li-Hsien Chen*, Shao-Yu Wang†, and Ming-Shuen Jian†

* lhchen@ntut.edu.tw , Department of Civil Engineering, National Taipei University of Technology

† Department of Civil Engineering, National Taipei University of Technology, Master

Key words: *Distinct Element Method, DEM, Finite Different Method, FDM,, Indentation Fracture Displacement Discontinuity*

Abstract

This study presents the numerical modeling approach with coupling of distinct element method (DEM) and finite different method (FDM) to simulate the quasi-brittle materials under indentation fracture test from the displacement continuity (elasto-plastic condition) to displacement discontinuity (linear fracture mechanics).

To verify the feasibility of this analytical simulation, both Biaxial compression and Brazilian test were calibrated first by comparing the numerical results from coupling model of PFC^{2D}/FLAC with experimental data (uniaxial compressive strength, q_u and indirect tensile strength, σ_t). Furthermore, both theoretical and numerical indentation fracture tests were investigated regarding the elasto-plastic interface as well as the initiation/propagation of crack. The results show that this coupled numerical modeling, which the quasi-brittle materials simulated by DEM while indenter/cutter simulated by FDM, can be used to understand the mechanism of indentation fracture test. With nice correspondence between the numerical modeling, experimental results and theoretical solution, the better understanding of the fracture mechanism during indentation cab be obtained. In addition, this study of indentation fracture can be applied to underground mechanical excavation in rock for tunnel engineering.

References

[1] Alehossein, H., Detournay, E. and Huang, H., (2000), Analytical model for the indentation of rocks by blunt tools, Rock Mechanics and Rock Engineering, vol. 33, no. 4, pp. 267-284.

[2] Johnson, K. L., (1970), “The correlation of indentation experiments,” J. Mech. Phys. Solids, pp. 115-126.

[3] Potyondy, D., Cundall, P., (2004), “A bonded-particle model for rock,” Int. J. Rock Mech. Min. Sci., vol. 41, pp. 1329-1364.

[4] Wanne, T., Johansson, E. and Potyondy, D., (2004), “Final coupled 3D thermo-mechanical modeling, Preliminary particle-mechanical modeling.” S. K. B. Rapport, R-04-03.

2013台灣工程計算力學暨邊界元素法研討會, 中興大學
Engineering Numerical Analysis & BEM in Taiwan 2013

Indentation Fracture with Coupling of DEM and FDM
耦合分離元素法與有限差分法模擬貫切破壞

陳 立 憲 北科大 土木系

日 期：2013.03.20

NTUT

簡報大綱

一 緒論
二 文獻回顧
三 耦合數值模擬方法
四 數值模擬結果與分析- PFC2D&FLAC
五 結論與建議

一、緒論

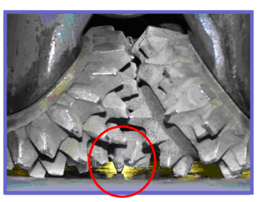

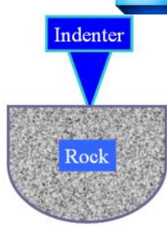

機械式地下開挖 ⟺ 應用 ⟺ 可挖性，破岩行為 鑽刀設計，動力參考

動機

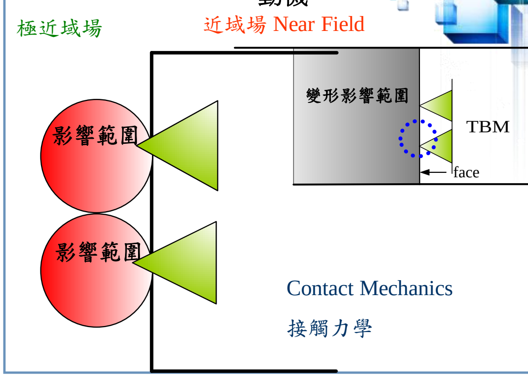

二、文獻回顧-分離元素法 (Discrete Element Method, DEM)

- 針對材料性質或形體為不連續的問題，所發展的數值分析方法
- 允許顆粒產生有限度的位移與旋轉，包括顆粒間完全分離
- 運算過程中，程式需能自動偵測產生的接觸點，並消除分離的接觸點

文獻回顧-分離元素法 (Discrete Element Method, DEM)

年代	重要事典	作者
1971	首創以分離元素法分析岩體問題	Cundall
1979	應用分離元素法分析砂性土壤	Cundall , Strack
1988	已完整敘述分離元素法	Cundall , Hart
1992	PFC之提出	Cundall , Hart

文獻回顧-貫入試驗沿革

年代	重要事典	作者
1881	最先圓錐形刃口探討彈性貫入行為	Hertz
1969	綜整彈性分析	Timoshenko
1970	彈-塑性理論建立孔洞擴展模式	Johnson
1975	應用破壞力學於開裂後之力學行為	Lawn
2000	廣義孔洞擴展模式	Detournay

文獻回顧-貫切破壞沿革(數值)

年代	重要事典	作者
1975	單點載重應力場分析（FEM）	Lawn & Swain
1975	比對Hertzian彈性解之接觸行為	Lawn & Wilshaw
1995	模擬岩材之貫切行為（FLAC）	Damjanac
1996	探討岩石貫壓行為（UDEC）	Alehossein
1997	模擬貫切破壞之破裂機制（BEM）	Tan et al.
1998	模擬岩材受側向圍壓之貫入行為（FLAC）	Huang
2002	模擬雙刀貫切之行為（R-T^{2D}）	Liu
2008	探求材料內部因子之影響（PFC^{2D}）	Huang

文獻回顧-廣義孔洞擴展模式(CEM)

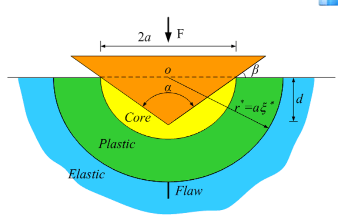

CEM：(延性, Ductile)
Lamé Solution (Elastic)
Mohr-Coulomb (Plastic)
(Cavity Expansion Model)

LEFM ：(脆性, Brittle)
(Linear Elastic Fracture Mechanics)

文獻回顧-線彈性破壞力學(LEFM)

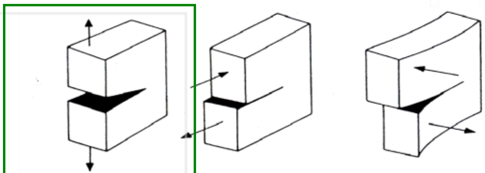

模式I：張裂型	模式二II：滑裂型	模式三Ⅲ：撕裂型

文獻回顧-數值耦合

年代	重要事典	作者
2004	利用PFC^{2D}與FLAC進行數值耦合，以模擬隧道開挖之裂縫生、衍行為	Potyondy & Cundall
2005	與FLAC模擬地下開挖產生之震動對於土層之影響，並得到初步之裂縫生、衍結果	Mercerat et al.
2005	PFC^{2D}與FLAC模擬墩柱效應之相互影響作用	Wanne et al.
2007	PFC^{2D}與FLAC之耦合模擬地下開挖之不同階段開挖產生微震造成之裂縫，並與現地AE監測與比對獲得相符合之結果。	Cai et al.

三、數值軟體模擬分析方式

PFC^{2D}

FLAC

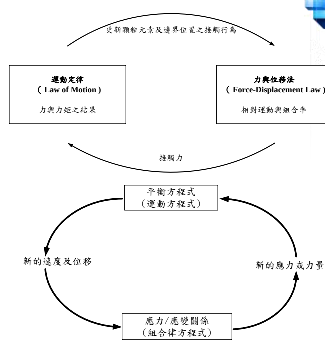

數值軟體之優缺點比較

	PFC2D	FLAC
優點	1.不需考慮組合律所產生之影響 2.可建立圓形或非圓形顆粒元素 3. 顆粒元素皆可視為單一個體，而由鍵結力所黏結，可模擬破壞行為 4.可模擬出試體峰後及裂縫生、衍之行為	1.採有限差分法，計算速度上有明顯的優勢 2.可自行定義新的組合律模式
缺點	1.試體由顆粒組成，產生邊界不平整之問題 2.牆面元素為剛體無法因受力而折損變形 3.當顆粒元素過多時，運算時間將大幅增加。	1.在模擬接觸式的破壞時，須考慮兩物體間的介面(interface)，此會影響模擬之結果是否正確，在設定上並沒有一定之標準。 2.無法完整模擬出試體破壞後之行為。

13

數值耦合之分析方式

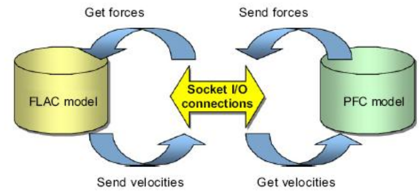

14

數值耦合之分析方式

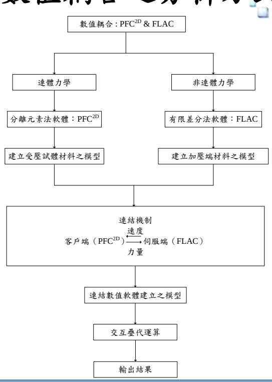

15

四、數值模擬與分析:PFC^{2D}&FLAC

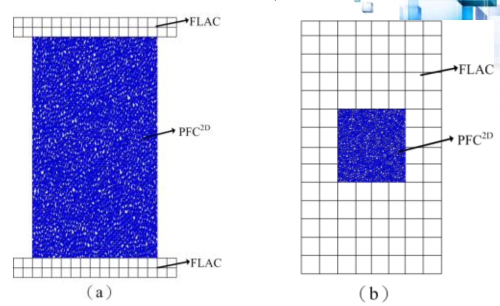

（a）非材料之數值耦合
PFC之加壓牆面由FLAC網格取代

（b）材料之數值耦合
較遠域之PFC顆粒元素由FLAC之網格取代

16

耦合之材料參數

高速鋼之材料參數		
幾何參數	長度（cm）	5
	寬度（cm）	0.5
材料參數（彈性）	楊氏模數（Pa）	2.25E+15
	體積模數（Pa）	1.25E+15
	剪力模數（Pa）	9.38E+14
	密度（kg/m^3）	8160
	柏松比	0.2

FLAC網格之參數設定（楊琳琰,2007）

17

數值耦合牆面元素之轉換

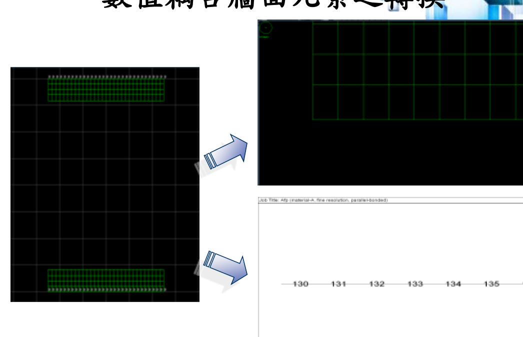

18

數值耦合模擬比對-單壓試驗

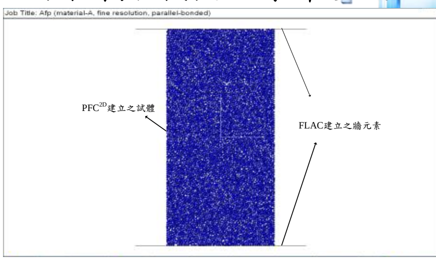

- PFC2D試體參數:花崗岩，Lac du Bonnet Granite
- FLAC網格參數：高速鋼

數值耦合模擬比對-單壓試驗

裂縫生、衍行為

PFC2D　　Couple

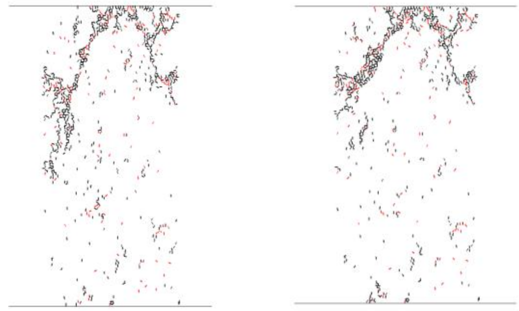

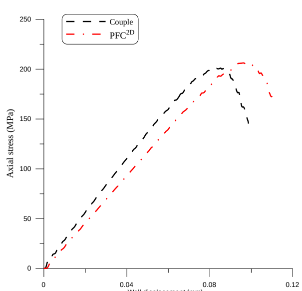

數值軟體	單壓強度 (MPa)
PFC2D	203.99
Couple	201.48
文獻	199.113 （n = 10）

數值耦合模擬比對-巴西試驗

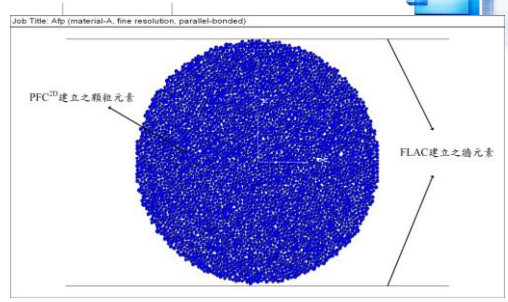

巴西試驗-裂縫生、衍行為比對

PFC2D　　Couple

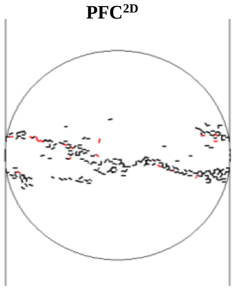

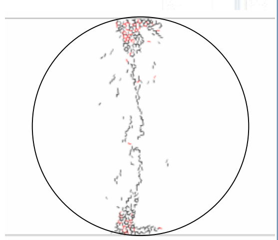

（黑色為張力裂縫，紅色為剪力裂縫）

壓應力:-3　拉應力:1

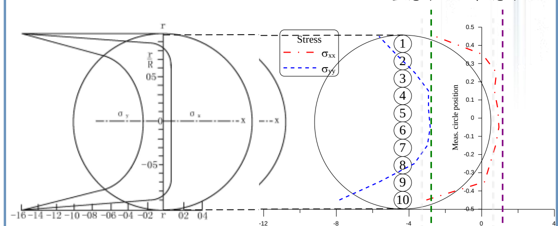

PFC2D

數值軟體	張力強度(MPa)
PFC2D	48.04
Couple	48.54
文獻 Couple	44.73.3 (n = 10)

壓應力:-2.5 拉應力:1

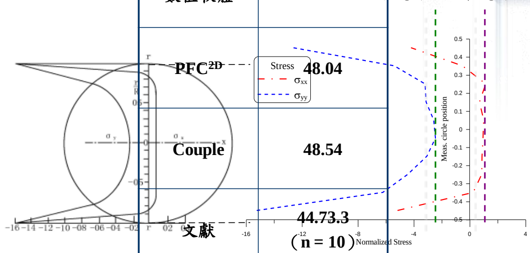

數值耦合模擬比對-貫切試驗

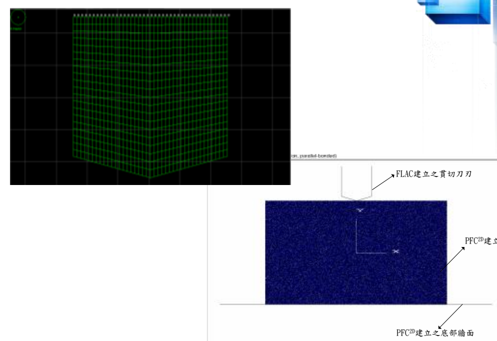

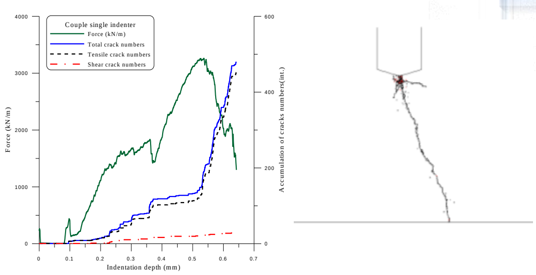

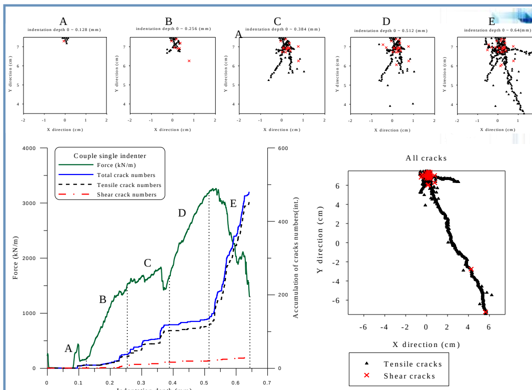

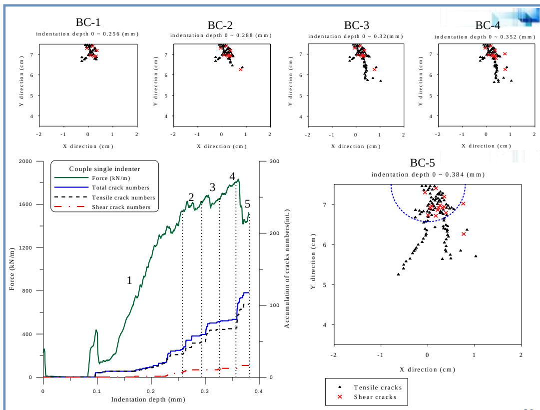

數值耦合模擬比對-貫切試驗

軟體種類	F_{max} (kN/m)	F_{ini} (kN/m)	d^* (mm)	r^* (mm)	a (mm)	ξ^*
單一數值模擬	3320.4	1526	0.25	9.5	0.746	12.73
數值耦合模擬	3258.1	1571	0.28	10.0	1.045	9.57

花崗岩, Lac du Bonnet Granite

Size of damaged zone, ξ_*

$$(1+\mu)\xi_*^{(K_d+1)/K_d} - \mu\xi_*^{(K_p-1)/K_p} = \gamma$$

$$\gamma = \frac{2(K_p+1)G\tan\beta}{\pi\sigma_c} f(\sigma_0)$$

$$1+\mu = \frac{(1-\nu)(1+K_p)(1+K_d)}{K_p+K_d}$$

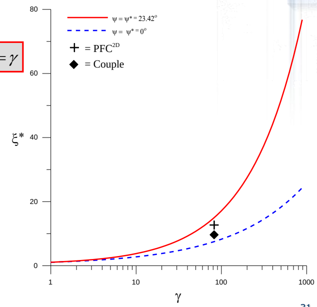

五、結論

❖ 數值耦合之模擬比對

1.單壓試驗

力系探討：單壓強度為201.48 MPa與203.99 MPa，且應力應變曲線相吻合。

變形行為探討：數值耦合之裂縫生、衍模式與單一數值模擬及文獻之結果接近。

2.巴西試驗

力系探討：張力強度分別為48.54MPa與48.04 MPa，並經由古典解比對之內部應力為-2.5:1與-3：1。

變形行為探討：加壓端兩側出現剪裂後，由兩端向中間開裂，並由顆粒元素之位移向量亦可證實確為張力破壞。

3.貫切試驗

力系探討：得與單一軟體模擬接近之初裂貫切力與最大貫切力。

變形行為探討：臨界彈-塑性區（r*）及無因次化之彈塑性區半徑（ξ*）皆與單一模擬之結果相近。

文獻比對探討：與廣義孔洞擴展模式理論解進行比對後，其數值結果落於理論值之上下限範圍內，驗證數值耦合應用於貫切試驗之適確性。

建 議

❖ 本研究之磨耗效應乃簡化後之模型，應可利用數值耦合之FLAC網格允許變形之優點，以取代取代貫切刀楔後，貫入試體觀察網格之變形量，或改為扭轉切削試體表面後，觀察其變形量與裂縫生、衍形式。

❖ 於數值耦合運算之形式，應再深入研究以網格取代顆粒元素之耦合形式，方可真正應用於大規模之工程實務，符合更多種類之工程實務之應用。

Applications of Displacement Discontinuity Method

位移不連續法之應用

Keh-Jian Shou
Department of Civil Engineering,
National Chung-Hsing University

壽克堅
國立中興大學土木系教授

Applications of Displacement Discontinuity Method

Keh-Jian Shou
Department of Civil Engineering,
National Chung-Hsing University

Abstract

The indirect boundary element methods are based on the superposition of influence coefficients and the numerical analysis procedure, which comprises the discretization of the boundary, superposing the influence coefficients, set up and solve the system of equations with the boundary conditions, applying the obtained fictitious loadings to calculate the stresses and displacements for the boundary and interior points. The displacement discontinuity element is an indirect method based on the fundamental solution of the fictitious loading, i.e., displacement discontinuity. The displacement discontinuity method is particularly suitable to model crack problems, as it possesses the property that the displacements at the two sides of the element are discontinuous, physically very similar to a crack. Therefore, the displacement discontinuity methods are quite popular in the simulation of fracture mechanics and rock engineering problems.

This paper intends to demonstrate the applications of the displacement discontinuity methods, focusing on the static problems in fracture mechanics and rock engineering.

The 2D displacement discontinuity was applied to the simulate the fault system in central Taiwan, and the results properly show the propagation of the faulting during the 1999 Chi-Chi earthquake. A special 3D displacement discontinuity method was developed and properly applied to the simulation of the fracture zone development in rock excavation. In addition, the new developments including the introduction of uncertainty consideration and the application to the reliability analysis were also investigated.

位移不連續法之應用

壽克堅
國立中興大學土木系教授

摘要

邊界元素法之間接法，其理論基礎乃建立於影響係數疊加之觀念上，其分析過程可分為以下四個步驟：對欲分析問題的邊界進行離散，將各元素對求解點之之影響係數進行疊加，利用邊界條件建立一聯立方程組並求解得於各元素之虛擬作用值，由求得之虛擬作用值來可求得邊界及內點之應力及變位。位移不連續法為使用位移不連續元素之間接法，係建立在彈性體內虛擬作用之位移不連續荷重的基本解上。由於位移不連續元素具有元素兩側位移不連續的特性，其物理性質近似裂縫，故除了可以分析一般之邊界值問題外，特別適用於包括岩石工程常見之節理、裂紋及採礦等問題。

本文主要探討位移不連續法之工程應用，包括破壞力學及岩石工程在內之靜力問題之分析。二維位移不連續法可應用於台灣中部地區之斷層系統模擬，成功模擬出1999 年集集大地震引發之地震斷層破裂相關行為。考慮裂紋發現而引入虛擬網格系統之特殊三維位移不連續法成功的被建立，可應用於模擬岩盤開挖引起破裂區之發展。此外，位移不連續法也有考慮參數及幾何不確定性之因素，以及用於可靠度分析之進一步發展及應用。

2013台灣工程計算力學暨邊界元素法研討會
Engineering Numerical Analysis and BEM in Taiwan 2013

位移不連續法之應用
Applications of Displacement Discontinuity Method

Keh-Jian Shou

Department of Civil Engineering,
National Chung-Hsing University,
Taichung, Taiwan
2013/3/20

CONTENTS

- Simulation of the Fault Propagation in 1999 Chi-Chi Earthquake
- Simulation of the Fracture Zone Development in Rock Excavation
- More Developments and Applications

I. Simulation of the Fault Propagation in 1999 Chi-Chi Earthquake


苗栗台中地區之斷層系統

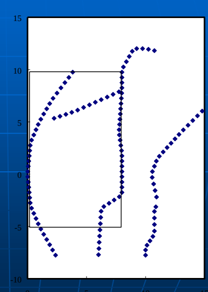
以邊界元素代表簡化之斷層系統及研究區

關刀山地震前強度因子分佈

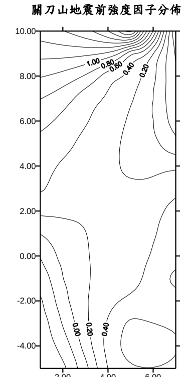

關刀山地震後強度因子分佈

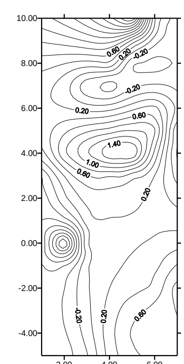

逆衝斷塊模型

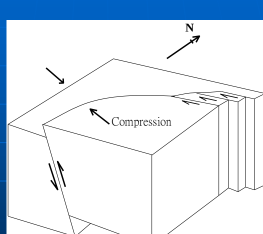

邊界元素模擬豐原－東勢新生破裂面之生成

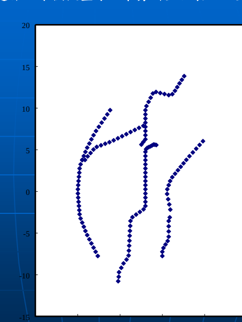

2. Simulation of the Fracture Zone Development in Rock Excavation

- *A tunnel approaching a weak zone may trigger slip along the interface or may induce stress concentrations within the weak zone leading to collapse as well as micro seismic activity.*
- *A weak zone can be considered as a layered system composed of formations with different material properties.*

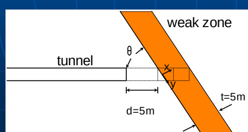

- **Solution for a Three-layer Medium**

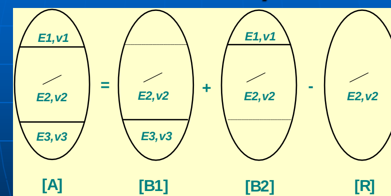

- (ui)[A] = (ui)[B1] + (ui)[B2] - (ui)[R]
- (σij)[A] = (σij)[B1] + (σij)[B2] - (σij)[R]

- **Strength Factor**

  strength factor (S.F.) is adopted to illustrate the stress concentration as well as the potential of failure

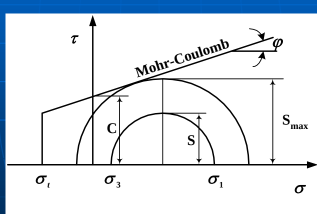

$$S.F = \frac{S_{max}}{S}$$

NUMERICAL RESULTS

- The approaching angle θ is defined as the angle between the mining direction and the dip direction of the weak zone. We let the thickness of the weak zone be t=5m, and the distance from the mining face to the first interface of host rock and weak zone be d= 5m.

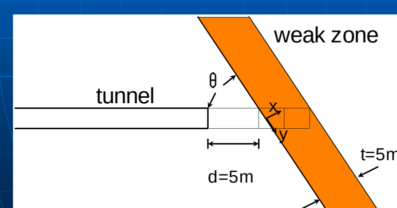

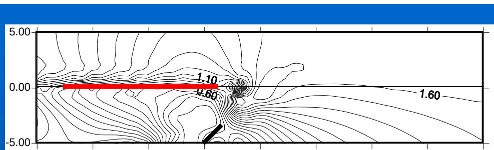

approaching angle 45∘

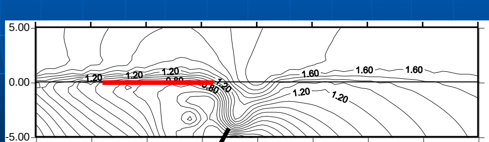

approaching angle 60∘

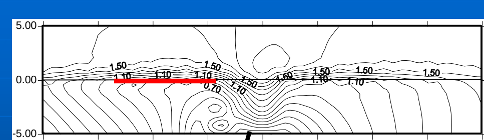

approaching angle 75∘

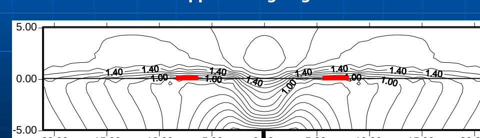

approaching angle 90∘

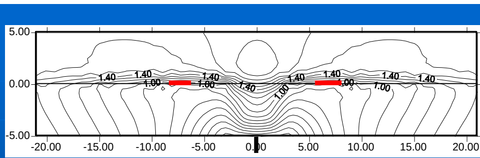

5m ahead of the interface

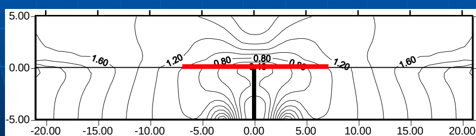

right at the interface of the weak zone

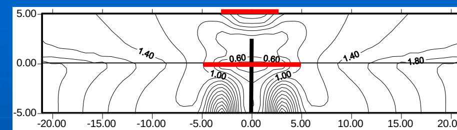

2.5m penetrating in the weak zone

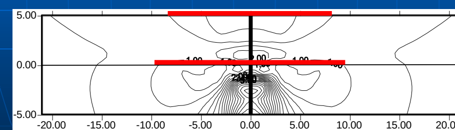

penetrating through the weak zone

tessellation simulation of fracture zone

- A set of pre-defined potential fractures is defined with a Delanauy triangulation procedure.
- The shear or tensile fractures activate when the failure criterion is exceeded and the fractures are included into the displacement discontinuity elements.
- The final activated fractures near excavation can be determined by a ***sequential activation calculation process***.

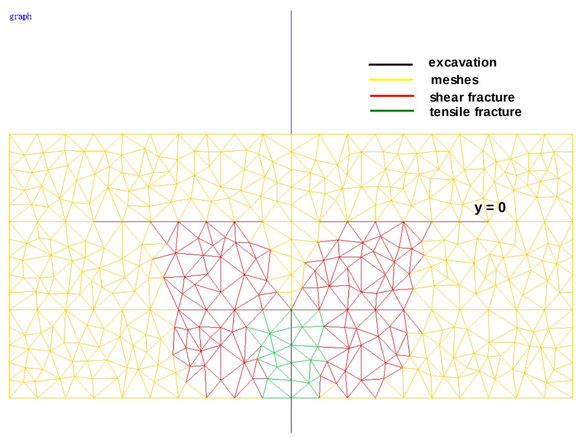

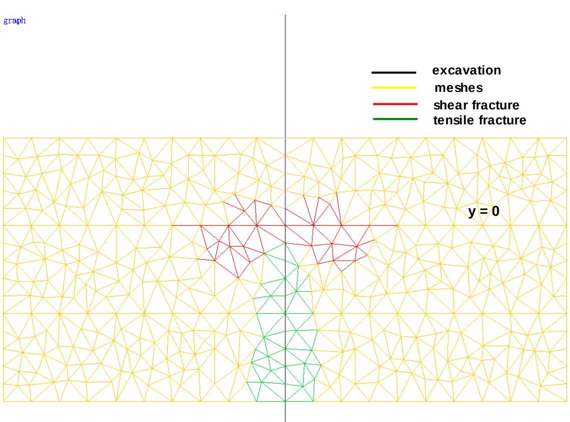

3. More Developments and Applications

2D→3D
Stochastic DD method

2D→3D

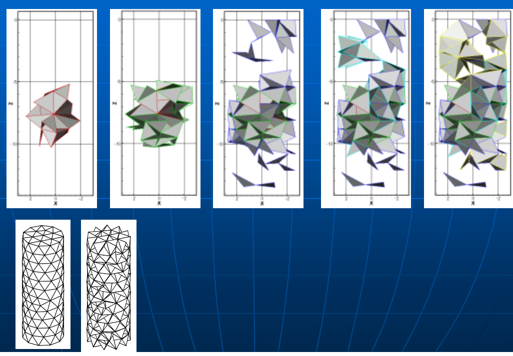

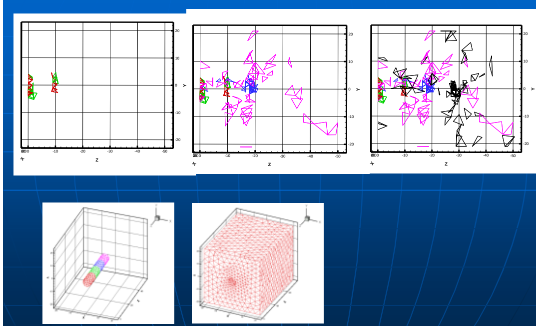

Development and Application of Stochastic Boundary Element Method

Fundamental solutions for the sdd element

$$u_x = D_x\left[2(1-\nu)f_3 - yf_5\right] + D_y\left[-(1-2\nu)f_2 - yf_4\right]$$

$$\frac{\partial u_x}{\partial x} = \frac{\partial u_x}{\partial y} = \frac{\partial D_x}{\partial y}\left[2(1-\nu)f_3 - yf_5\right] + D_x\left[(-3+2\nu)f_5 + yf_7\right]$$

$$+\frac{\partial D_y}{\partial y}\left[-(1-2\nu)f_2 - yf_4\right] + D_y\left[-2(1-\nu)f_4 - yf_6\right]$$

$f_2=f_{,x}$, $f_3=f_{,y}$, $f_4=f_{,xy}=f_{,yx}$, $f_5=f_{,xx}=-f_{,yy}$,
$f_6=f_{,xyy}=-f_{,xxx}=f_{,yyx}$, $f_7=f_{,yyy}=-f_{,xxy}=-f_{,xyx}$,
$f_8=f_{,xyyx}=f_{,yyx}=-f_{,xxxx}=-f_{,yyyy}$,
$f_9=f_{,xyyy}=f_{,yyyx}=-f_{,xxxy}=f_{,yyxy}$

水平直線裂縫上位移之比較(μ_s=0., SD_s=0., μ_n=10., SD_n=1.)

元素 (中點座標)	AVERAGE			
	U_x		U_y	
	MC	S	MC	S
1(0.5,0.)	-8.82E-05	-8.82E-05	4.04E-04	4.04E-04
2(1.5,0.)	-3.75E-13	-2.90E-13	4.85E-04	4.85E-04
3(2.5,0.)	8.82E-05	8.82E-05	4.04E-04	4.04E-04

水平直線裂縫上位移之比較(μ_s=0., SD_s=0., μ_n=10., SD_n=1.)

元素 (中點座標)	VARIANCE			
	U_x		U_y	
	MC	S	MC	S
1(0.5,0.)	8.08E-11	4.40E-17	1.70E-09	5.95E-18
2(1.5,0.)	5.90E-24	1.55E-18	2.44E-09	4.14E-17
3(2.5,0.)	8.08E-11	4.27E-17	1.70E-09	1.31E-16

水平直線裂縫上應力之比較(μ_s=0., SD_s=0., μ_n=10., SD_n=1.)

元素 (中點座標)	AVERAGE					
	σ_{xx}		σ_{yy}		σ_{xy}	
	MC	S	MC	S	MC	S
1(0.5,0.)	10.00	10.00	10.00	10.00	0.00	0.00
2(1.5,0.)	10.00	10.00	10.00	10.00	0.00	0.00
3(2.5,0.)	10.00	10.00	10.00	10.00	0.00	0.00

水平直線裂縫上應力之比較(μ_s=0., SD_s=0., μ_n=10., SD_n=1.)

元素 (中點座標)	VARIANCE					
	σ_{xx}		σ_{yy}		σ_{xy}	
	MC	S	MC	S	MC	S
1(0.5,0.)	1.04	1.66E-07	1.04	1.66E-07	0.00	9.16E-09
2(1.5,0.)	1.04	4.69E-22	1.04	4.69E-22	0.00	0.00
3(2.5,0.)	1.04	1.66E-07	1.04	1.66E-07	0.00	8.99E-09

THANK YOU FOR YOUR ATTENTION